AD-A060 837 AIR FORCE INST OF TECH WRIGHT-PATTERSON AFB OHIO SCH--ETC F/G 6/16
KINESIOLOGY OF THE LOCKED TORSO AS A FUNCTION OF COMPONENT WEIG--ETC(U)
MAR 78 A J NESTLE

UNCLASSIFIED AFIT/GAE/AA/78M-10 AMRL-TR-78-63 NL

1 OF 2
AD A060837

IFIED

1 OF 2

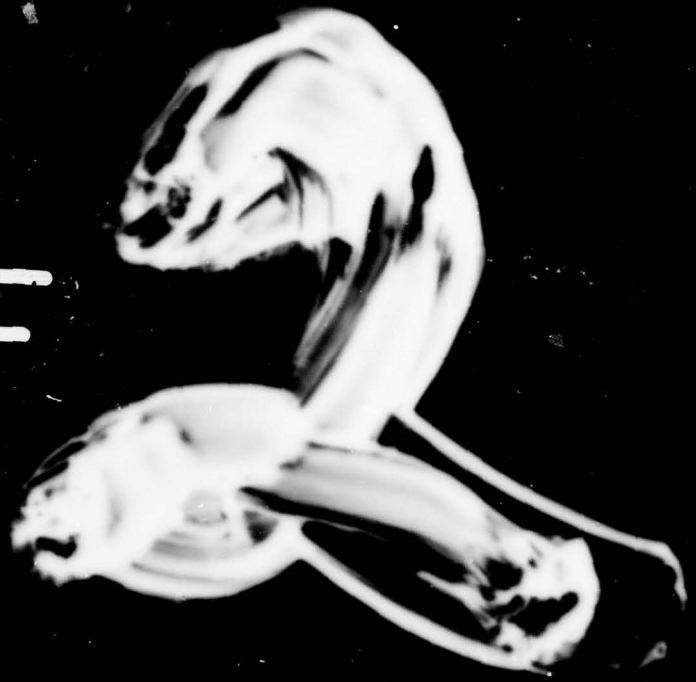

AD
AO 60837

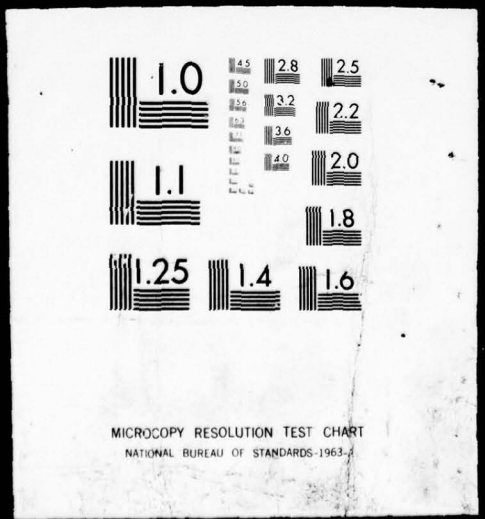

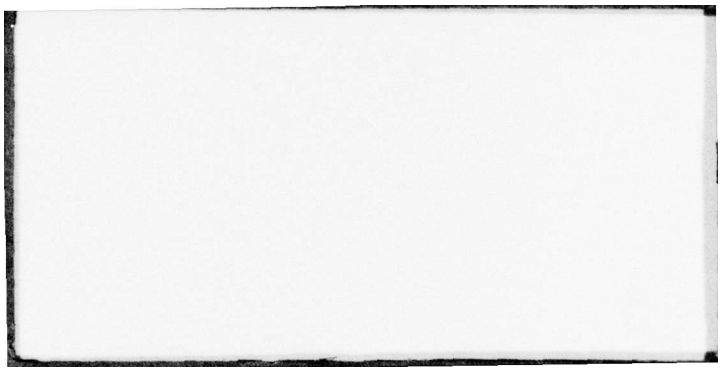

GAE/AA/78M-10

LEVEL II

AD A060837

DDC FILE COPY

KINESIOLOGY OF THE LOCKED TORSO AS A FUNCTION OF COMPONENT WEIGHT

THESIS

GAE/AA/78M-10

Arthur J. Nestle
Captain USAF

Approved for public release; distribution unlimited

GAE/AA/78M-10

KINESIOLOGY OF THE LOCKED TORSO AS A FUNCTION OF COMPONENT WEIGHT

THESIS

Presented to the Faculty of the School of Engineering

of the Air Force Institute of Technology

Air University

in Partial Fulfillment of the

Requirements for the Degree of

Master of Science

Arthur J. Nestle, B.S., M.S.

Captain USAF

Graduate Aeronautical Engineering

March 1978

Approved for public release; distribution unlimited.

Preface

The author gratefully acknowledges the guidance furnished by his advisor, Dr. Peter Torvik, AFIT/EN, and sponsor, Dr. Leon Kazarian, 6570 AMRL, throughout the course of this endeavor. The facilities of the 6570th Aerospace Medical Research Laboratory, Aeronautical Systems Division (ASD), Wright-Patterson AFB, OH were used in this investigation, and the author wishes to thank those people and agencies for their assistance. Special acknowledgement is made of the substantial time and talent devoted to this project by Major Steve Combs, USAF, MC.

The experiments reported herein were conducted in accordance with current Air Force and DOD policy and directives controlling research use of nonhuman primates.

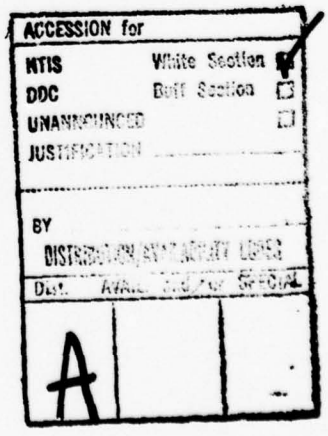

Contents

Contents

List of Figures

List of Figures

List of Tables

List of Tables

Abstract

Two subhuman primates were utilized to experimentally record the contribution of the musculoskeletal substructures to overall torso stability. Each specimen was euthenized and four small diameter surgical pins drilled into the spinous processes. A Stengstaken-Blakemore esophageal tube was threaded into the proximal esophagus and balloons inflated to define the diaphragm. One experiment consisted of static load application to the torso so that flextural, extensive and lateral bending were introduced. Abdominal pressure was taken from a transducer and multiple exposure photography used to measure the vertebral deformations corresponding to load increment from 0-2309 grams. A second experiment involved rotation of the pelvis, with the C-4, C-5 vertebrae fixed, from 0-110° and associated pressure recorded. For each experiment a progressive necropsy was accomplished and experimental steps repeated.

Deformation measured, from scaled photographs, versus applied load was graphically compared. Both quantities were geometrically reduced along the axis of the spine and slope data tabulated.

Relative reaction to loading for vertebrae C-4, T-3, T-8, L-2 and L-6 is tabulated for abdominal pressure and deformation in flexion, extension and side-bending and abdominal pressure from torsion.

Castigliano's theorem was applied to a circular arc representation of the bent torso.

INTRODUCTION

The general functions of the musculoskeletal system are movement and support. The spinal column serves as the skeletal anchor for maintenance of the vertical posture of the torso and, as a result, experiences a complex system of externally applied forces and moments. Contributions made by the musculature, integument and thoracic and abdominal body cavities distribute these forces through the trunk and allow for a greater load acceptance before the bioengineering structure "fails". Engineering studies of the body can provide valuable understanding of the component and substructure interaction - much like evaluation of the isolated reactions of any framework or mechanical system to determine its physical limits of performance.

Thesis. To investigate the constitutive relationship of musculoskeletal substructures to overall torso kinesiology in subhuman primates and, to apply the principles of engineering mechanics to determine the functional contribution of the anatomical parts to body stability and movement.

Literature Review. Kinesiology of the torso is an extension of the much addressed problem of stability and normal movements of the spine.

Historical motivation for this research emanated from the medical quest for understanding and treating the dysfunction scoliosis (lateral curvature of the spine) and lumped maladies of low-back pain, sciatic pain, low-back syndrome, disk degeneration and related conditions, including disruption of the skeleton by trauma. The goal was to decrease crippling and death. The desire to predict internal injury from extent and type of skeletal or surface injury is of current engineering attention.

Man's interaction with a sophisticated technology has greatly expanded the hazards and demands characteristic of his environment and has necessitated the evaluation of his capability to perform successfully in the mechanical systems and conveyances. As a result, an engineering idealization of biological man has evolved as an attempt to conform with design demands for data of an anticipated load bearing structure: man. Biomechanics is this blending of physiological and engineering disciplines and is a relatively new investigative concept.

Experimental research has involved human volunteers, animals such as subhuman primates, intact human cadavers and segments of the human spine. Most recently, computer generated models have been investigated. Because of the medical and engineering cohesion necessary to achieve the kinematic perspective of an anatomical unit, major areas of research parallel the professional backgrounds or supportive agencies of the investigators. Approaches consider the spine as major unit composed of many subunits (vertebrae, disks, et al); interface of spine and musculoskeletal substructure; and the mathematical and mechanical modeling of exhibited properties under impact, load and movement.

In 1905, Dr. Robert W. Lovett presented his investigation, "The Mechanism of the Normal Spine and its Relation to Scoliosis". Lovett described the kinesiology of the spine; its normal mobility, its restrictions, and its weakest points of resistance, using cadavers and live volunteers. This was an extensive study of the gross properties of regions of the spine. This thesis applies a more analytical perspective to the movements of the nonhuman primate torso, but does approach the raw data with the kinesiological intent of the previous study. Direct comparisons

are made with specific human findings, reported by Lovett, and comprise a portion of the discussion of torso kinesiology from experimental results (Section IV).

The kinematics of the spine (and body substructures) receive investigative attention from orthopedic and biomechanical viewpoints, generating substantial documentation of specific phenomenon, all of which will not be explored here. The core of this thesis is Lovett's procedure, modified and expanded in a desire to utilize in an engineering analysis the observed torso mechanics of movement.

BIOMECHANICAL DEVELOPMENT

Man is a unique creature in his habitual assumption of the upright posture. Reports in the literature suggest that there is general agreement that the change from quadruped to the biped stance has imposed certain mechanical disadvantages on man [46:70]. There are divergent opinions regarding the significance of these disadvantages and of the engineering stresses that are involved. Some investigators believe that there is an extreme inadequacy of adaptation and that anatomic and physical physiologic defects in skeletal structures are exhibited in poor functional health [12:22]. There is a general acknowledgement of the great magnitude of the forces that operate within the trunk, and specifically the skeletal system, when a load is applied by some variety of ways: locomotion [42,55], distribution of movement [62], dysfunction [21,39,46,59,64,73], torsional resistance [19,24], sitting [24,46], standing [24,46], caudal mechanics [43], body positions with respect to gravity [46], and interaction with structures [1,15]. In some instances the effective load is no more than the arithmetic sum of the upper trunk and weight. However, in bending, moving or lifting, moments exist which create substantial forces, especially

in the lumbosacral spine. The applied loads that appear during violent actions must be considerably higher. It is the mechanics of the musculoskeletal substructure that enables the torso to tolerate these forces by distribution of the load throughout the framework of the trunk.

A series of bones, supplemented in certain regions by pieces of cartilage, form the framework of the body. The bony part of the framework is held together by ligaments and constitutes the skeleton. Covering the surface of the body is the skin or integument. The spinal column serves as a sustaining rod for maintenance of the upright position and, as such, is subjected to a complex system of forces and loads of different types. This column is considered to have both an intrinsic and extrinsic stability [43:327]. Intrinsic stability is provided by the alternating rigid and elastic components of the spine which are bound together by the system of ligaments, whereas extrinsic stability is provided by the paraspinal and trunk muscles. This column is attached to the sides of and within two chambers: the thoracic and abdominal cavities, separated by the diaphragm. The action of the trunk muscles converts these chambers into nearly rigid-walled cylinders of air, liquid and semisolid matter. Both of these cylinders are capable of relieving the load on the spine [43], by increasing the effective area of support (Fig. 1).

It is desired to analyze this relationship between structure and function. A standard approach is to isolate the system with the logic being that a study of the subunits will elucidate their contribution to the whole system. Biomechanics is this straightforward study of the human body as an engineering problem and involves the application of engineering principles to analysis of the human musculoskeletal system. The general functions of the musculoskeletal system are movement and

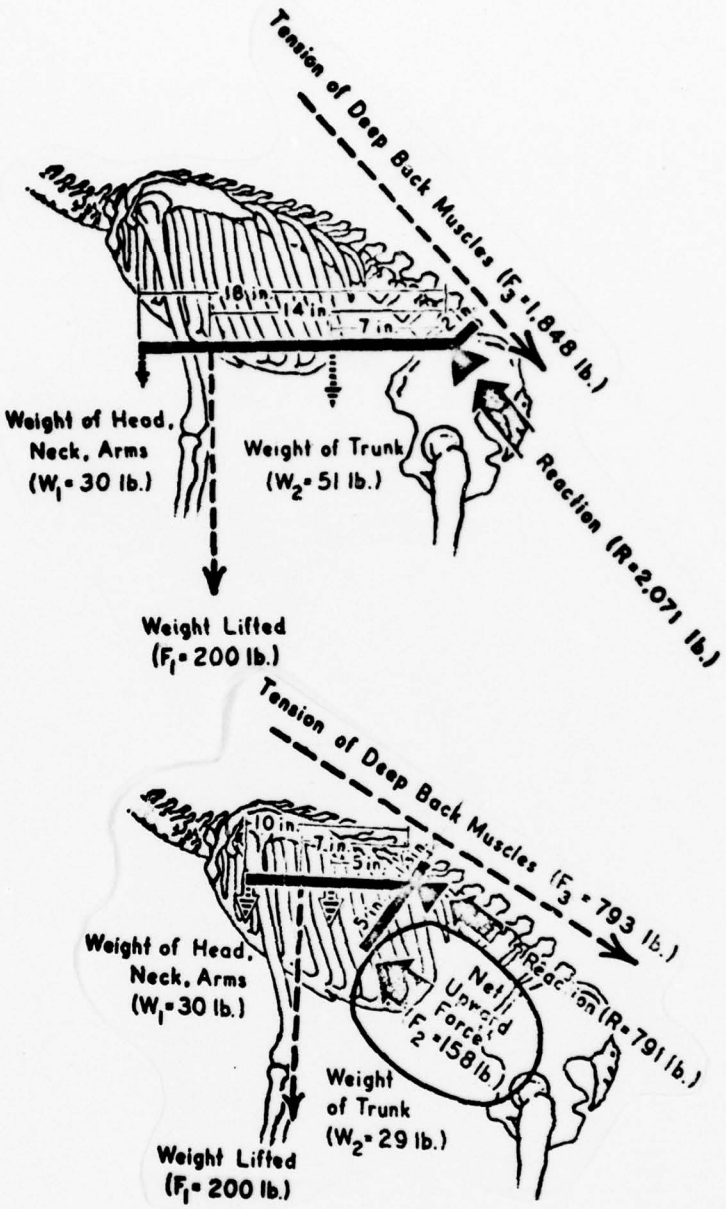

Figure 1. Abdominal Cavity Participation [40]

support. In order to perform these functions, the musculoskeletal system must contain basic elements that provide kinematic alignment motor power and structural stability and rigidity. In order to understand the complex structures of the musculoskeletal system, it is desirable to determine the properties of the material constituents of the components. Clinical problems in orthopedic biomechanics are related to particular structures of the skeletal system and their mechanical properties. To understand the biomechanical perception of the torso, integument, tendon, muscle and bone will be discussed as they ideally represent conventional mechanical structures [21].

Integument - skin - covers the surface of the body and shelters it from injury. Skin is also, from a bioengineering approach, a flexible and extensible casing which effects its containing function of resisting lateral pressures by sustaining membraneous stresses [21]. These are predominantly tensile and shearing stresses. At points of articulation, buckling or wrinkling and folding, the resistance of skin to compressive stress is exhibited. The integument is visibly arranged in a preferential manner to facilitate certain large movements so that anisotropy of its elastomechanical properties is a salient feature. The reticular layer (deep layer) of the skin consists of fibroelastic connective tissue. When a penetrating wound with a sharp conical instrument effectively relieves the natural prestresses of the integumental membrane a round hole does not result, as might be expected, but a slit. Maps from a series of punctures (Langer, 1861) substantiates that there are definite lines of tension within the skin which are characteristic for each part of the body (Fig. 2). Skin is not axially fibrous but becomes fully oriented with tensile stresses under loads imposed laterally in any

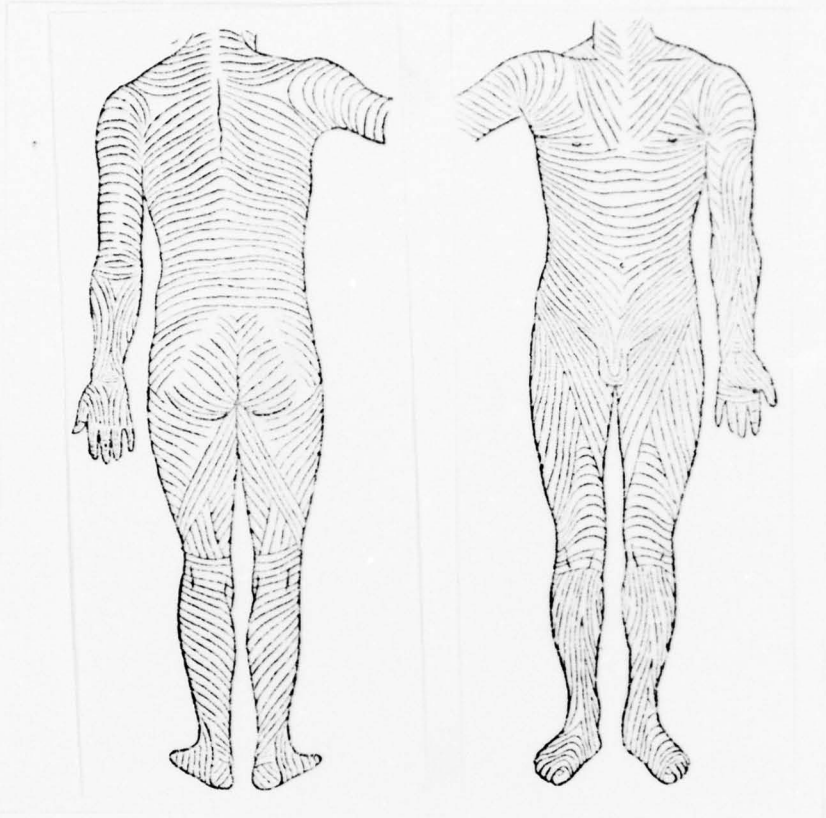

Figure 2. Langer Lines: Integumental Stress Alignment [25] (Eller)

direction in the integumental plane. The unorganized dense fibrous tissues are interwoven and able to stand strong tensional stress in many directions. Mechanically, the skin can be idealized as a bubble of composite material having a constant surface stress resultant, when other musculoskeletal substructures are not considered.

Tendons (and ligaments) are organized dense fibrous tissue arranged in compact parallel bundles. They are pliable and inelastic, and withstand great tensile strength, particularly in one direction. Ligaments are attached to bones at both ends. Tendons connect muscle to bone. The function of each is to transmit uniaxial tensile force and not to respond to compressive, shearing or bending effects. The tendon generally makes

possible the precise application of force. This kinematic arrangement allows the complex range of movement of the musculoskeletal torso. It is generally accepted that working stress is about one quarter of that at ultimate tendon failure and tendon strength exceeds that of its muscle by a factor of two [21:141-175]. The structural engineering properties normally associated with rod elements is evidenced by these anatomical substructures.

Muscles are contractile tissue and control the position and movement of the complex of bone comprising the skeletal framework of the torso. Motion and articulation in vertebrates are by means of skeletal levers acted upon by muscles. The energy of their contraction is made mechanically effective by means of ligaments which secure the ends of the muscle and control the direction of pull [25]. Muscles form the mass of the torso commonly known as flesh and account for about 40% of body weight. The *origin* and *insertion* of the muscle are the terminal attachments of the ligament to a bone. Three types of muscle action are generally recognized in the literature, (i) individual action, (ii) group action, and (iii) action correlated with the nerve supply [25]. Mechanically, the individual action is directly associated with the attachment points and the effect may therefore be anatomically deduced. Group actions tend to relate to functions as well as anatomy and may possibly be remotely apparent or even antagonistic. Frequently, there can be seen a correspondence between groups of muscles and nerve supply arrangement. Because of this variety and redundancy in the muscular subsystems, individual muscles cannot always be treated as single mechanical units. Furthermore, retarding and controlling the movement caused by gravity may cause the antagonist of the apparent effective muscle to act. This variety lies

in the structural anatomy as well as intrastructural profiles. The muscle is basically a machine which converts chemical potential energy, electrically excited, into mechanical energy. The dynamics of motion is concerned with the operation of the leverage system exhibiting shortening of the fiber from the development of tension. In an equilibrium condition (or state of rigor mortis) muscle activity is more of an isometric nature and approximates a static framework.

Biomechanically, bones are the beam elements of the skeletal structure. They are not absolutely rigid, but possess some degree of plasticity and will support tension, compression, and shear stresses. Stresses can produce a transient deformation which is followed by recovery of original form. Bone is porous and mechanically and morphologically nonhomogeneous. Adaptation to the mechanical function concerns the gross shape: cross section, material distribution and inner structure. Bone has been mechanically hypothesized as a composite, compound bar and a prestressed member [31:241]. The relative ease of adapting structural testing from conventional substances of an engineering interest, to bone, has propagated substantial amounts of data on bone, such as: strain rate, creep rate, Young's modulus, etc. In compact bone, the breaking stresses are comparable to those widely employed in engineering materials. A "failure" in the musculoskeletal system occurs when a bone fractures or a tendon separates. The degree of force necessary to produce a fracture depends on the properties of the bone, application of force in relation to the structure, and the speed of application (loading rate). Although the general form of the skeleton is hereditary, it also responds to external mechanical factors, such as pressure and stresses and internal strains will stimulate bone formation, overtime [2]. The internal position of

bones and their central position in limbs provide firm support. While the component parts of the skeletons of vertebrates are uniform in basic plan, there are wide superficial differences associated with adaptations or environments. In addition to strength, bones can provide a marked degree of flexibility in many directions when strategically placed.

The substructures - integument, tendon, muscle, and bone - cohesively form the human skeletal system and coaxially provide trunk stability. The vertebral column constitutes the longitudinal axis of the musculoskeletal system and sustains the upright position for the body. This column possesses a number of unique features that make it distinctive in an engineering sense, and those characteristics will be explored now.

The vertebral column or spine constitutes the longitudinal axis of the skeleton (Fig. 3). It is a flexible, segmented spring resembling the form of the letter "S". In humans, there are twenty-four (24) separate bones, so joined to each other as to permit forward, backward and sideways movement of the column. The interactions of the spine with the whole body can be generally grouped into four different types - support, protection, motion, and anchoring of muscles.

The distinctive characteristic of man with respect to other mammals is his erect posture, which has necessitated adaptation of the skeletal system to insure support and stability. The trunk has been brought into erect position over the hip joints by the development of lumbar curvature. The spinal column possesses an intrinsic as well as an extrinsic stability. A series of ligaments placed under tension by an expanding intradiscal force firmly bind the vertebral segments together. These ligaments include: (i) a longitudinal system that binds all the vertebrae together into a mechanical unit, and (ii) a longitudinal system that secures one segment

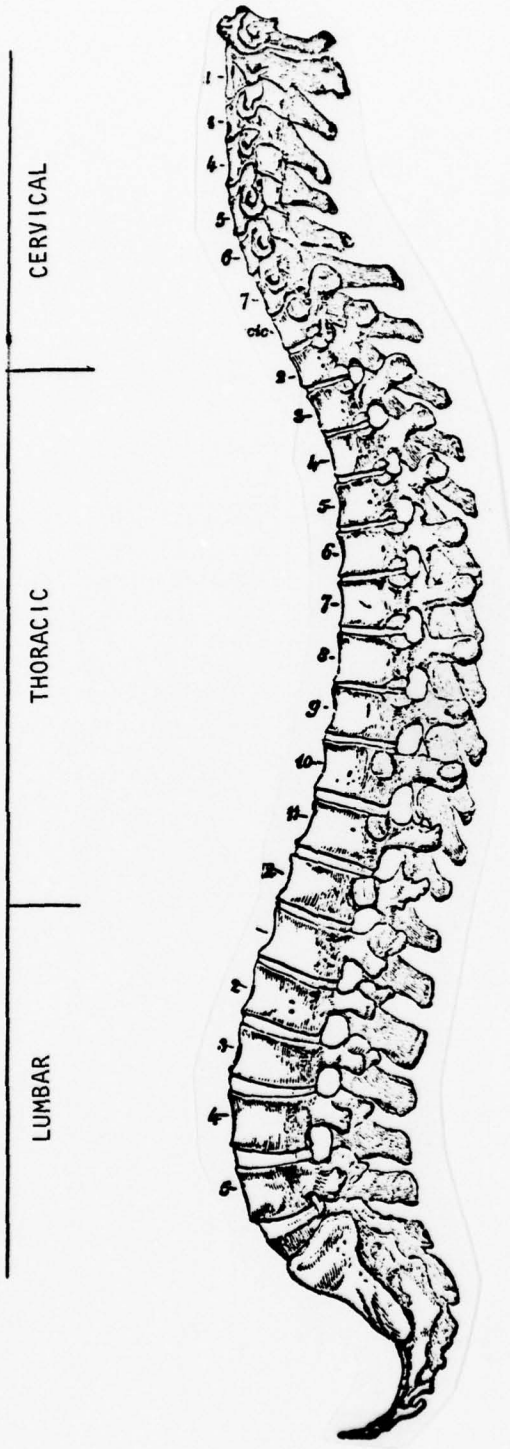

Figure 3. The Spinal Column [25]

to another [42:313]. When uniaxial load is applied, the intervertebral disks distribute and convert the load to a tangential annulus force attended by the viscoelastic mechanism of the annular walls [34:16]. Additional support is provided through stabilizing paraspinal musculature, the action of the intercostal muscles and the muscles of the shoulder girdle rendering the thoracic cage quite rigid, and the contraction of the diaphragm and muscles of the abdominal wall making the abdominal cavity semi-rigid. The extrinsic support distribution increases with load bearing requirements [42:325-326]. The curvature of the spine allows it to absorb vibration and shocks of movement. Additionally, weight distribution of the whole body is effected by this "S" curvature. The upper sector carries the head, the middle sector the organs and structure in the chest and the lower sector the abdominal cavity contents. The curvature creates a more uniform distribution of load and is far less vulnerable to breakage than a straight column would be since the load is not strictly supported at the lowest point.

The protective function is most conspicious in relation to the central nervous system [52]. The heavy bodies of the vertebral column, the intervertebral disks and interlaminar ligaments encase the tracts of nerve fiber traveling to and from the brain. The spinal vertebrae transmits forces and guides and limits the overall motion of the column. The vertebrae in different parts of the column show regional differences reflecting the degree of motion and load bearing requirements. The ligamentous attachment of the ribs to the spinal vertebrae provides a flexible and elastic protective covering for the organs of the chest.

The motion of the body (and its parts) is made possible by a large number of different suborindate and variously interacting engineering

arrangements between muscle and bone. To voluntarily change its position a skeletogenic organism must contain elements capable of producing controlled forces and necessarily maintaining the body's center of gravity within the zone of support [55:514]. It is the necessity to maintain stability that determines the functional sequence of movement. The feet raise the body from the ground, and serve to anchor it, while the vertebral musculature allows forward progression by contracting isometrically to create the energy for propulsion. The elimination of lateral undulations of the vertebral column as the main propulsive agent is accompanied by the development of torso-central flexibility of the chain of vertebrae: the distance between successive footfalls would be less if the vertebral column remained rigid.

The vertebral column is also important in the anchoring of muscles. Many attached muscles are so arranged as to move either the column itself or various segments of it. The large erector spine muscle provides axial stability. Small muscles run between the transverse and spinal processes of adjacent vertebrae giving mobility to the segmented bony column.

Biomechanically, the spine has been modeled structurally as a flexible elastic rod and as a discrete parameter sequence of rigid bodies. Because of its many interactions with other body structures, the spine is medically and mechanically the focus of torso investigations.

Movements of the Torso (Spine). Motion of the torso is directly reflective of the spinal segments involved. The shape and position of the articular facets of the vertebral bodies controls the type and range of motion possible. Motion between the vertebral bodies occurs in four directions: three rotary and one translatory.

Flexion is the forward downward bending in the sagittal plane (Fig. 4). It involves compression of the anterior body cavities and intervertebral disks and elongation of the muscles of the back.

Extension is a backward and downward movement in the saggital plane (Fig. 5). In the thoracic region extension is limited by the overlapping of the spinous processes. Major muscles of the chest must elongate to allow extension of the torso.

Side-bending (Fig. 6), or lateral flexion, is flexion in the frontal plane about a sagittal-horizontal axis. The ribs limit the range of side-bending motion evidenced by the thoracic region of the trunk.

Rotation (Fig. 7) is movement about the spine in the horizontal plane about a vertical axis. Rotation is accompanied by a slight amount of side-bending and is most free in the cervical and thoracic regions of the spine.

Lovett [34:349] demonstrated three points in movement of the trunk:

(i) Side-bending and rotation of the spine are parts of a compound movement and cannot be disassociated.

(ii) The rotation accompanying side-bending varies dependent on extended position.

(iii) Every rotation manifests lateral curving or side-bending.

The mechanical redundancy is evidenced by the compound movements of the trunk and associated substructures of the torso.

EXPERIMENTAL METHODS

Selection of Specimen. In investigating the human system, an understanding of the mechanical interaction of the tissues is necessary. When any substance is subjected to a load, it exhibits some deformation as a reaction to the stress. The material may recover its original geometry

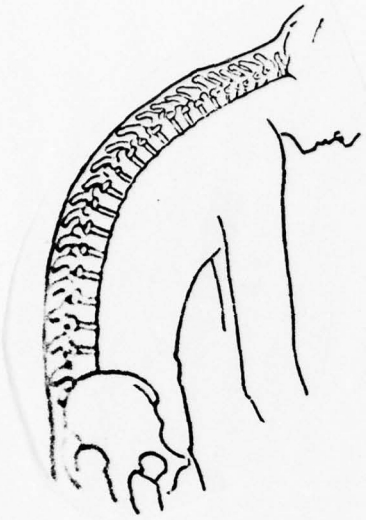

Figure 4. Kinesiology of Torso: Flexion

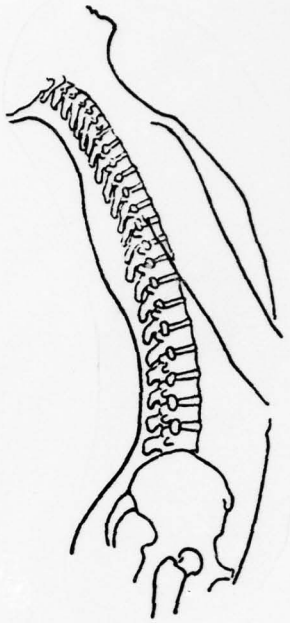

Figure 5. Kinesiology of Torso: Extension

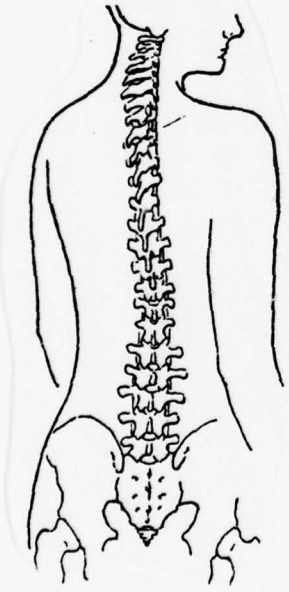

Figure 6. Kinesiology of Torso: Rotation

Figure 7. Kinesiology of Torso: Side-Bending

when the load is removed - an elastic substance - or the deformation may remain to some degree - a plastic or inelastic substance. The biological tissues are deformed by stress and, these deformations of an anatomical geometry resulting from imposed loads, can be investigated. When the mechanical properties of the specimen have been obtained from the stress configuration, it is possible to calculate some of the material properties of the tissue. When a substructure is investigated, exhibited material properties may be determined for the gross specimen and subunit contributions, as the component parts are separated. This will be the general concept of accomplishment in this thesis.

To investigate the kinesiology of the restrained torso in a destructive sequence of separations, a suitable model necessarily must be selected. The use of nonhuman primates has historically offered biomechanical responses to a contrived environment which have allowed acceptable hypothesization of human performance. Accounting for morphologic and functional kinesiologic differences improves the usefulness of results. As diversified as primates are in terms of appearance and ecological adaptations, they have avoided extreme anatomical specializations and have preserved a generalized structural likeness (Fig. 8). The primate vertebral column shows a similar basic pattern of components, reflecting adaptation for the verticality of the trunk. Man does exhibit some mechanical characteristics that have been imposed by the change from quadrupedal to habitually bipedal locomotion. However, normal musculoskeletal geometry and torso kinesiology of man and other primates is grossly alike and tempered comparison of biomechanical responses is a realistic investigative perspective.

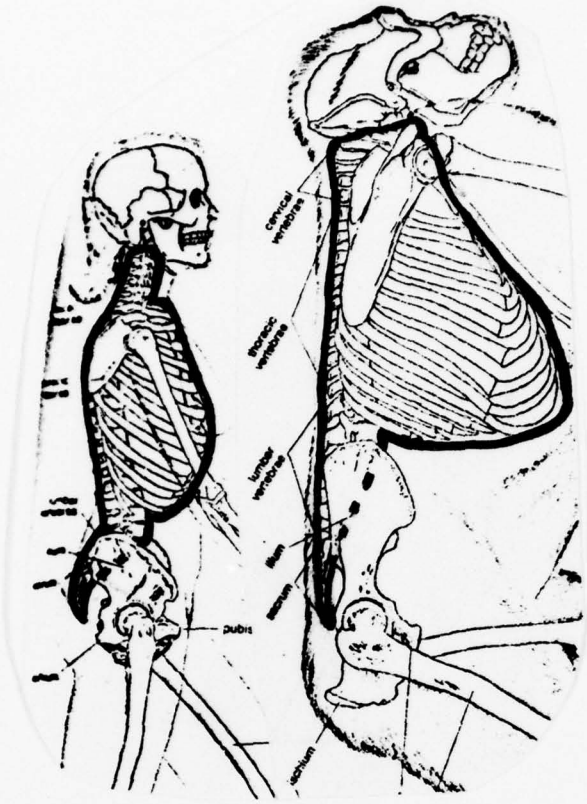

Figure 8. Primate Comparison [52]

The field of mechanics seeks to develop mathematical laws which define the common properties of an idealized body in both the static and dynamic sense, and on the basis of these laws derive constitutive equations which illustrate their application to different specific situations [21:3]. Physiology deals with the study of the functional behavior of living structures, with the objective of establishing the relationships that underlie the phenomena [82:3]. Biomechanics is a general blending of these disciplines, and others, to facilitate the investigation of a topic from that special perspective. Inherent in this combining is also the compounding of premise, assumptions and limitations used to make the

investigation manageable. The general stipulations and understandings essential to successfully achieve an acceptable engineering description of biological material and processes, and most applicable to the use of nonhuman cadavers for research, are briefly presented now.

a. The functional characteristics of integument, muscle, tendon and bone interaction are so complicated and the overlapping of so many individual actions that factors of lesser importance must essentially be eliminated in formulating a model of musculoskeletal substructures.

b. Movements resisted by contracted muscle (or muscle in the state of rigor mortis) depends upon the angle of application of the muscle to the bone and this angle changes with the position of the joint. It is also known that applied tension is a function of the geometrical properties of the muscle, consequently, mean values must be accepted [62:6].

c. Density of biological material is complex and using an average value is most realistic.

d. In primate movement, bodies, as parts of irregular morphological shapes composed of tissue of varying density and specific gravity and inertial properties, interact. To do an engineering evaluation of the structure one must approximate the body, or its anatomical part, to standard geometric forms of homogeneous structure. The composite nature of anatomical material is a property that is not readily manageable without creating precise geometries and accepting general characteristics.

e. There are few precise points of force resolution in the body. The musculature generally acts to distribute loading to the surrounding area.

f. Biological tissues are inelastic and a process of preconditioning is necessary to obtain repeatable results. Preconditioning is a repetition of the same procedure a sufficient number of times until a state of homostasis develops [65:655]. With cadaver material the problem of rigor mortis further complicates the tissue reaction.

g. Musculoskeletal complexities of the vertebral column are an area of investigation alone. For general purposes the behavior of this subunit is considered to be like many rigid bodies with interspersed elastic material [72:405].

h. The response of the abdominal and thoracic cavities can be likened to a uniform cylinder, with load intensity and duration of sufficiently small magnitudes that pressure values are considered constant, after stabilizing, until the applied force is changed and the sequence progresses.

i. The viscoelastic characteristics - material stress-strain relationships dependent on the loading rate - will not be of concern to this investigation. Load application will be deliberate, but not of such rapid increase as to be considered an impact force [6:56].

j. The interchangeability of primate and human response data must be done judiciously because of morphological and kinesiologic differences. Animal responses parallel injury (force application, mode, severity and site) similar to man, after accounting for static and dynamic musculoskeletal differences [33:961]. Morphologic considerations are elaborated in a later paragraph and applied in a discussion of the experimental results.

k. Cadavers possess unique material response characteristics. Muscles are generally absent. In the state of rigor mortis, the extensibility and transience of tension disappears and the muscle is very stiff

[39:349]. The specimen is generally less flexible [39:349] and drying of the tissues produces unnatural limitations [39:349].

It is the goal of this work to provide a relative understanding of the functional contribution to torso stability of musculoskeletal substructures by applying a known load with a known orientation and isolating the contribution of the substructures by removal - necropsy. Accepting the foregoing qualifications, use of nonhuman primates is still a viable model of the complexities of the human system for investigative study and interpretation.

There are some morphological characteristics of the Rhesus (Macaca Mulatta) monkey which warrant presentation by their difference or nonexistence in humans and, more fundamentally, their contribution to a biomechanical response of the complete torso. Generally, the upper torso of the Rhesus has more encompassing musculature attachment and greater pelvic-cranial muscle travel than man.

The shoulder and upper torso area exhibit more distributive musculature attachment in the monkey. The spinodeltoid attaches to scapula and exhibits a well developed fascial connection. This is interpreted as offering the monkey a greater mechanical advantage in lifting the humerus [63]. The existence of the long tricep (caput longum) offers greater upper torso mass in the area along the border of the scapula and cohesiveness at the shoulder than man has. The Rhesus has a cervical portion of the serratus anterior, a large muscular sheet between the ribs and the scapula. The latissimus dorsi, a broad flat muscle, arises from the T-5 or T-6 vertebrae distally to the lumbar region [63]. The upper torso portion of the muscle connects to the teres major. This is a further torso support that organizes the entire trunk in a support effort,

maximizing the redundancy of a given effort and enhancing vertical support. This pelvic to cranial expanse of substructures is not as predominate in man. Man does exhibit a greater chest covering musculature in the overlapping layers of the pectoralis major [63]. The abdominal continuation of this muscle is unique to the monkey. The Rhesus has a more well developed sternocostalis muscle, extending from the upper sternum laterally to the first rib. This amplifies the mass concentration in the upper torso. Man also has a much less cranial attachment of the rectus abdominius muscle than other primates [63]. The gastric morphology is similar. The monkey does exhibit a longer more narrow thorax, wider intercostal spaces and a longer attenuated sternum than human primates [63].

This generally means the Rhesus is more compact and better equipped to sustain and distribute external forces applied to the upper torso. This apparent fortification and predominance of the thoracic region will be explored with the experimental results.

Apparatus. The test apparatus consisted of the mechanism for loading the specimen (Fig. 9), a three-part support stand with rotatable top plate, a restraining box, a pulley system, calibrated steel weights, and the means of recording the resulting deformations with a pressure transducer, two plane photography equipment and the associated electronic equipment. The loading and support apparatus was fabricated by the industrial shops of the 6570th Research Laboratory.

The steel support stand (AMRL drawing No. 77MRL-C-232) was pinned to the floor through eight evenly spaced 9/32 inch holes drilled into the circular 16 1/2 inch base plate. A seven inch diameter axially symmetrical collar welded to the base plate was threaded to accept the 36 inch high

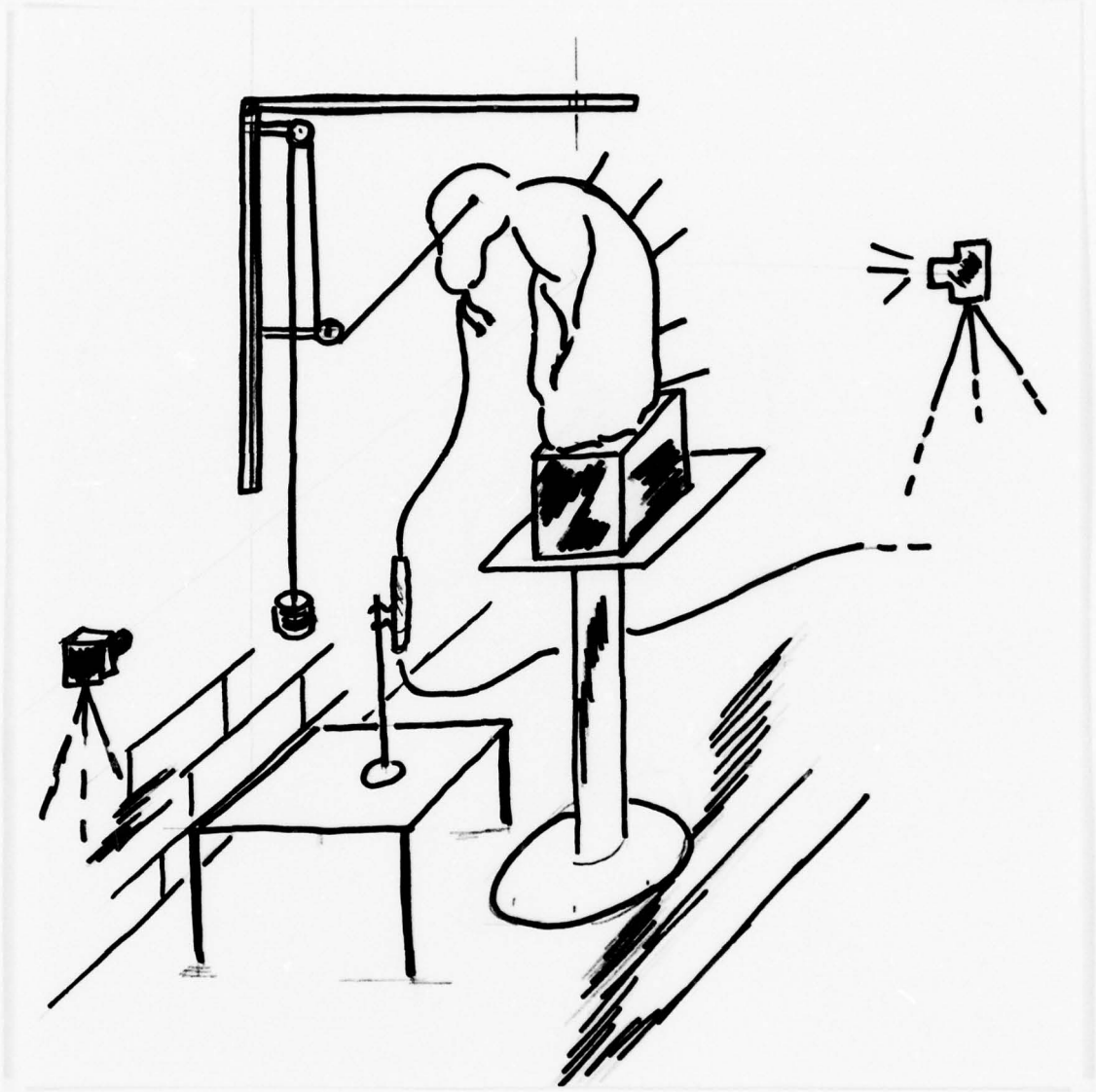

Figure 9. Experimental Apparatus Set-Up

stand shaft (AMRL drawing No. 77MRL-B-234) onto which the stand top plate (AMRL drawing No. 77MRL-C-233) is screwed. The steel top plate was twelve inches square and 3/8 inches thick with four 9/32 inch holes, drilled symmetrically, for securing the restraining box. The thread interface between top plate and stand shaft was 5 7/16-16UN. This is such a fine pitch thread that rotation of 180 degrees does not manifest significant change in the distance from the floor to the top plate. The restraining box (AMRL drawing No. 77MRL-C-231) was 3/8 inch plywood construction, with 9 1/4 inches square inside dimensions. It was affixed to the support stand top plate with 1/4-20 bolts and hex-head nuts. The stand-box apparatus was pinned to the floor, 28 inches from the wall mounted pulley and weight hardware.

For the flexion, extension and side-bending experiments a movable pulley, constructed to slide on a thin aluminium track bolted vertically to the wall, was adjusted to maintain the desired angle of load application. The weights are each about 481 grams, slotted to be additive on a hook and end stop center rod. Nylon cord was used in the pulley system.

For the rotation experiment, aluminium channel bar was secured perpendicular to the wall track so as to extend horizontally from the wall above the specimen. The cadaver was aligned by rotating the top plate of the support stand so that the large cross Steinmann pins inserted through C-4 are parallel to the channel bar and they are wire wound to it.

The abdominal pressure was sensed by a linear differential pressure transducer attached to the open stomach tube of the Stengstaken-Blakemore tube (Fig. 10). The electrical response of the transducer was coupled to a Hewlett-Packard 3440 digital voltmeter and a Rustak chart recorder to monitor abdominal pressure change and display it in millivolts.

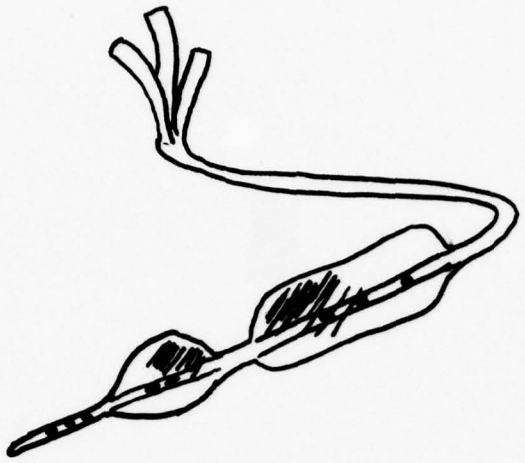

Figure 10. Stengstaken-Blakemore Esophageal Tube

Two multiple exposure cameras were positioned about six feet from the specimen, one photographing the saggital plane and one the transverse plane. Deformation was recorded by multiply exposing the specimen sequentially with load application and measuring from the photograph movement of small Steinmann pins drilled into the spinous processes. A millimeter measure was affixed to the restraining box for scaling purposes and a corner of the box marked as an origin, in each plane, to allow relative measurement of sequences. A horizontal and vertical axis was placed on the photographs with the previously marked "spot" as the system origin. Millimeter values of X and Y for no loading applied are measured and subsequent relative changes in those components measured, for each load applied.

Throughout the bending experiment steel weights were manually stacked onto the hook-center-rod.

The support stand top plate collar was painted at five degree increments at the junction with the stand-shaft. The top plate with the specimen and restraining box affixed was rotated through ten degree increments for measuring abdominal pressure.

The necropsy sequences were accomplished with the facilities of the 6570 AMRL Veterinary Services Branch. The specifics of the necropsy activity are presented in the section on procedure which follows.

The pressure transducer/recorder printouts were calibrated with a mercury manometer and abdominal pressure voltages graphically compared to the calibration run to determine appropriate value.

Preparation. The subject was anesthetized with sodium pentothal and euthanasia was accomplished by drug overdose. Four small Steinmann pins, 3/32 inch diameter and about four inches long, were inserted into the spinous processes of the thoracolumbar spine of the fresh specimen at predetermined locations (C-4, T-3, T-8, L-2, L-6) by means of a surgical drill. The specimen was then positioned into the wooden restraining box in such a way that the rim of the pelvis was at the top edge plane of the box and the torso was aligned laterally with the load application apparatus. Three large, crossed, Steinmann pins (NSN 6515-00-310-7920; Pins, Trocar Point, Steinmann) were introduced through the sides of the restraining box and pelvis of the specimen, securely transfixing the specimen to the restraining box, through the pelvis. A quantity of acrylic resin (NSN 6520-551-8150; Resin, Acrylic, Dental (denture base repair)) insured immobility of the pelvis.

In the flexion, extension and side-bending experiments, two large crossed Steinmann pins were introduced through the skull anteriorly-posteriorly and medially-laterally at the plane of Reid's baseline [25:50] and transverse loading applied to the torso through the second respective pin.

The torsion experiment preparation consisted of making a circumferential incision through the skin at the base of the skull. The jugular veins and carotid arteries were identified and ligated distally and proximally. The musculature of the neck was then sectioned and the cervical spine was disarticulated at the C-4, C-5 level. Two large cross Steinmann pins were introduced through the cervical vertebral bodies parallel and secured to the aluminium channel bar, extending horizontally from the wall mounted track over the specimen. This sustained the torso in a vertical posture.

For all experiments a Stengstaken-Blakemore tube (LRR 6516L, Blakemore-Esophageal Nasogastric Tube, Doval No. 9211, Fidelity Medical Company) (Fig. 10) was introduced into the proximal esophagus of the primate cadaver, and advanced into the stomach. Normal (0.9 percent) saline solution was used as a lubricant. The Blakemore tube is three tubes, one inside the other, with separate openings at the external end for application of pressure to inflate the internal gastric and esophageal balloons or for introducing a substance directly to the stomach through the innermost tube, which does not have an enclosing balloon, but is completely open. The gastric balloon was inflated and tube clamped. Tension was placed on the Blakemore tube until the gastric balloon rested at the gastroesophageal junction (the diaphragm). The esophageal balloon was then inflated and tube clamped. This effectively "sealed" the

gastrointestinal track at the diaphragm. Saline was injected through the nonballoon third tube of the Blakemore device directly into the stomach until the pressure transducer, connected to the external end of the nonballoon third tube, detected the pressure change resulting from the filling of the stomach cavity with saline. This tube was then clamped, also.

At this point the experimental preparations consist of the immobile specimen sustained in a vertical posture by a channel bar extending from the wall mounting. The Blakemore tube has both balloons inflated and clamped to define the diaphragm and the third tube from the stomach attached to the pressure transducer. The three-headed Blakemore tube hangs from the specimen's mouth with two tubes clamped and one connected by hose to a pressure transducer being held in close proximity by a laboratory clamp-stand. An electrical connection extends from the transducer. Five small pins extend from the spinous processes of the cadaver and two multiple exposure cameras, one viewing laterally and one viewing from the specimen's back, are focused to record the pin movements. A point has been marked on the restraining box to define an "origin" for each plane and subsequent data reduction. The particular experimental sequence progresses from this point.

Procedure. The elapsed time spent in preparation was approximately five hours. Rigor mortis is a viable concern and must be considered when interpreting experimental results. After the integument is removed, the specimen was periodically bathed with normal saline solution to retard tissue dehydration. Preconditioning was not done due to extreme flexibility of the specimen.

One primate, dimensioned in Appendix C, was used in each experimental sequence: bending, which includes extension, flexion and side-bending and torsion.

To begin the bending sequence the specimen was released from the artificially vertical posture, sustained by the overhead support, and manually guided to seek equilibrium with a torso kinesiology conducive of the type of trunk movement (Figs. 4, 5, 6) to be forcably manifested by applying the static load. In this no-load hanging condition of static equilibrium, the nylon cord applying the load from the pulley system was looped around both extended lengths of the laterally drilled, large cross Steinmann pins in the skull and allowed to hang freely, awaiting the hook and load. Additionally, 0.9 percent saline was introduced into the abdomen, by opening a T-valve at the junction of the stomach tube of the Blakemore tube and the pressure transducer attachment point, until a reading was acquired. This value was recorded as the "no load" abdominal pressure and is used as a zero reference for subsequent abdominal pressure values reflecting load application. Two different procedures were exercised:

Experiment 1: Extension, Flexion, Side Bending. Loads from 0 to 2604 grams were applied so as to produce greater relative torso displacements in flexion, extension and side-bending. The abdominal pressure differential was recorded and the two-plane photographs exposed immediately after each new load increment was added. Care was taken to insure load application was deliberate, but not so fast as to necessitate an oscillatory damping to an equilibrium position.

Experiment 2: Rotation. The specimen was held stationary at the C-4, C-5 disarticulation level by the large cross Steinmann pins wire wound to the overhead channel bar. The pelvis was rotated from 0 to 150 degrees by moving the support stand top-plate. Abdominal pressure was recorded concurrent with achieving each 10 degree movement and two plane photographs also exposed at that time.

Each experiment was systematically reaccomplished after completing stages of a necropsy sequence described in the next paragraph.

Progressive Necropsy [7]:

a. Intact cadaver.

b. Pelt removed. A circumferential incision was made through the skin at the base of the skull and the pelt removed from the thoracic and abdominal torso to the pelvic rim and to the elbow joints of the upper limbs.

c. Limbs removed. The arms and shoulders were removed en bloc after litigation of the axillary artery and vein. The specimen included the clavical, pectoralis muscles, scapula serratus anterior and posterior, trapezius rhomboids (a ligament and two muscles), latissimus dorsi, shoulder and arm.

d. Musculature removed. The abdominal musculature was removed from the thorax to the pelvic brim, not including the psoas musculature.

e. Viscera removed. The major portion of the ribs, the heart, lungs and abdominal viscera were removed leaving the thoracolumbar spine and pelvis.

f. Spinal muscles removed. The paravertebral musculature, including the psoas muscles, were removed leaving the ligamentous, discal and asseous thoracolumbar spine.

Removed anatomical material was weighed and the values recorded (see Appendix C). Beginning pressure values were recorded as zero-load equilibrium for each sequence of the necropsy during the experiment. No additional saline needed to be injected, through the Blakemore tube, into the stomach as the pressure transducer sensed a readable abdominal pressure differential throughout the experiments.

After each sequence of the necropsy the cadaver was again restrained in a vertical posture to facilitate the surgical activity achieving the subsequent specimen condition by removing appropriate anatomical material. After maximum loading for each sequence, a zero-load pressure value was recorded to determine the leakage or plastic deformation of the stomach.

The abdominal pressure data was recorded in millivolts by instantaneous digital printout and continuous chart recording. This value was changed to millimeters of mercury (MM Hg) by comparison to the manometer calibration recording, then multiplied by conversion factor to pounds per square inch (psi) at 0°C. Pressure values are differential values above ambient.

Photographs taken of the side and back of the cadaver were printed to 8 by 10 inches. A rectilinear millimeter scale was embossed on a clear plastic overlay and placed on top of each multiply exposed photograph of a single sequence of loading for one step of the necropsy, with the marking on the restraining box, identified as the origin, aligned with the origin of the overlay. Values of the coordinates of the inserted point and exposed end of the small Steinmann pins protruding from the spinous processes were measured in millimeters in horizontal, "X", and vertical, "Y", directions (Fig. 11). The scale in the photograph and the millimeter overlay were compared with dividers and the derived conversion factor used to change all values to corrected actual millimeter readings. Angles are measured directly. The length of the bent torso was measured along the arc and compared to the before-bending length to determine an appropriate distance to the pins from the rim of the pelvis. The change in X and Y were considered legs of a right triangle and a change in length, the normalized displacement, calculated by the Pythagorean Theorem. A best fit radius was determined by inspection of the photographs and a theta angle measured from the horizontal to the C-4 pin insertion. The center was forced to be on the horizontal axis.

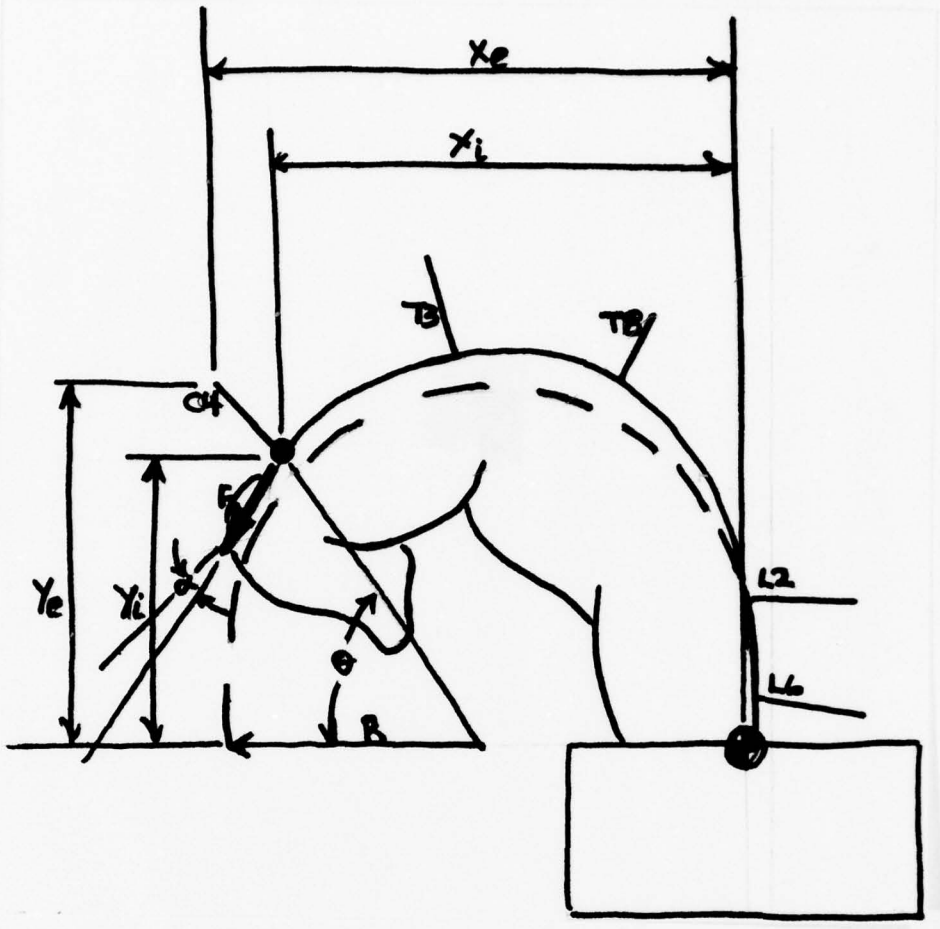

Figure 11. Coordinate and Angle Measurements

The angle Alpha (Fig. 11) to determine resolution of the total load to horizontal and vertical is measured directly for each load application, and total load geometrically resolved into vector components. Radial and tangential vector displacements are X, Y angular resolutions defined with respect to the best fit circular arc terminated at the load point. Data is graphically presented for directional displacements (X, Y, tangential and normal) versus applied loads (horizontal, vertical, radial and tangential). "+" α indicates F is directed outside the tangent to the arc.

Observations of the photographs were made to detect compound movement of the torso; i.e., a side-bending component associated with flexion.

The narrative of this investigation appears in the results.

Torsional data consists of abdominal pressure differential versus the angle of rotation of the pelvis, rigidly fixed to the support stand top plate.

EXPERIMENTAL RESULTS

Flexion. Beginning torso position is shown in Fig. 12. Application of an external load on the specimen produced an obvious arcing of the torso (Fig. 11) and an immediate pressure differential was recorded. The pressure changes observed for various values of load are presented in Figs. 13 and 21, with reduced data given in Appendix A. The load is given as horizontal and vertical components of the total load applied. The small geometric figures are actual observations joined, for convenience in visualizing the trends, by smooth curves. The code on each line denotes the stages of necropsy at which the data was taken corresponding to the progression outlined in the preceding experimental procedures section (i.e., a. intact cadaver, triangle; b. pelt removed, circle; c. limbs and shoulders removed, square; d. torso musculature, parallelogram; e. viscera including rib cage, inverted triangle; and f. spinal musculature removed, circle with dot). Dashed lines indicate the plotted load component is vertical, Y, while the solid graphics are horizontal, X, resolution, unless otherwise keyed differently by the legend.

The intact, sequence a, experimental loading evidenced an increasing pressure with increasing load until the abdominal musculature was removed, sequence d (Fig. 13). At 850 grams and 1350 grams for X-component, horizontal, and Y-component, vertical, the load pressure response becomes dramatically sensitive to the externally applied load for sequence a and b experiments. Pressure increases at a greater rate for unit of horizontal

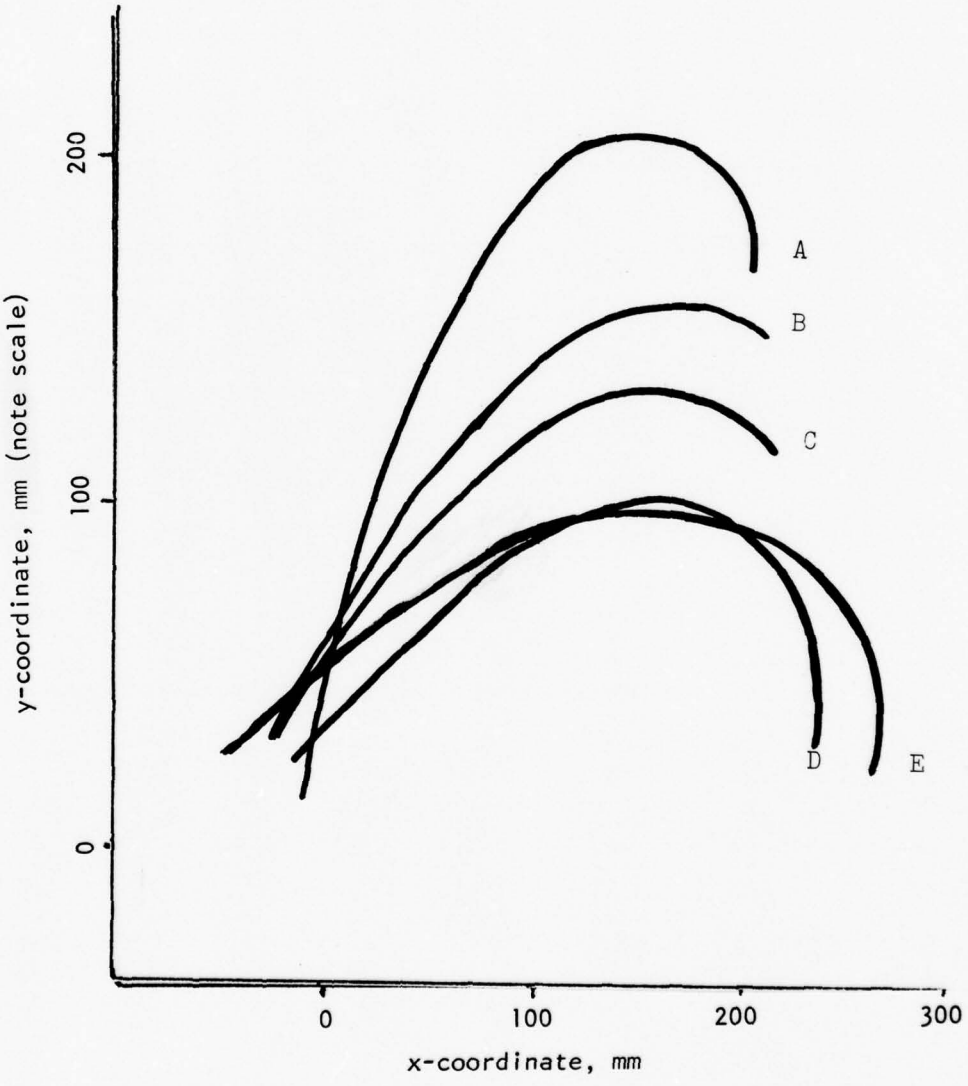

Figure 12. Spinal Displacement for Initial Position (Appendix A: X_i and Y_i for Step 1)

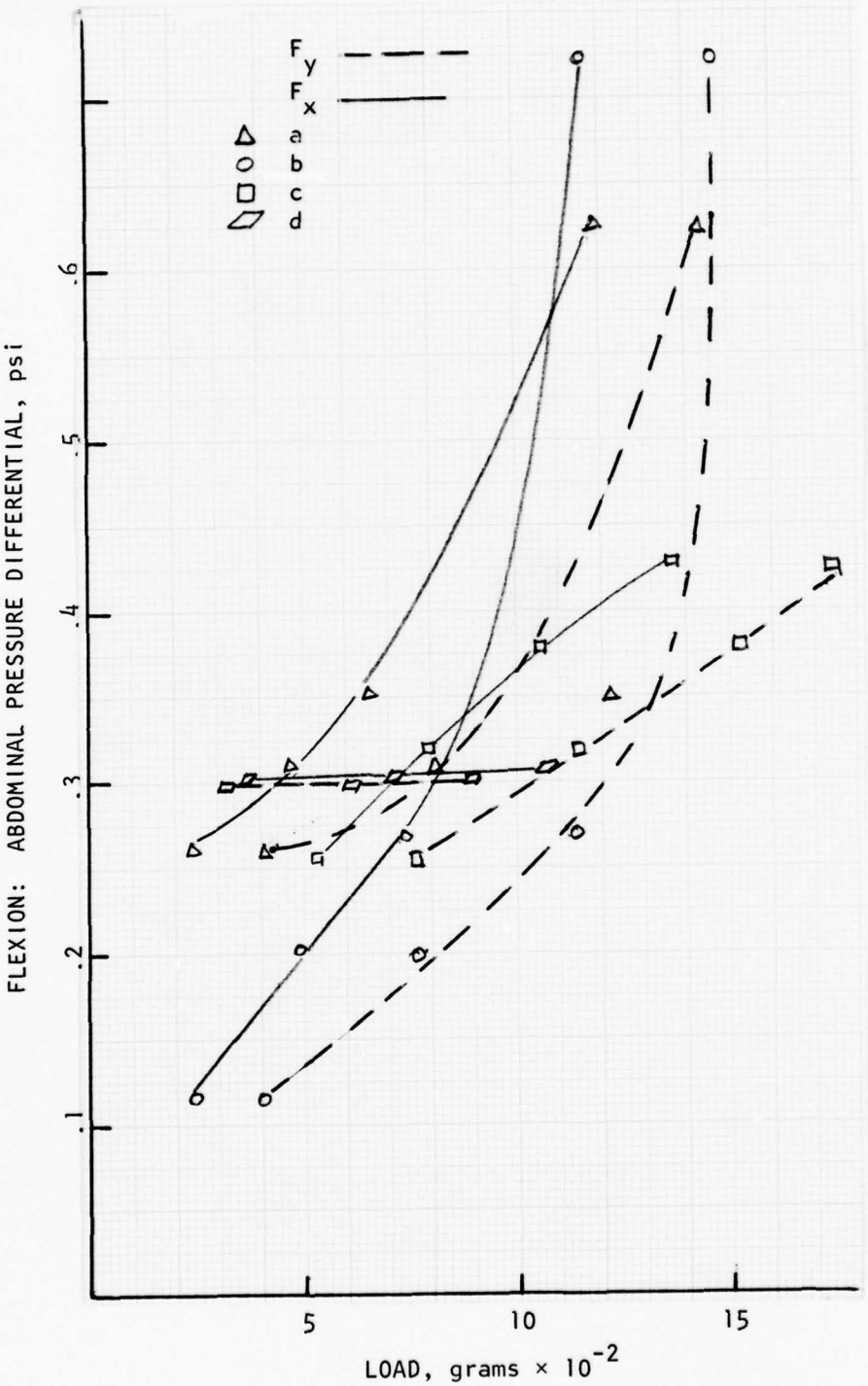

Figure 13. Abdominal Pressure vs. x and y Component Load: Flexion

load, than for vertical component, throughout the experiment, as is visualized by the generally greater slope of the horizontal load data in Fig. 13. For the same initial load recorded pressure is greater for the intact specimen than for sequence b. The rate of increase per unit of applied load is less for sequence a, than b, as is the final pressure for maximum applied total weight.

Sequence d was accomplished with no recorded differential pressure change, although the initial value is greater than the previous experimental sequence, c. Except for sequence a, all experiments evidence increasing pressure for the same value of applied load and a decreasing pressure load response as the necropsy progresses (b to c to d).

The displacement at several spinal stations (C-4, T-3, T-8, L-2), resulting from the load application is given in Figs. 14-17. In each case, the total displacement is plotted versus the x-component and y-component of total force. Each displacement has been normalized by division by the length from the rim of the pelvis to the spinal station observed. The data points are denoted by geometric figures joined by smooth lines which are coded to denote the stage of necropsy and load component; as described on page . The unreduced data is given in tables of Appendix A.

The fourth cervical vertebrae (C-4) experiences a decreasing value of normalized displacement for the same external load as the necropsy progresses, Fig. 14. Trunk musculature is still present in sequences a, b and c, which evidence a greater elastic response to loading. The greatest strain is experienced by the intact specimen. Without torso musculature and viscera (sequences d and e), there is a propensity to a constant strain value.

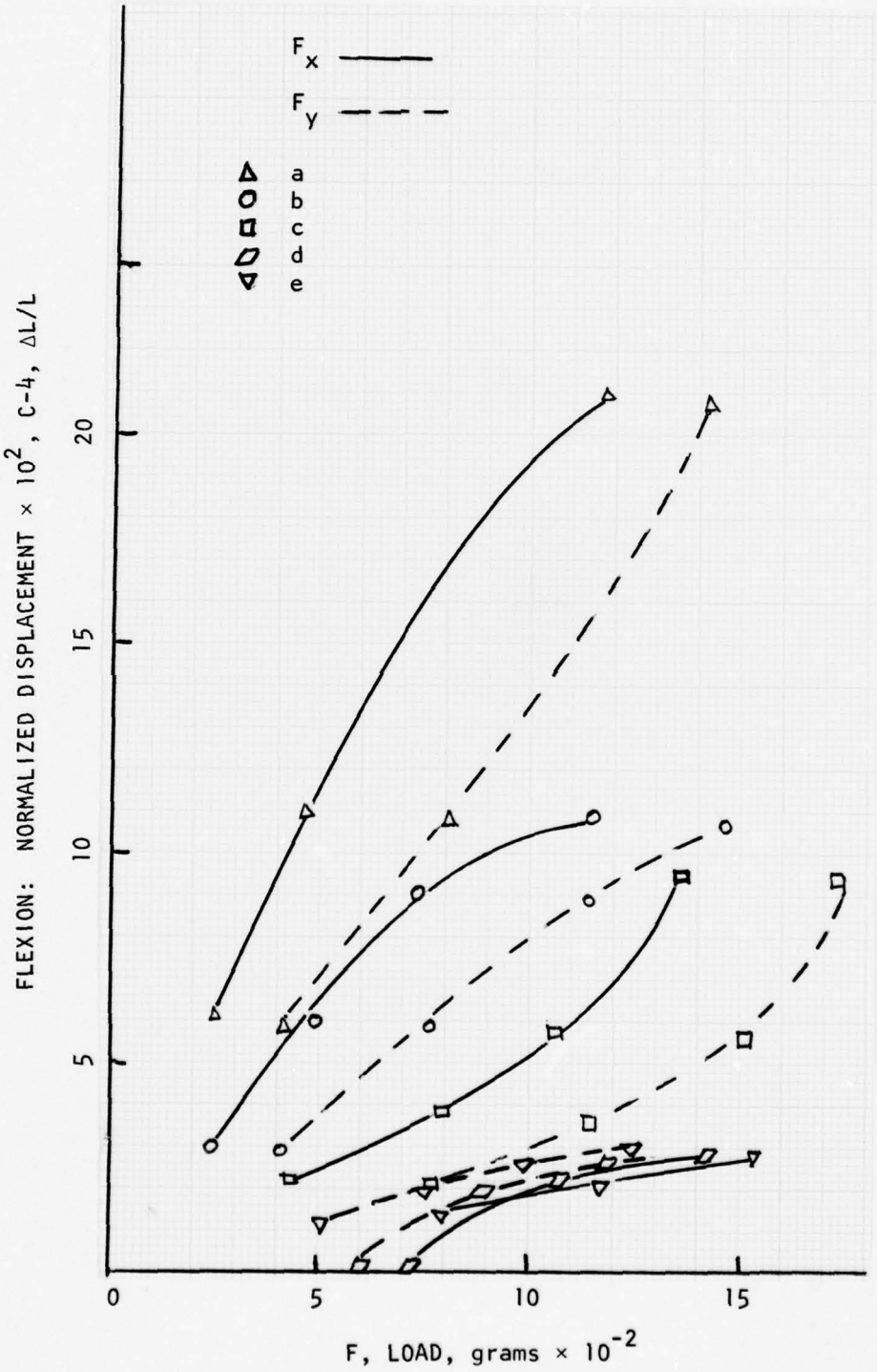

Figure 14. Normalized Displacement vs. Load, C-4: Flexion

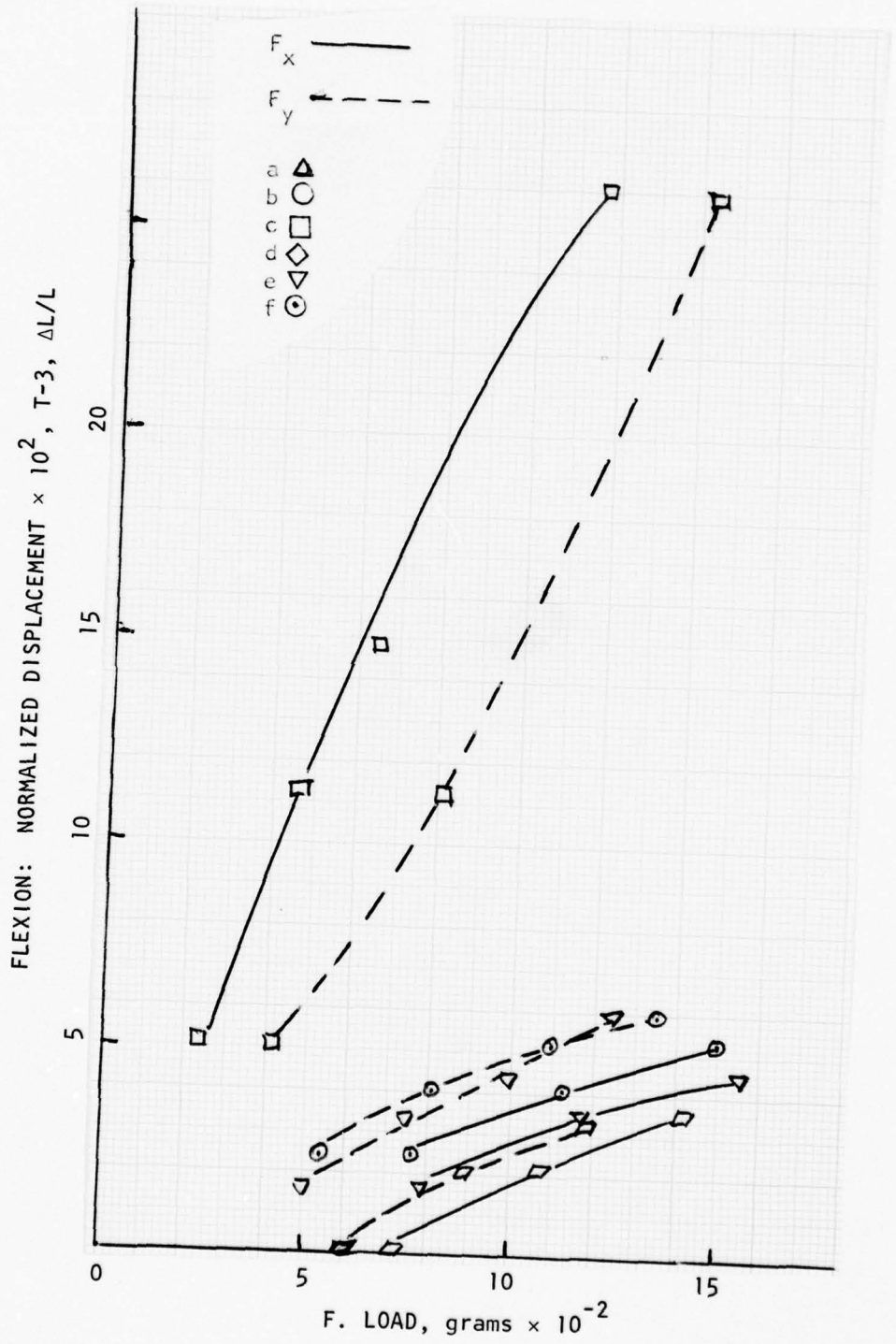

Figure 15. Normalized Displacement vs. Load, T-3: Flexion

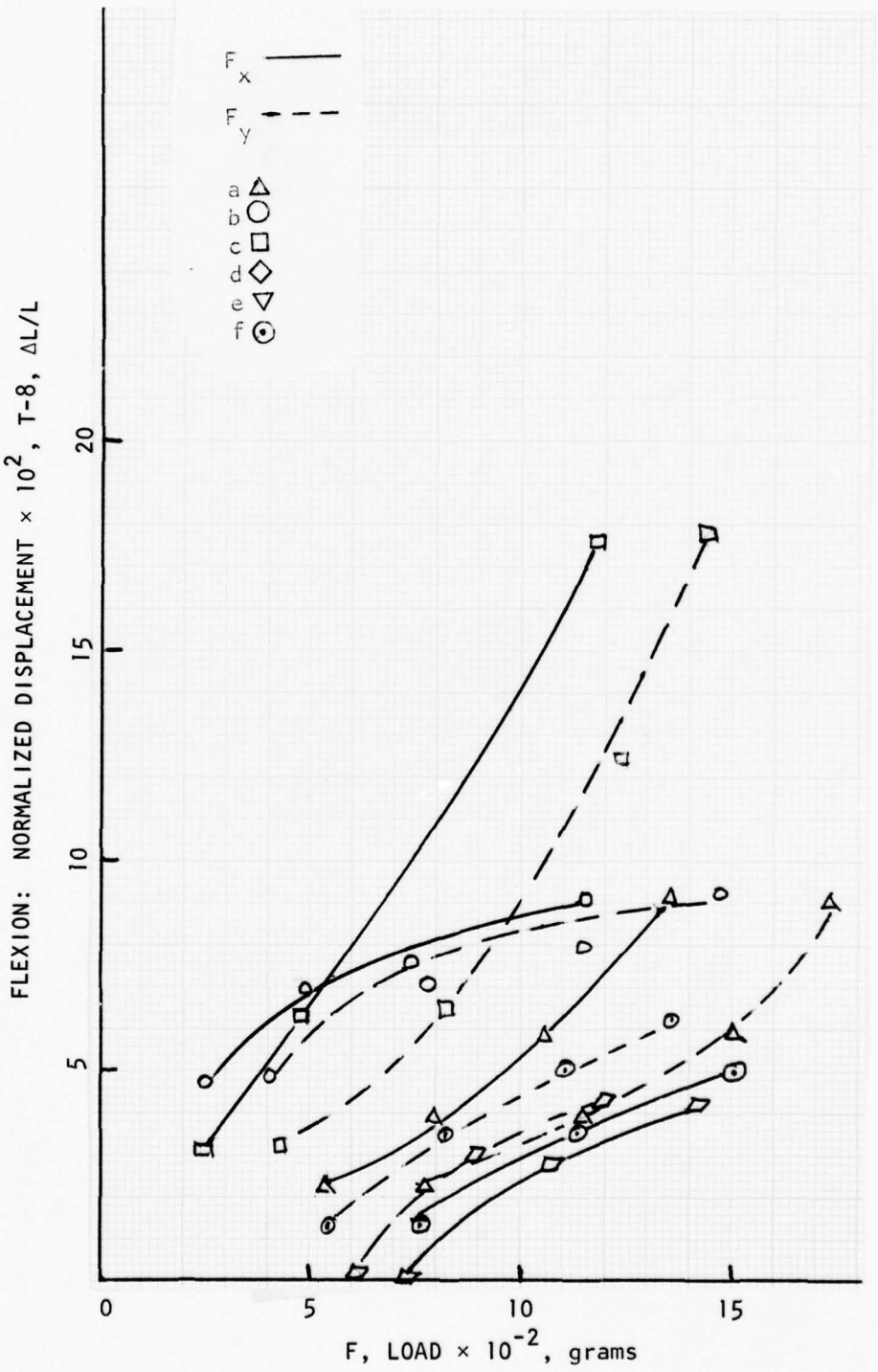

Figure 16. Normalized Displacement vs. Load, T-8: Flexion

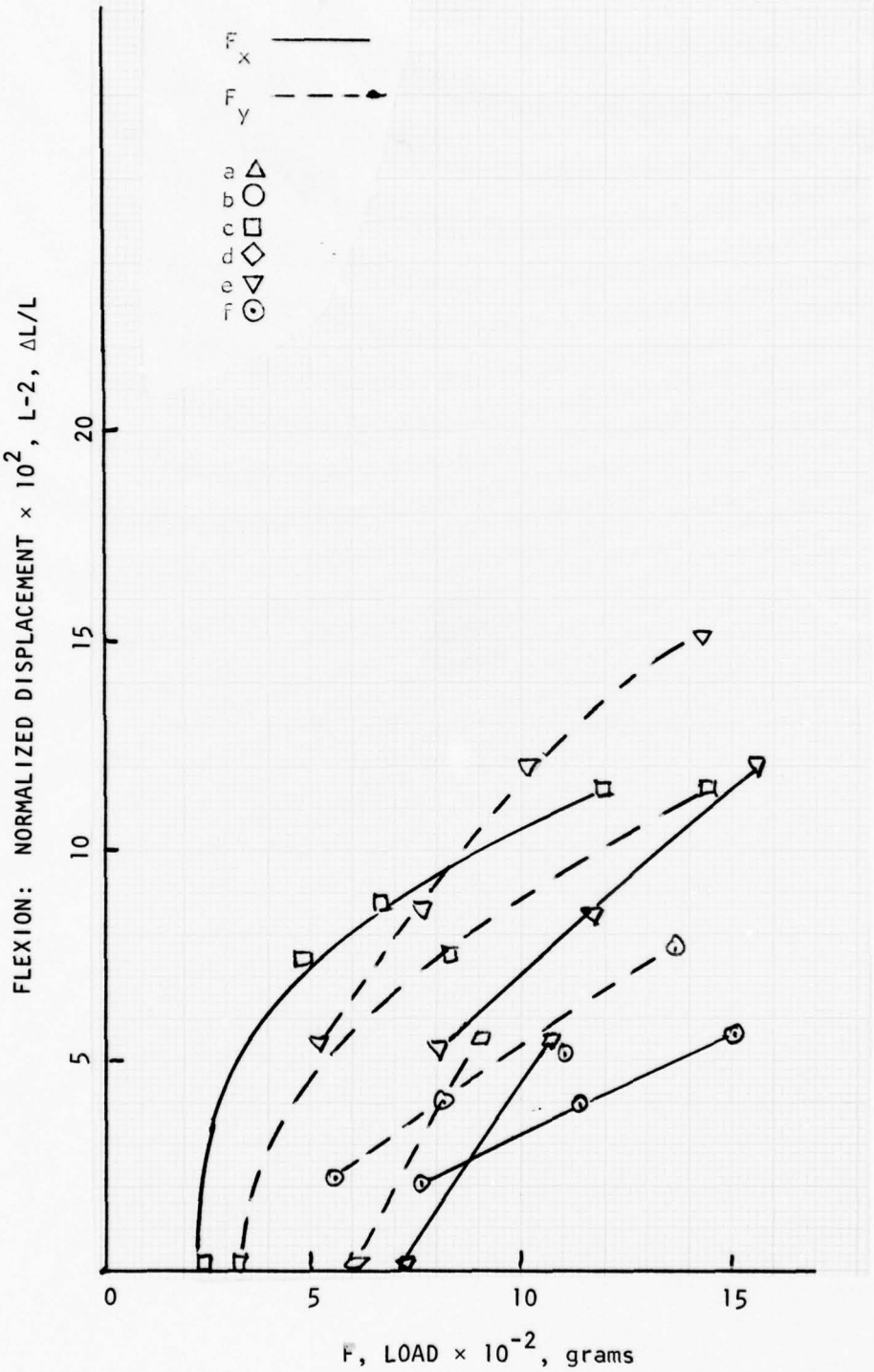

Figure 17. Normalized Displacement vs. Load, L-2: Flexion

T-3, the third thoracic vertebrae (Fig. 15), experiences a dramatic convergence to a constant stiffness subsequent to the intact sequence a experimental loading. A greater value of strain is measured for identical loads as the necropsy progresses (d, e to f). This was not substantiated by the data measured from C-4.

Figure 16 displays the response of the eighth thoracic vertebrae, T-8, to loading. As in the case of C-4 and T-3, there is a convergence to the stiffness measured at the final sequence of the necropsy. Sequence c shows increasing stiffness with increased loading, approaching the stiffness of the intact specimen. Sequence b vividly displays an opposing transition of response to loading as the graph parallels sequence a (intact animal) for loads less than 500 grams, with the response being more characteristic of the latter stages of the necropsy for loads greater than 800 grams.

The lower lumbar spine, L-2, evidences (Fig. 17) a diverse response to applied external load with questionable correlation of the data. There is no tendency to a constant stiffness rate as the experiments progress. The sequence a L-2 load response does become stiffer with increasing load.

Vertebral rotation (Fig. 18), the summation of which composes the flextural bending, generally decreases as the portion along the torso decreases; i.e., the lower thoracic and lumbar vertebrae rotate less than those of the cervical region. The greatest rotation is measured from the intact specimen. T-3 evidences the widest range of movement for an applied load as the necropsy progressed. T-8 responds with the same deformation to load for sequence a and b. T-3 and T-4 approach a limit of vertebral rotation around a lateral axis as the maximum load is reached for sequence a. The same phenomenon appears as the T-8 response

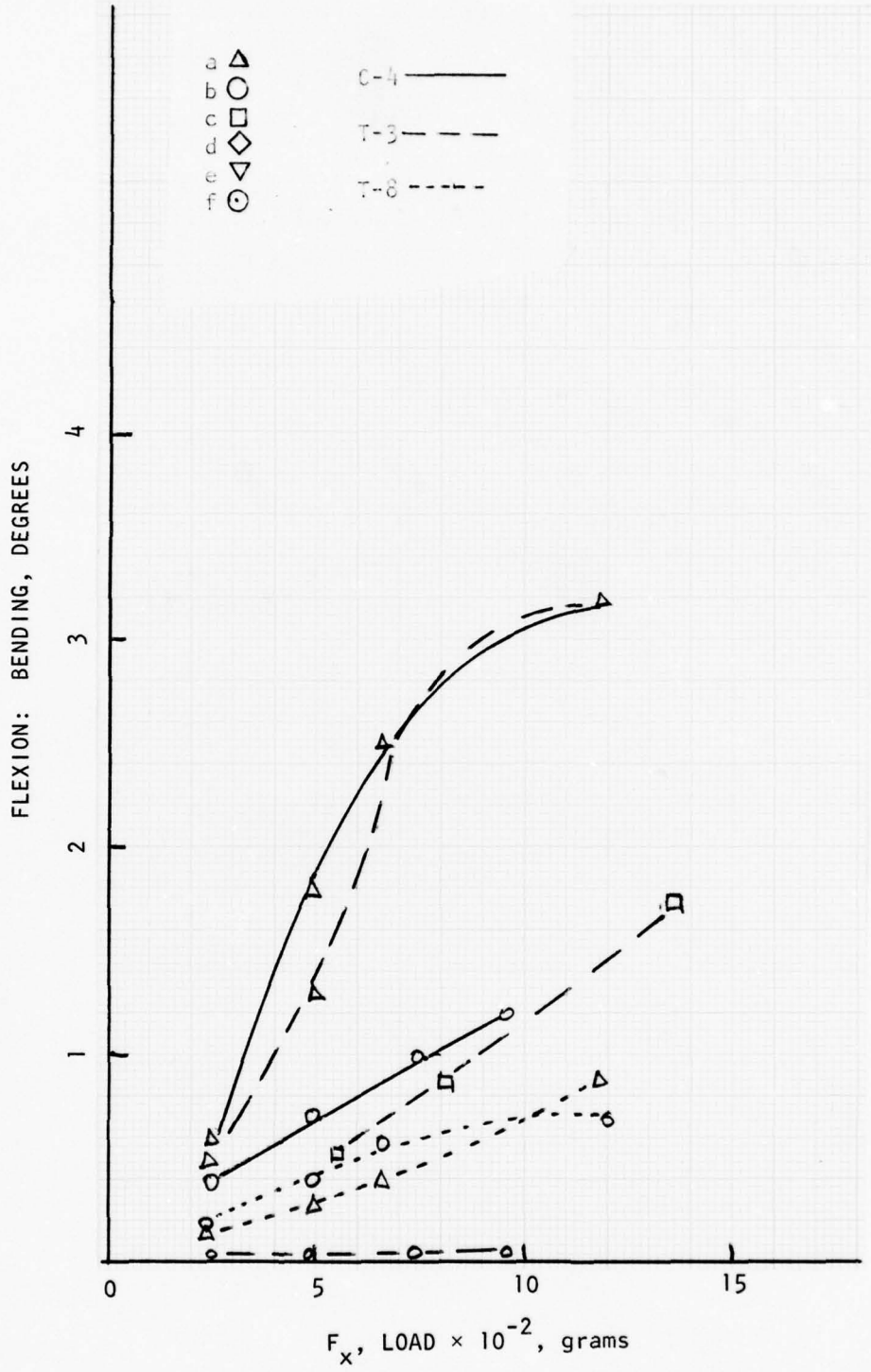

Figure 18. Bending in Spinal Plane vs. Load, C-4, T-3, T-8: Flexion

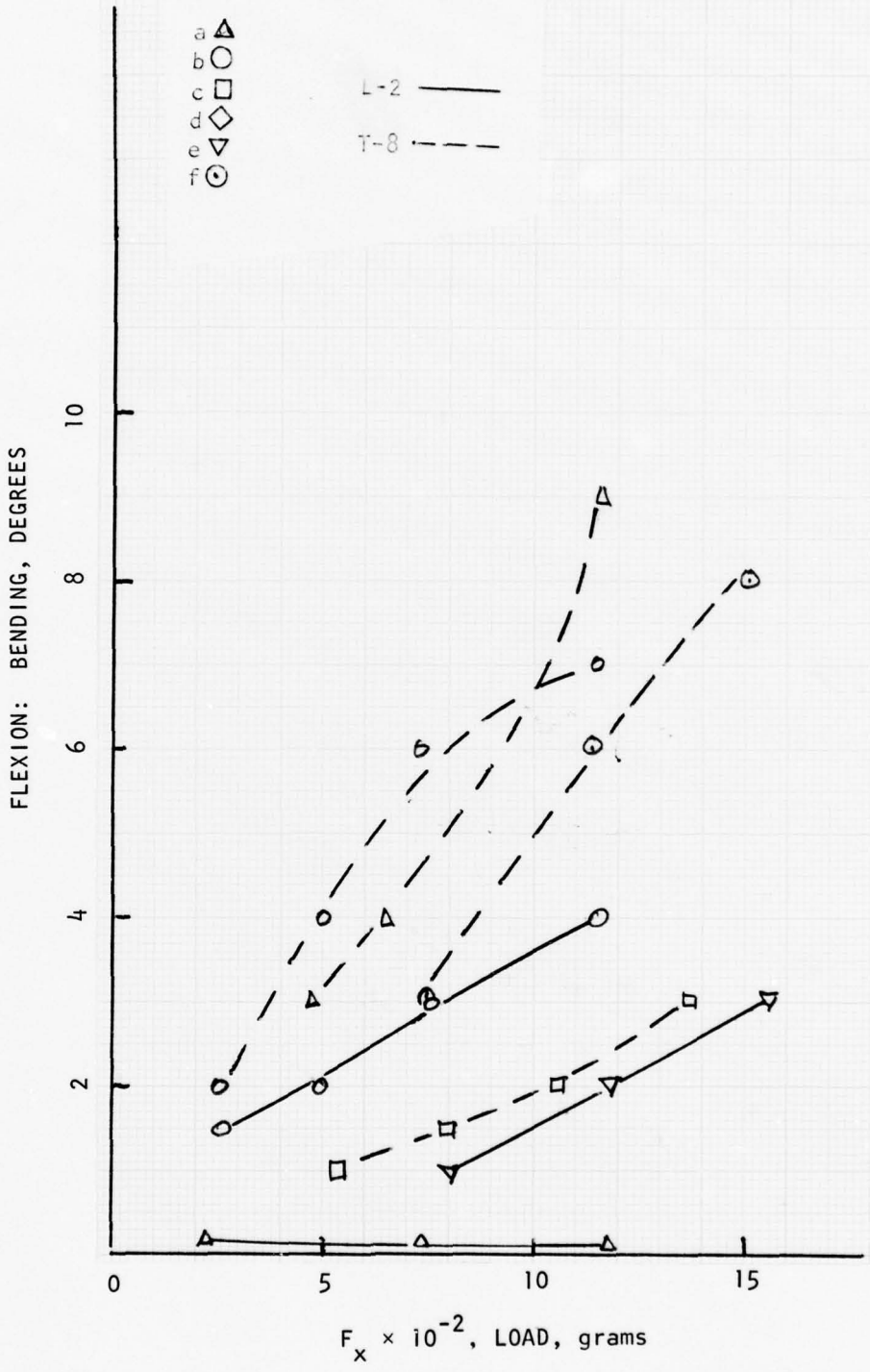

Figure 19. Spinal Plane Bending vs. Load, L-2, T-8: Flexion

to maximum loading under sequence b conditions approaches a constant value of degrees. Sequence b and e (Fig. 19) elicit the same slope of bending versus applied load from L-2. The response is almost linear and of constant rate. Excepting sequence c, T-8 responds with the same rate of change for each examined sequence. Sequence b loading appears to move T-8 to a bending limit near 1200 grams. The lower lumbar (L-2) remained stationary during experimental loading of the intact cadaver.

Figure 20 shows convergence of normalized displacement data to .27 psi abdominal pressure differential at values less than .08 for the intact animal. Each vertebrae reaches a stiffness which causes the pressure response to become much more sensitive to displacement. The value of this occurrence is a larger normalized displacement as the investigated point examined is a longer distance from the rim of the pelvis along the axial spine.

Extension. Pressure versus applied load data for the extended specimen, Fig. 21, a generally constant slope for the entire experiment with the exception of sequence d which shows no measurable pressure differential response to external load components less than 1100 grams but rapidly converges to the gross constant slope of .0027 psi per gram with continued loading beyond that value. Sequence c response is initially more sensitive but converges to the relative linearity of the other experimental data.

Figure 22 shows the T-8 plot of normalized displacement versus component of applied load approaching a constant value slope between .005 and .012 for sequences c and e. The intact animal, sequence a, exhibits a linear deformation with loading.

The L-2 vertebrae (Fig. 23) increases in the stiffness of response to loading as the experimental sequences are accomplished. Sequence e

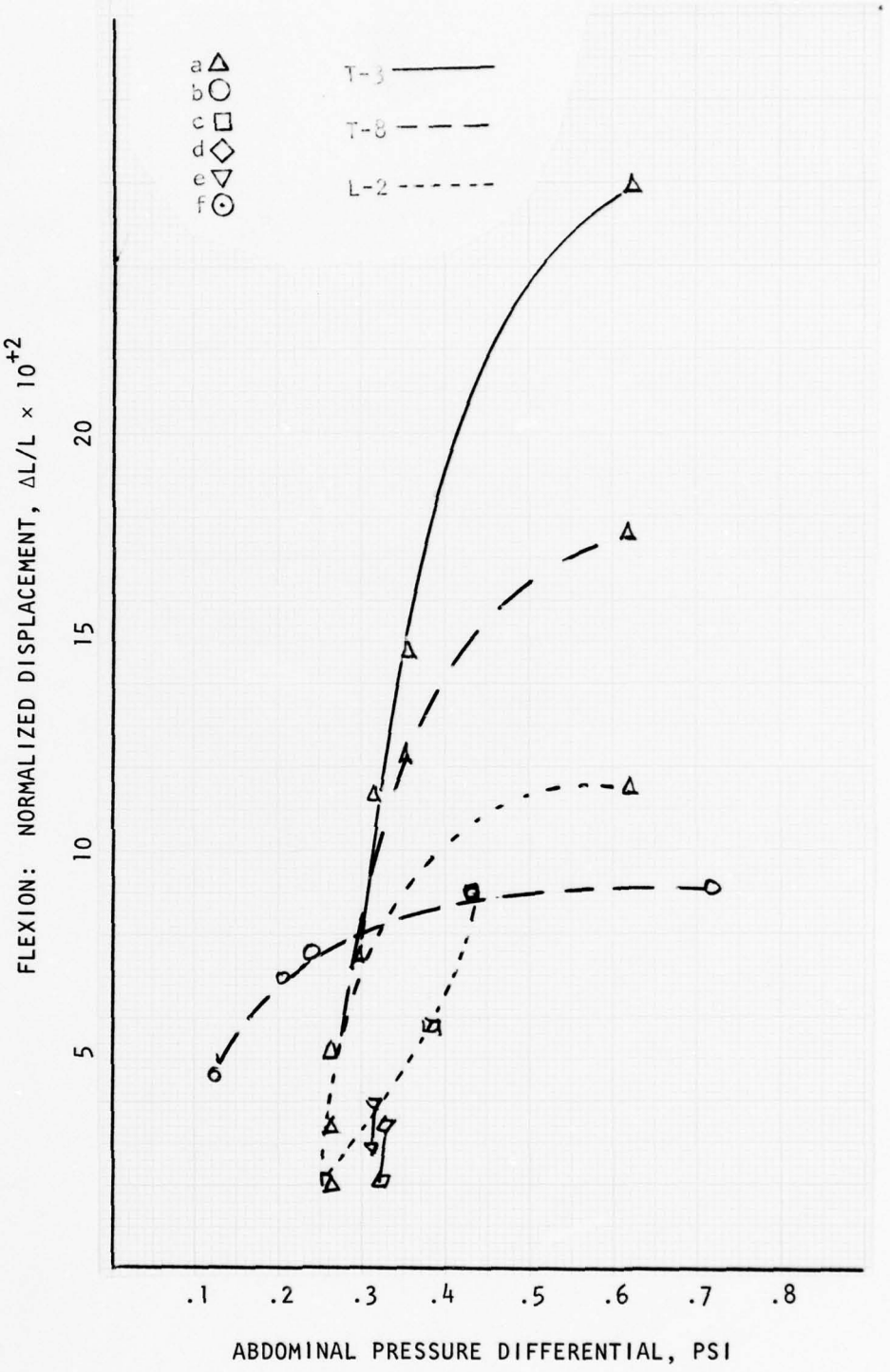

Figure 20. Normalized Displacement vs. Abdominal Pressure, T-3, T-8, L-2: Flexion

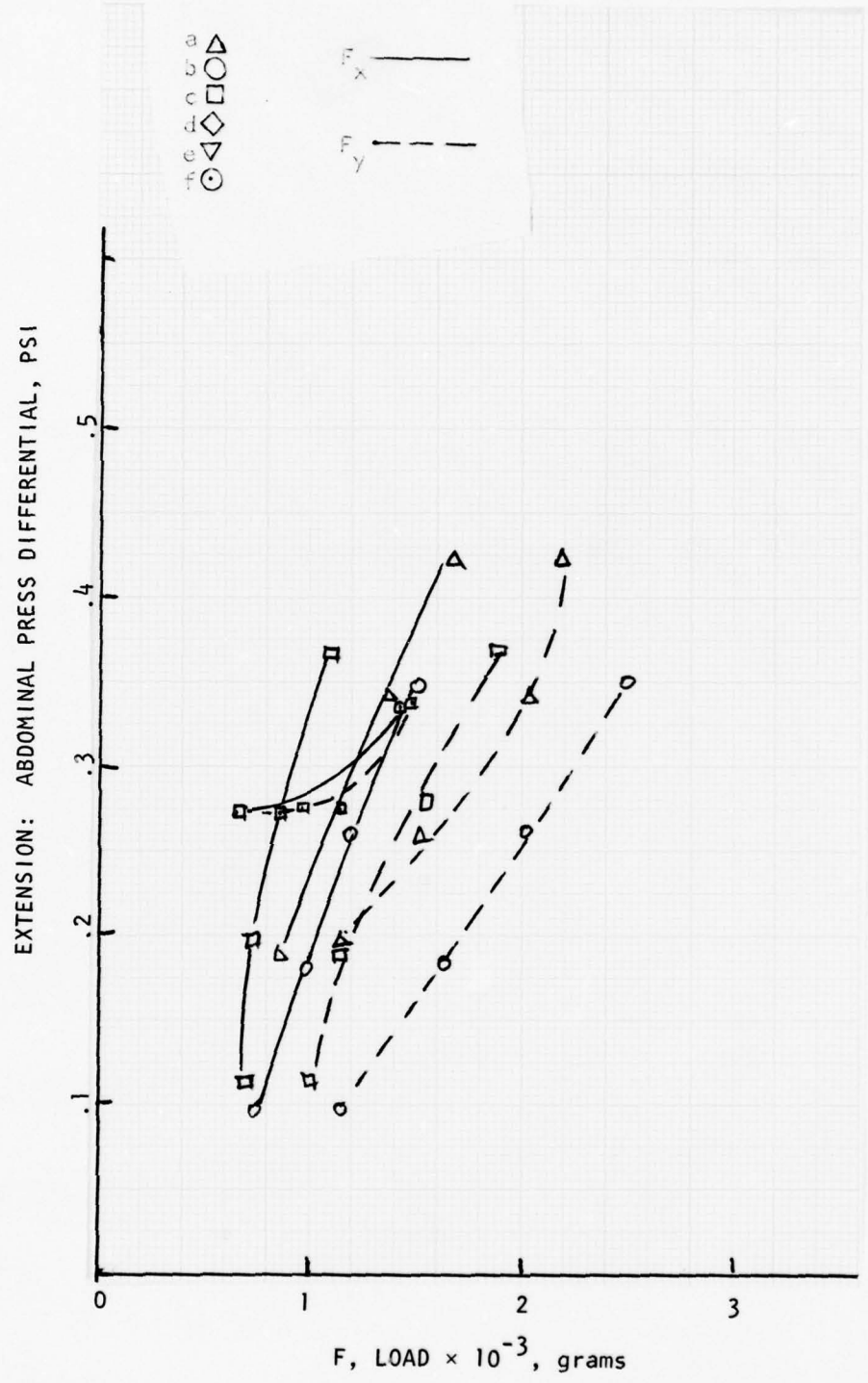

Figure 21. Abdominal Pressure vs. Load: Extension

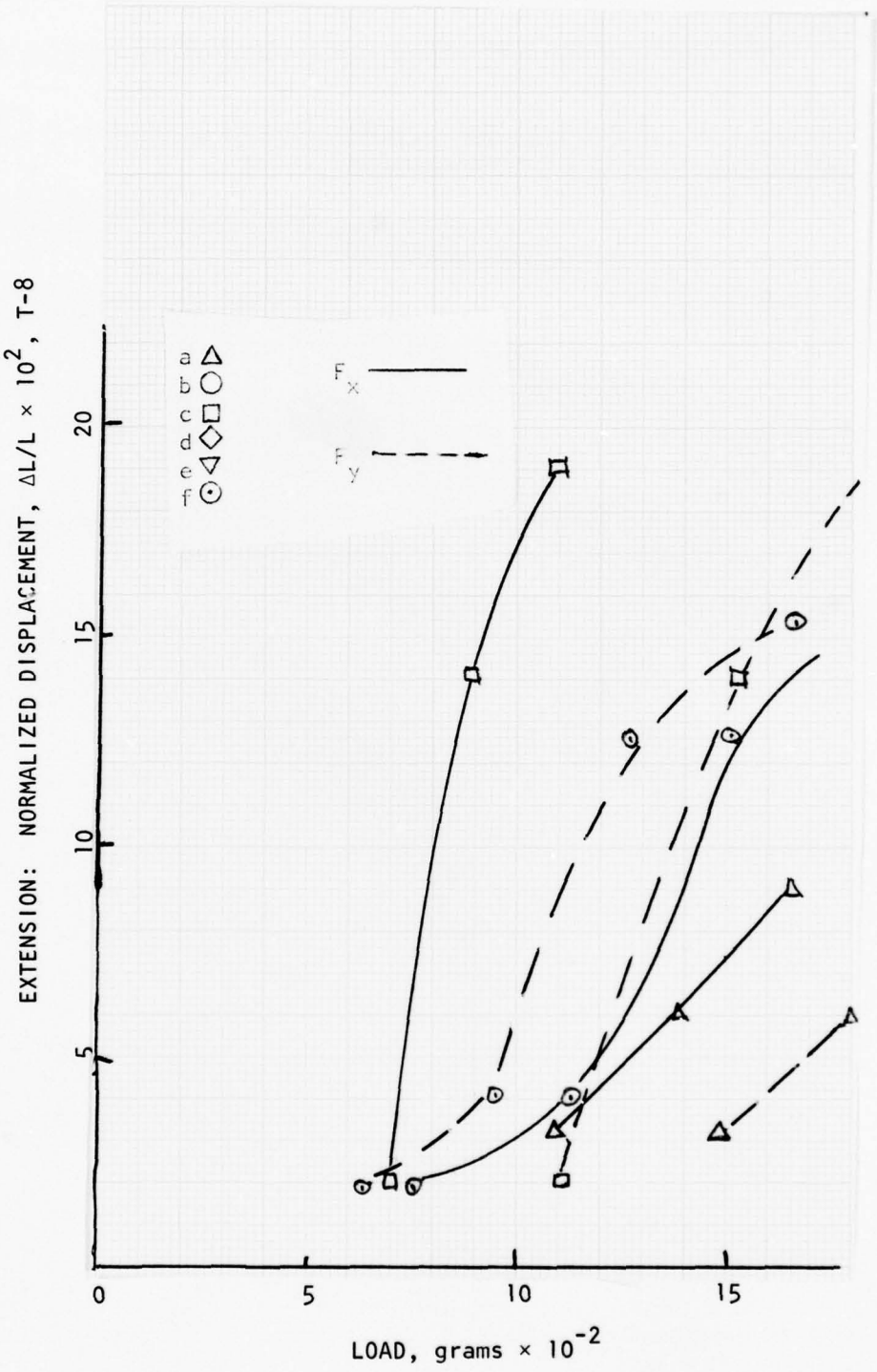

Figure 22. Normalized Displacement vs. Load, T-8: Extension

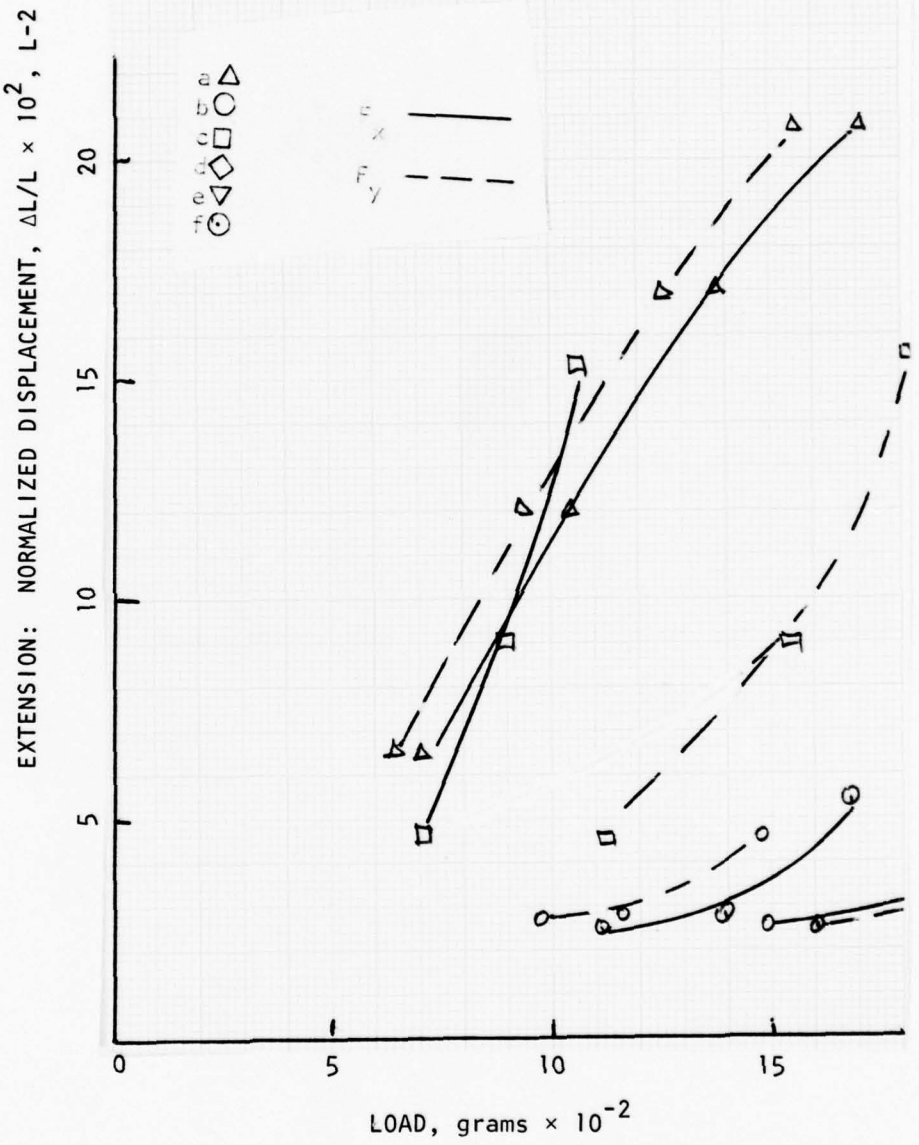

Figure 23. Normalized Displacement vs. Load, L-2: Extension

stiffness is in marked contrast with the greater incremental deformation of the intact animal and sequence c results.

Rotation of C-4 and T-3 (Fig. 24) about a lateral axis is significant but difficult to measure, because the Steinmann pins become impressed in the torso and are not visible on the photographs. Rotation of L-2 increases as the necropsy progresses and an increased flexibility as well as greater gross deformation values for the same external load are recorded. T-8 responds in a similar manner.

Sequence c (Fig. 25) recordings provide generally common slopes for T-3, T-8 and L-2 spinal level, abdominal pressure response to normalized deformation. The progression from sequence a to c has the effect of decreasing the absolute values of abdominal pressure differential for the same normalized strain value at T-8 and L-2. The rate of the response is not dramatically different and maximum pressure differentials recorded about the same. There is no deformation versus abdominal pressure differential correlation apparent from the L-2 vertebral level data.

Normalized displacement decreases as weight is removed (Fig. 26). The C-4 data shows a stronger relationship of displacement to percent of weight removed for all progressive necropsy actions. The T-8 vertebrae experiences a more constant deformation - weight relationship, especially for sequences subsequent to the intact animal segment.

Side-Bending. The resulting data is of questionable usefulness. Photographic extraction of deformation was practically impossible due to confusion of defining the multiply exposed spinal pins in the lower spine, from those in a more cranial location on the lateral photograph, and defining the pin inserts from the overlapped imposed angular length of the pin, viewing the side-bent animal from the back. The torso propensity

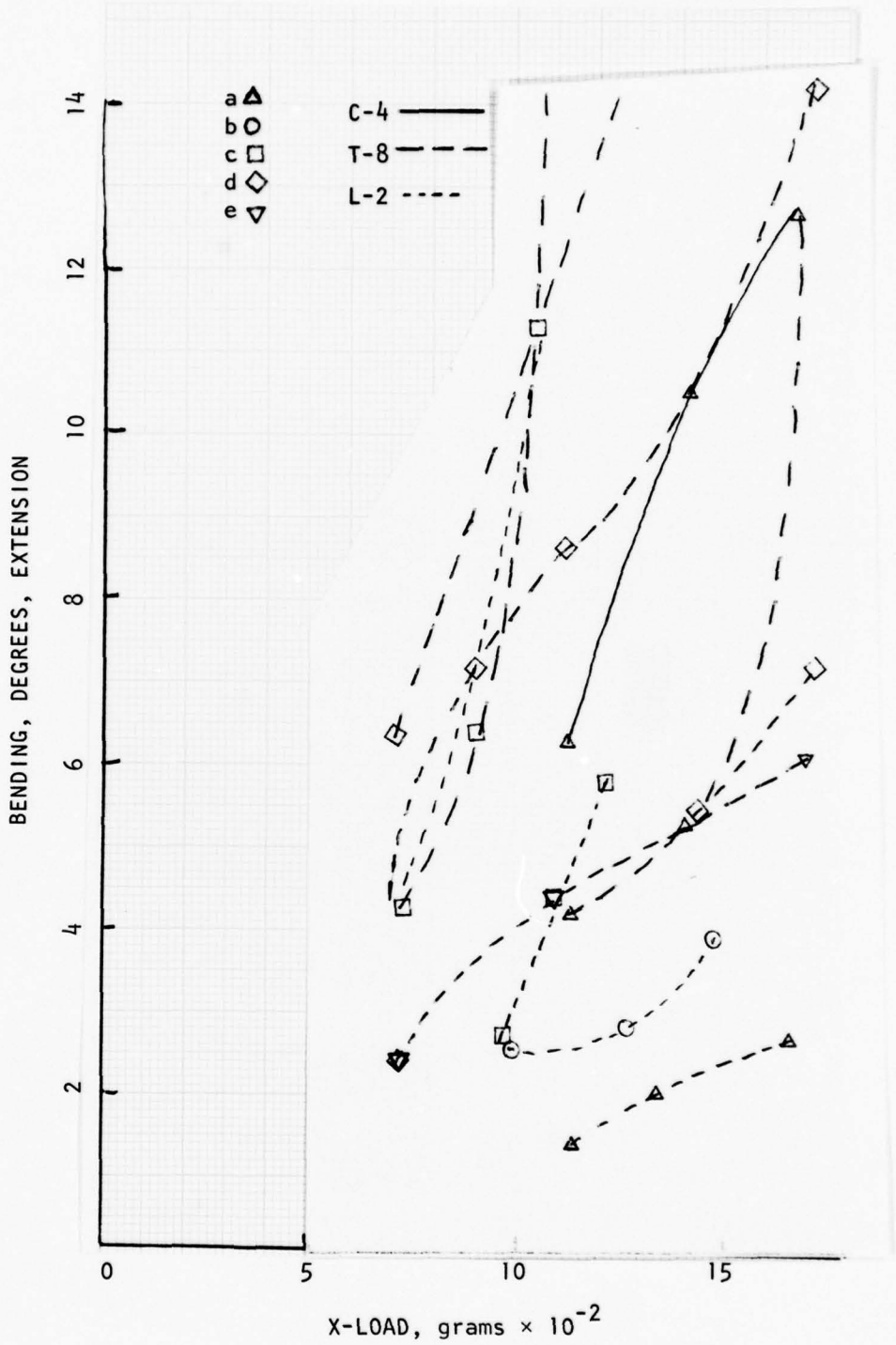

Figure 24. Bending in Spinal Plane vs. X-Component of Load, C-4, T-8, L-2: Extension

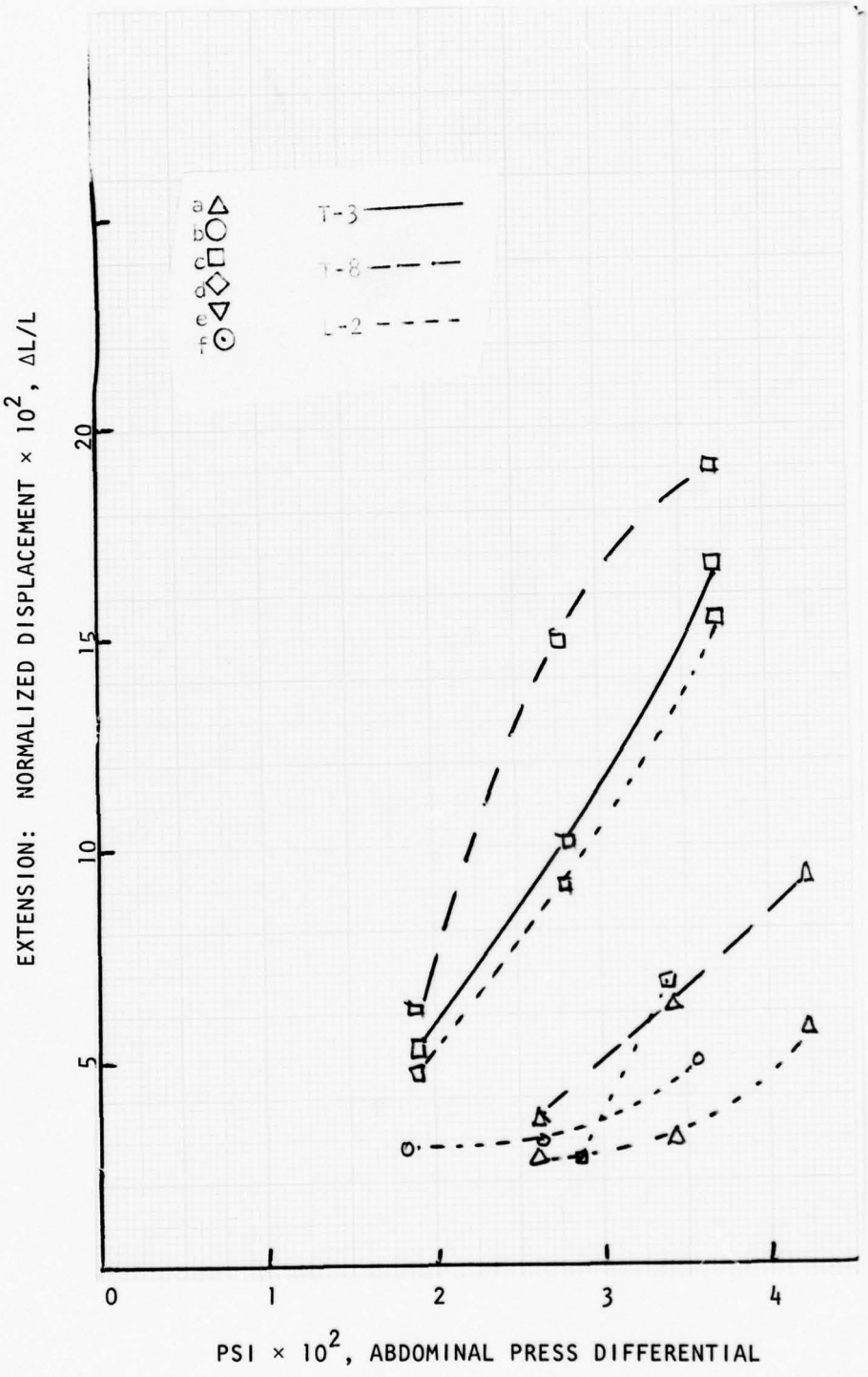

Figure 25. Normalized Displacement vs. Abdominal Pressure, T-3, T-8, L-2: Extension

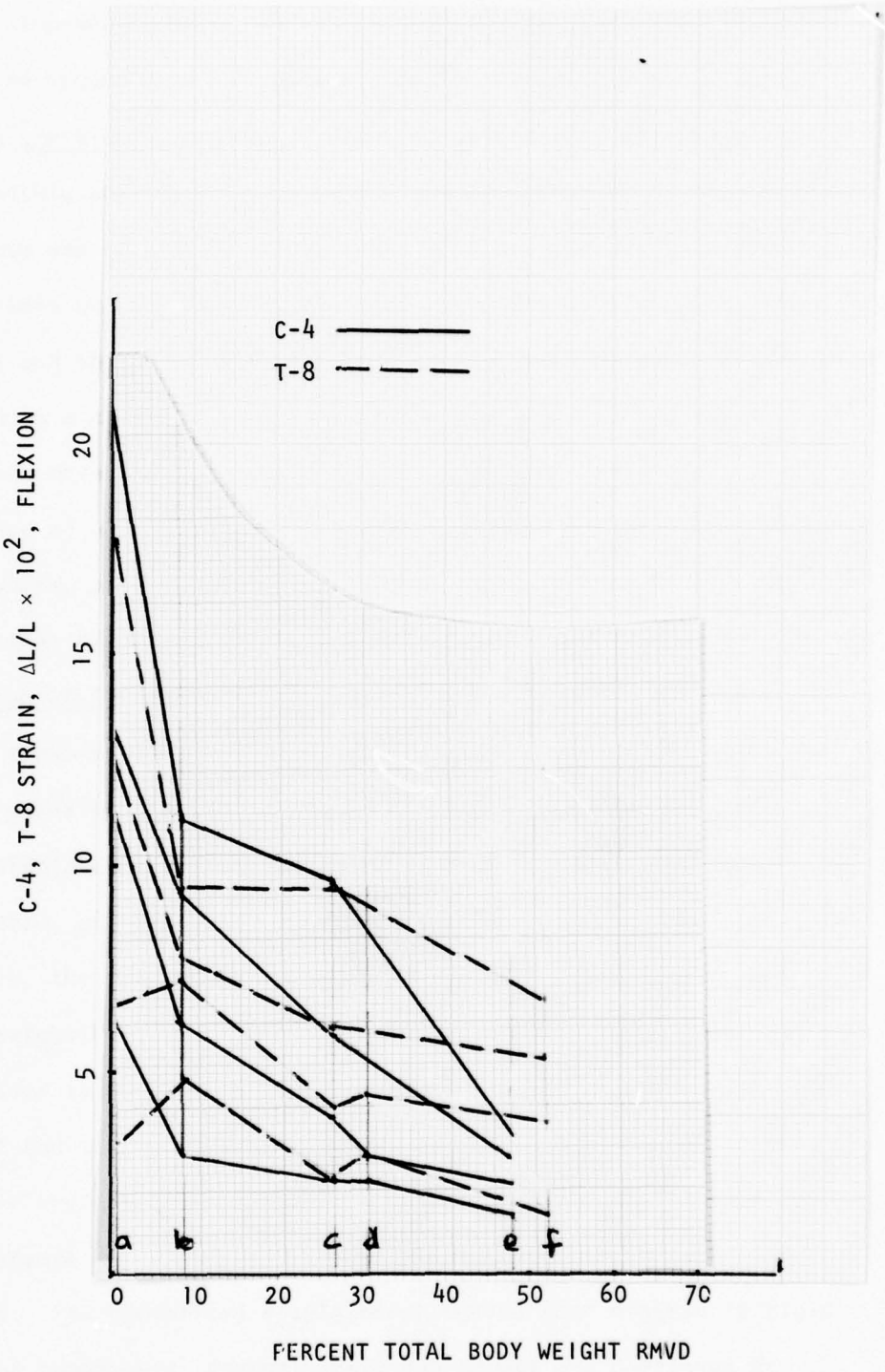

Figure 26. Normalized Displacement vs. Percent Weight Removed, C-4, T-8: Flexion

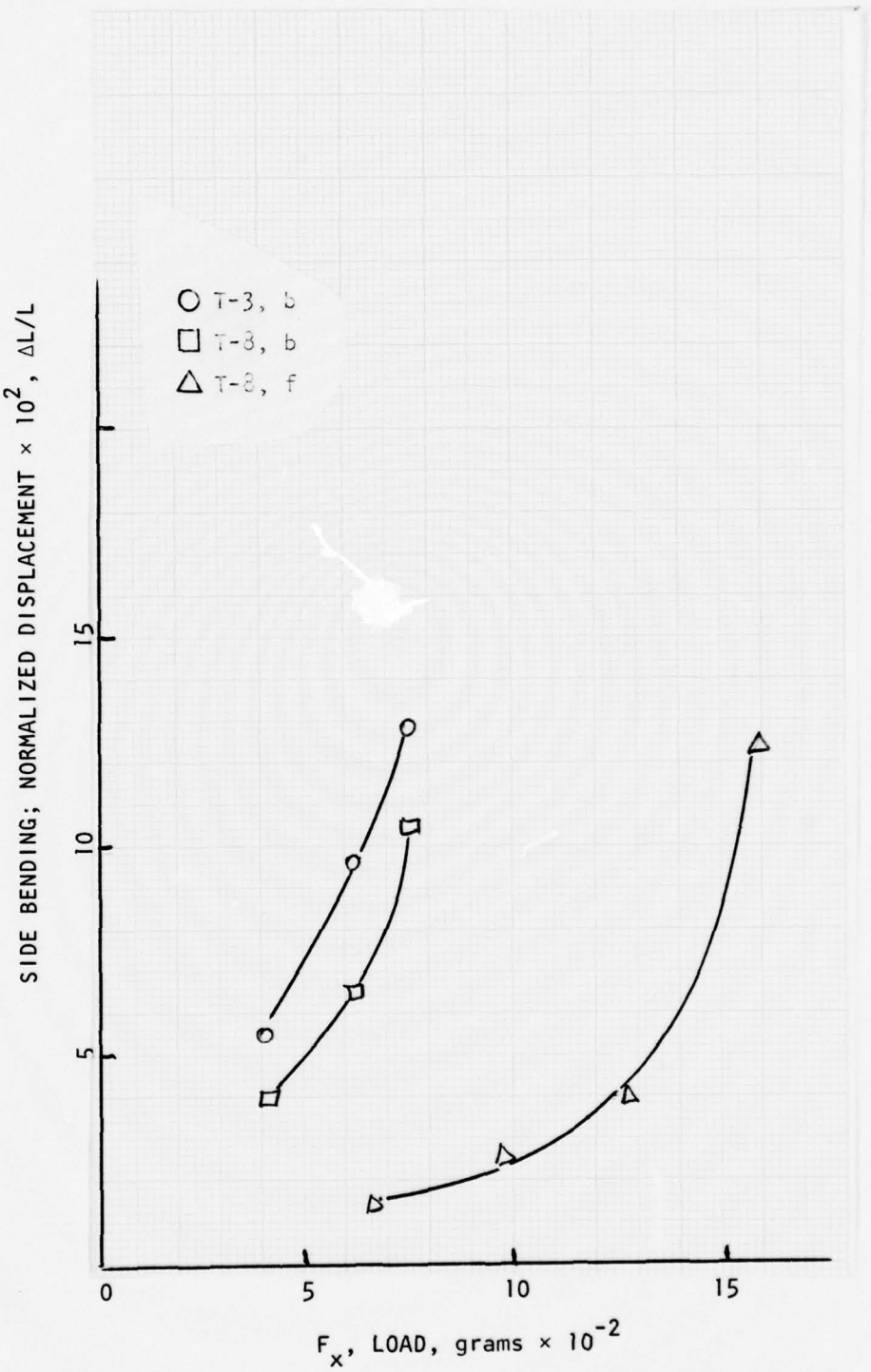

Figure 27. Normalized Displacement vs. Load, T-3, T-8: Side-Bending

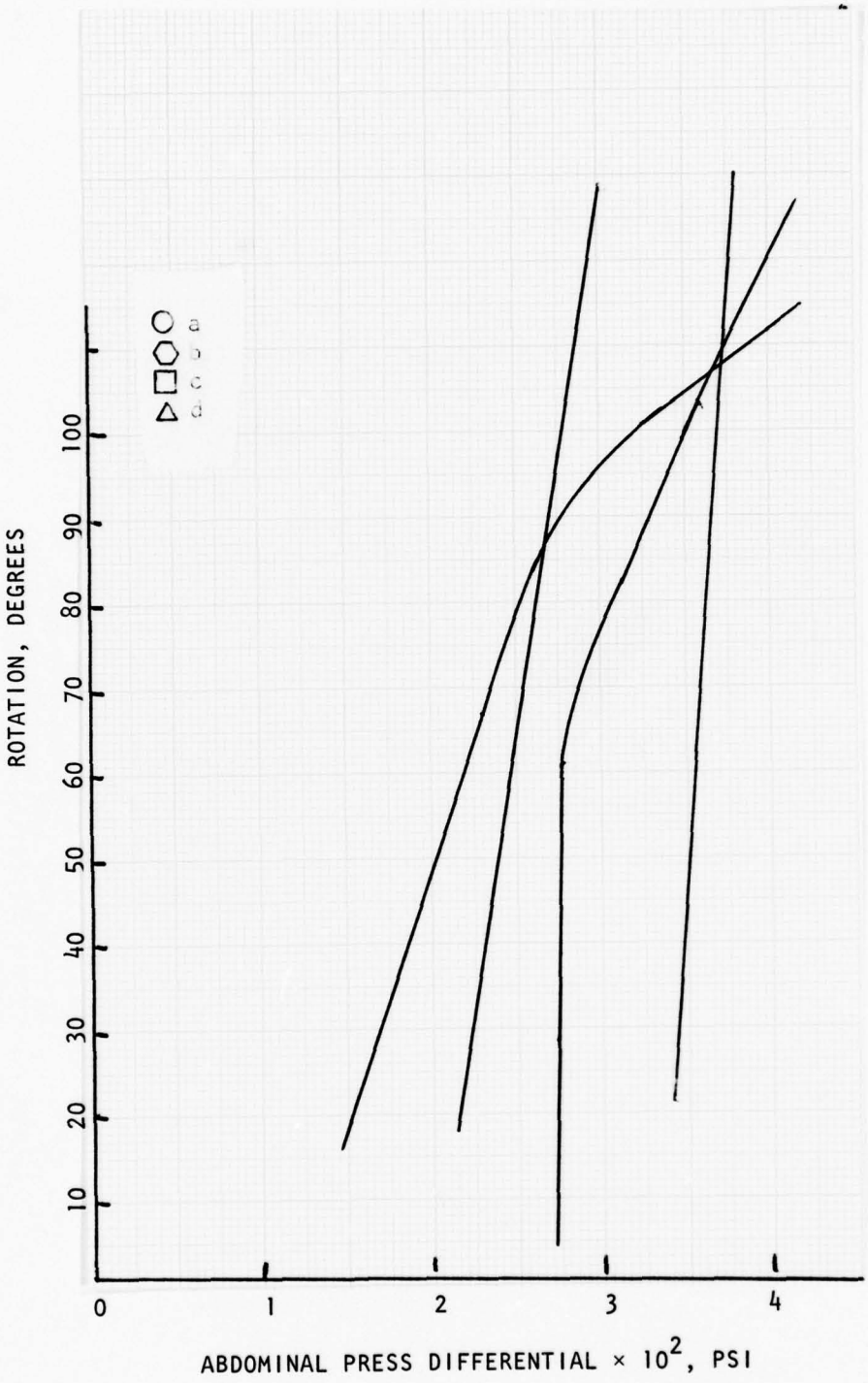

Figure 28. Abdominal Pressure vs. Degrees Rotation of Pelvis

restraining box, with epoxy resin to the brim of the pelvis as a means of securing the cadaver, it is plausible that the initially less rigid stiffness data observed at the L-2 vertebrae (Fig. 17) reflect the flexible properties of the restrained integument and that the structural response of the spine and other substructures are only obvious at larger loadings (subsequent to the pelt failing in a tensile loading environment created by the arched trunk). The intact animal exhibits a similar stiffness at each vertebral level (Figs. 14, 15, 16). The thoracic spine, T-8, exhibits a resistance to displacement, when subjected to small vertical load components, which is also mechanically characteristic of the trunk devoid of substructure and viscera (Fig. 16). The lumbar spine is most rigid when experiencing applied load components of relatively medium magnitude, for this experiment (Fig. 17). Abdominal cavity pressure differential, for the intact primate sequence, increases at a greater rate when graphically compared to horizontal load component than is evidenced when plotted versus vertical load component (Fig. 13), indicating greater abdominal cavity incremental volume change from bending than compression. Beyond the point of application of the 600 gram total external load, a review of Appendix A flextural compilation indicates the torso has been deformed approximately 70 degrees from vertical. Slight pressure differential increases with large increases in total applied external load can be attributed to the overriding support and distribution of the load through the musculature of the upper torso and the protective capacity of the ribs and sternum. At this point of the sequence the cadaver does contact the epoxy support at the chest. The load pressure relationship increases at about the same rate (Fig. 13), without evidencing a decreasing stiffness with higher applied loads, after the pelt and

gross shoulder musculature are removed. Upper thoracic musculature of the trunk and scapula most probably assumes a resistive role, opposing the flextural motion of the torso and at the same time relieving the abdominal and thoracic cavities of accepting a greater portion of the load from bending the specimen.

With the pelt removed a marked stiffening is observed. The thoracic region, T-3 and T-8 spinal pins, immediately exhibit (Figs. 15, 16) the very stiff mechanical properties of the vertebral column with only isolated variance from a general response slope of 2.2×10^{-5} MM/MM/gram. The C-4 cervical location evidences a more gradual stiffening transition with progressive necroptic component removal, indicating a greater mechanical flexibility of the regional substructures. The pelt was 7.7 percent of the total weight. There is a greater observed contribution to torso stability from the integument than the percentage of total body weight contained in the pelt or intuitive conceptions of component participation would predict. The "locked" mounting of the specimen at the rim of the pelvis provides an anchoring capability to the integument by effectively pinning it at the level of epoxy containment - a mechanical phenomenon not physiologically present in nonclinical torso environment where large deformations are easily performed with no resistance from the membraneous integument.

Removing the arms en bloc, with the major supportive musculature and scapula, increases the evidenced stiffness at all levels of the trunk. This removed material was a substantial 16 percent of the total body weight and combined with the pelt to reduce the remaining specimen weight by one-fifth of the intact torso, at this point of the progressive necropsy. The arm shoulder musculature provides substantial stability

to the trunk, extending beyond the upper thoracic region. This morphological expansion of musculature is characteristic of brachiators and is elaborated in previous sections (Section III, Selection of Specimen). Subsequent to this sequence, c, of the necropsy, differential pressure values in the abdominal cavity do not evidence the steep slope of the pressure response to high load values recorded during previous sequential completions, a and b (Fig. 13). The rate of abdominal pressure increase with load application is not appreciably changed. Abdominal pressure differential versus load applied graphic comparison is uniform for the resolved horizontal and vertical components of total applied loading at 2.78×10^{-5} psi/gram.

Removing the musculature (in sequence d), physiologically recognized as the abdominal wall, causes the abdominal pressure differential to become a constant value at 0.26 psi (at 0°C), Appendix A. Without the containment provided by the musculature, the intestinal membrane loses the ability to function as a semi-solid cavity and offers no resistance to loading. Observations confirm the intestine withdraws from the point(s) of load application and seeks equilibrium pressure through lateral expansion, in the instance of trunk flexion. The cervical vertebrae (C-4) shows the most marked increase in stiffness for flexion with the abdominal musculature gone and a sum of about 1/4 the total weight removed by necropsy. This is also evidenced by the T-3 and T-8 vertebrae. In the lumbar spine the slope of the load normalized displacement data does not tend to be more rigid with removal of the abdominal musculature, but generally exhibits a constant reaction to loading. For the lower thoracic and cervical regions, the greatest value of normalized displacement for a given load is measured at this sequence, d, of the experiment.

Visceration reduces the vertebral displacement and has no effect on the trunk response slope. There is a slight flattening of the curve for lumbar flexion in response to a vertical load at relatively large values. The viscerate was approximately 17 percent of the body weight and completion of this sequence has eliminated almost half of the original specimen total weight.

The greatest normalized displacement in the lumbar region and greatest rigidity is existent after the paravertebral and psoas musculature are removed. At this point of the experiment the osseous thoracolumbar spine is all that remains and the applied load versus normalized displacement measured in the lumbar region (L-2), 2×10^{-3} mm/mm/gram, is less than that calculated for the thoracic 2.2×10^{-5} or cervical 2.0×10^{-5} mm/mm/gram regions.

In all instances, the measured deformation for a particular loading of the locked torso gravitated to the mechanical properties characteristic of the ligamentous spine at that same region. Abdominal pressure differential to load relationships also grossly aligned to the constant value of the osseous spine. A weight to normalized displacement correlation is not evidenced. The sequential steps (a), (b), and (c) of Appendix A evidenced the greatest changes in data slope with the relationship becoming progressively more rigid. There was no perceivable axial rotation of the trunk/spine during this sequence. Rotation in the sagittal plane generally decreased with progressive component necropsy and was most pronounced in the cervical (1.25×10^{-3} degrees/gram) and upper thoracic region and least measurable in the lumbar region (2.64×10^{-3} degrees/gram).

In extension (Fig. 21), the abdominal pressure evidences a generally constant correlation to load of 6.75×10^{-5} psi/gram: a substantially more rigid relationship than in flexion. The lumbar region is almost totally rigid in load response as the sequence progresses. This is also evidenced by the thoracic region, but with less severity.

As was observed in the flexion sequence the measured data indicates a greater mechanical participation by the pelt than can be morphologically justified in a displacement load relationship. In the lumbar region the flat plot of normalized displacement versus load must be considered to be the extensible material properties of the integument. The greatest displacement values for extension are measured in the thoracic region (T-8), Fig. 22.

The strain rate is consistency mollified when the gross necroptic removal of the arms is accomplished. This is evidentary of the substansive trunk stability provided by the abdominal and upper thoracic musculature which in the rigor mortis state resist to failure. Even with the musculature removed, the extension is of such a severe arc for about 1 Kg loading that the viscera is evidencing tension in a dramatically changing abdominal pressure which aligns with the pressure differential versus load relationship of subsequent sequences rather rapidly.

The ligamentous spine alone is less rigid initially at the thoracic level than the lumbar region, but with increased loading the limits of the spinous processes are reached and all measured deformations are slight and very rigid approaching a constant data slope of 3.85×10^{-5} mm/mm/gram.

The greatest rotation for an increment of load is seen in the thoracic (T-8) region (Fig. 23) where, subsequent to the en bloc arm removal, the vertebral movement is of relatively substantial magnitude.

Most of the sagittal plane rotation measurable in this experiment is in the thoracic region with the lumbar spine (L-2) remaining almost fixed for the entire sequence and evidencing only 4° of movement after necropsy.

The side bending sequence was not productive (Fig. 27). The primate cadaver necessarily had to be stabilized to prevent rotation around the vertical axis to such a magnitude that the slight deformations measured are compromised. The thoracic level (T-8) data is available and indicates a less rigid behavior for the integuous torso becoming a more predictable displacement load relationship, as the spine is approached through necropsy.

For a single observation, abdominal pressure remains unchanged for a substantial portion of the bending movement but increases dramatically near the maximum total loading. This is a manifestation of the tendency of the specimen to "rotate-out-of" the bending configuration into flexion. Generally, this phenomenon was less pronounced as the necropsy progressed, substantiating the hypothesis that the action of the trunk and subcomponents was enhancing the tendency of the vertebral column to align with limitations of the articular facets. The limitation of the technical photography and the multi-plane response of the torso to a side load precluded accumulation of a predictive quantity of data.

Torsional pressure values were measured. Pressure generally increased, as the necropsy progressed. For the torso alone no change was evidenced in abdominal pressure until rotation surpassed about 65° when a .001 psi per degree gentle increase began. This was not evidenced after the pelt was removed. Then a constant increase of .0008 psi per degree of rotation was exhibited throughout. When the en bloc arm necropsy was done an abrupt increase appeared at about 87°. Abdominal muscle removal exhibited

a smooth pressure differential versus deformation curve. For this reason, the cross-tension of the pelt and similar phenomenon of the abdominal muscles are thought to have extended to a limit at 65° and 87°, respectively, and subsequently compress the abdominal cavity as they "wrap around" the torso.

Comparison to Lovett's Data for Human Specimens. The Rhesus did exhibit some rotation of the torso during flexion unlike the human models in Lovett's study. This was particularly evident for the intact animal and other early sequences of the necropsy (Appendix A, Table 10). Because that activity was not observed after removal of the arms and shoulders and because the relative weight of that anatomical mass is substantial compared to the whole animal; it is plausible that an imbalance would not be resisted by the trunk and rotation occur. The Rhesus did arc into a near perfect circle during extreme flexion, as Lovett observed. That propensity is used in Section V of this thesis as motivation for applying a strain energy equation to the experimental data in an effort to predict displacement of flextural movement of the torso. The pins at thoracic positions T-3 and T-8 evidenced the greatest bending participation in the monkey, with L-6 remaining virtually stationary for the entire flextural experiment. This is different from Lovett's observations of flextural movement more predominant in the lumbar region of man. The nonhuman primate evidenced a greater bending action at the crest of the shoulders when intact, and generally less participation by the lumbar and cervical regions until subsequent necropsy sequences were accomplished. It is believed that the morphological fortification discussed in Section III, Selection of Specimen, contributed to this condition. The lumbar region, (L-6) specifically, did not actively display a bending contribution

until the rib cage and associated musculature were removed. Because of the geometry of the externally applied load the cervical region exhibited uniaxial displacement, without bending, during advanced sequences of the necropsy; d, e and f.

The extended Rhesus paralleled Lovett's observation of humans and exhibited a purely anterior-posterior extensive kinesis. After removing the viscera and then the spinal musculature, there was a dramatic tendency for the specimen to rotate while in an extended posture. It is believed this was caused by the attempted alignment of the intervertebral articulations as an extended semicircular arc was being approached by this point in the experiment. Most of the extensive bending occurred in the lower cervical and upper thoracic regions. The lower lumbar is active in this bending mode from the onset. Removing the ribs and musculature effectively allows the specimen to "fail" in a mechanical sense and gross extensive displacement is evident.

In side bending, the Rhesus continually "rolled out" of the contrived posture. The propensity to return to a flextural movement subverted data collection attempts using photography. The specimen, with musculoskeletal substructures removed to the osseous spine, could be "set" into a bending equilibrium position which would sustain the applied external load and not rotate from the posture. This false kinesiology was not consistent with naturally sought positions of the spine or previously complete specimen.

The thoracic region of the nonhuman primate appeared to participate to a greater extent in all movement than that degree described by Lovett, observing humans. The immobilized pelvis may have manifested this activity in the particular specimen observed. The gross anatomical differences

of the upper torso surface as a plausible reason for this difference in primate torso kinesiology.

Because the experimental results evidence a trend contrary to the thesis preposition - removing body weight did not cause the specimen to become less stiffer but actually more stiffer - it is now plausible to attempt a theoretical review which might lend some insight as to the cause of this phenomenon.

THEORETICAL INVESTIGATION

Matrix Approach. A review of the experimental data, Appendix A, evidences that in flextural motion the total external applied load achieved an axial orientation, due to the severe bending of the specimen. This is shown analytically in Figs. 29 and 30. While there is a bending process taking place during sequences a and b of the experiment, the total applied external load sustained by the torso is of greater axial than transverse component for subsequent sequences.

This is further evidenced by comparing ΔX, ΔL and Δt in Appendix A. The displacements of X-coordinate value, "length" computed from allowing the X-component and Y-component to be sides of a triangle and calculating the change of hypotenuse length, and the tangential component, respectively. These values are relatively large and of substantial difference, initially. As the sequences progress beyond a and b, the values ΔX, ΔL and Δt approach each other. This indicates the alignment of the small Steinmann pins in the spinous processes (along the axis of the spine) with the X-axis of the grid overlay, which is also horizontally set, and substantiates the large axial component of the resolved total applied external load.

The data is geometrically resolved into normalized tangential displacement and normalized radial displacement, and tangential and radial resolved load component.

The relationship of appropriate normalized displacement and load component is acquired by measuring the slope of the graphical presentation from the most consistently linear region of the exhibited data (Figs. 31, 32, 33, 34). The tabulated slopes, viewed as some "coefficient" of the relationship, are presented in Table 1.

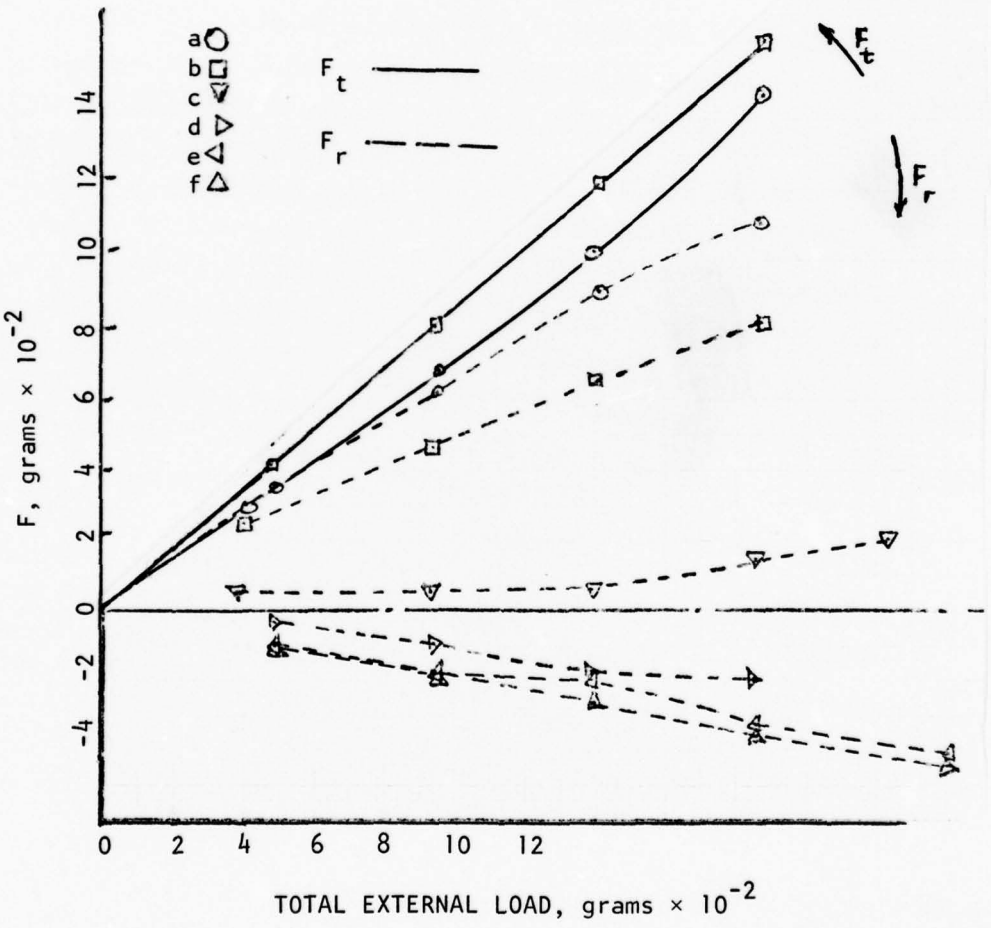

Figure 29. Coordinate Resolution into Radial and Tangential Component

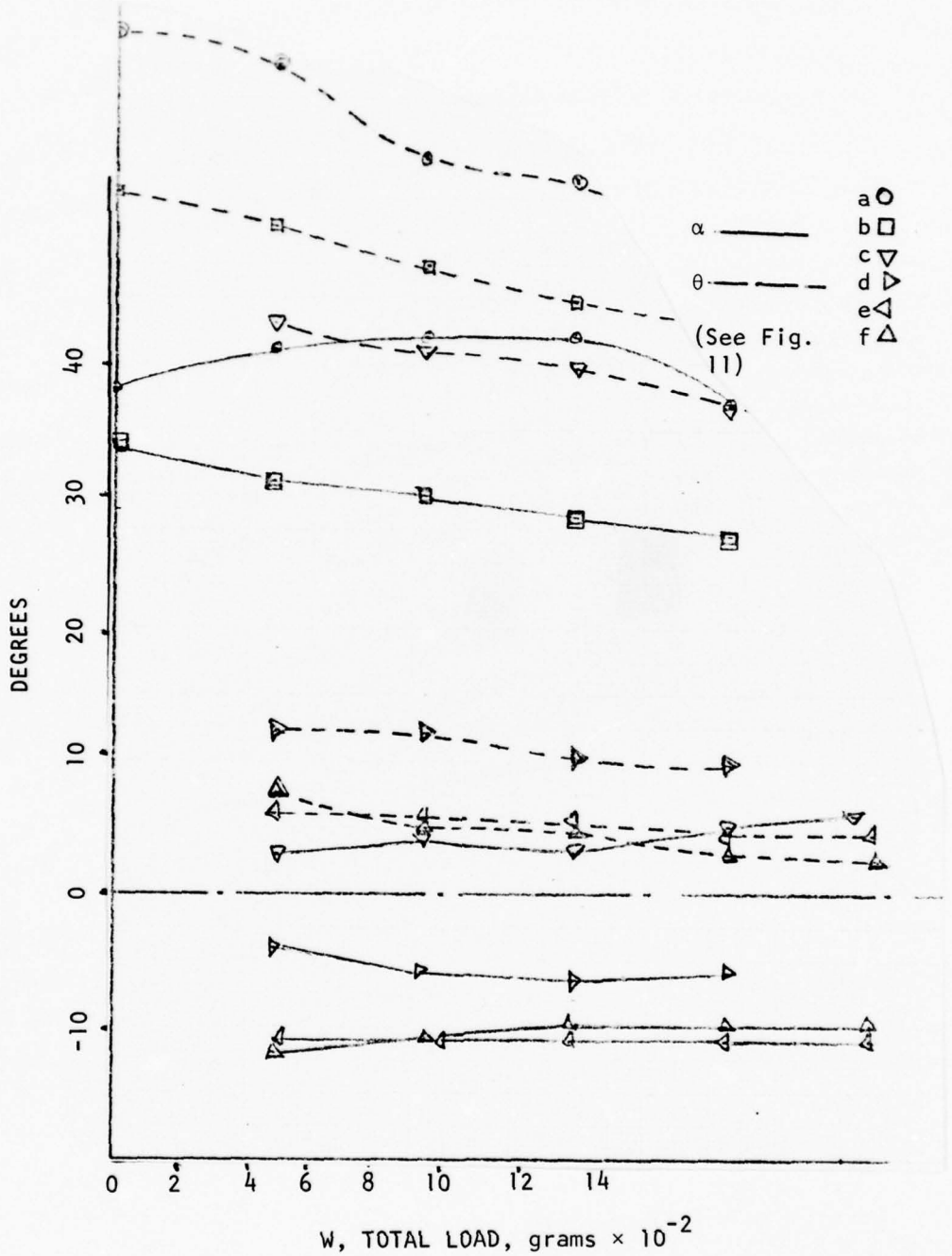

Figure 30. Total Load vs. θ

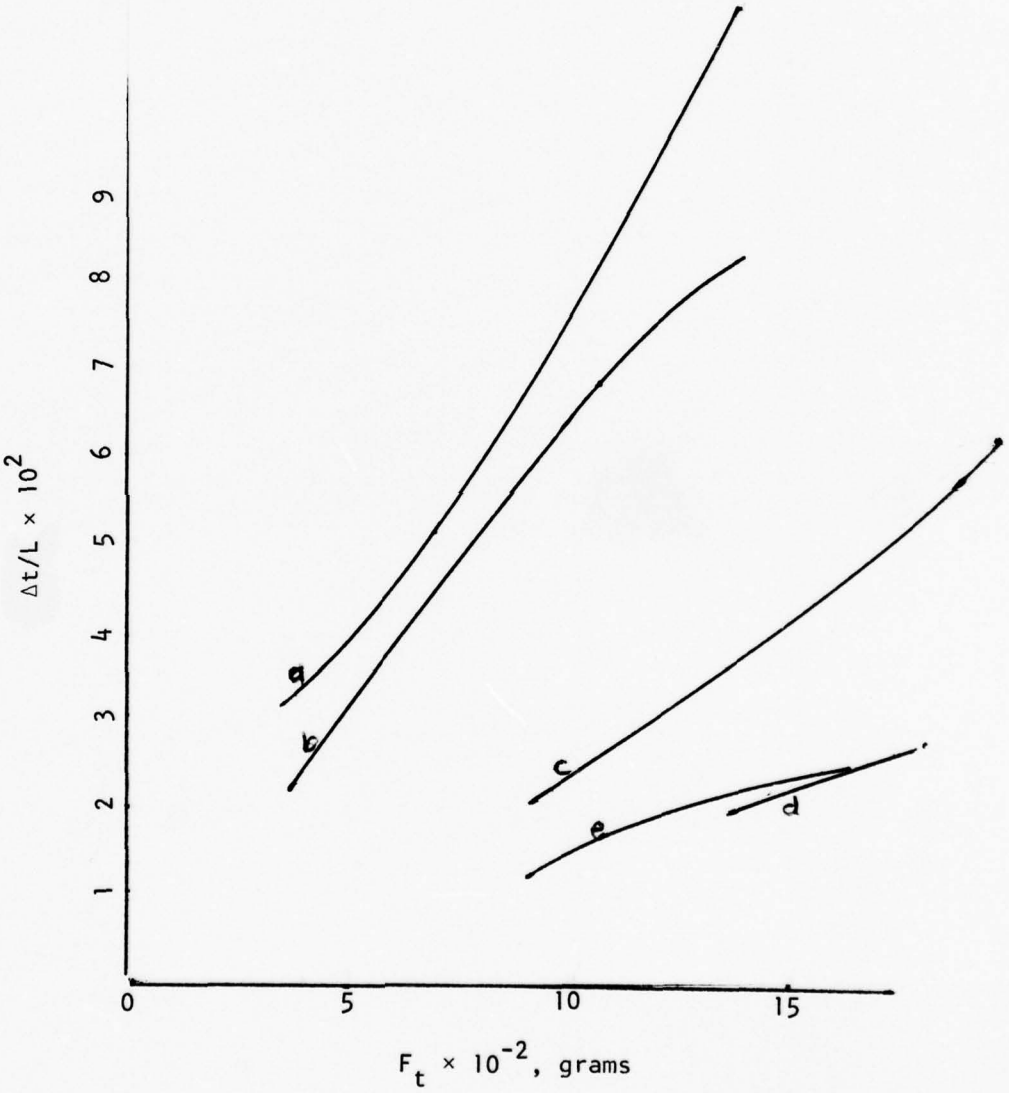

Figure 31. Normal Displacement vs. Normal Load, C-4: Extension

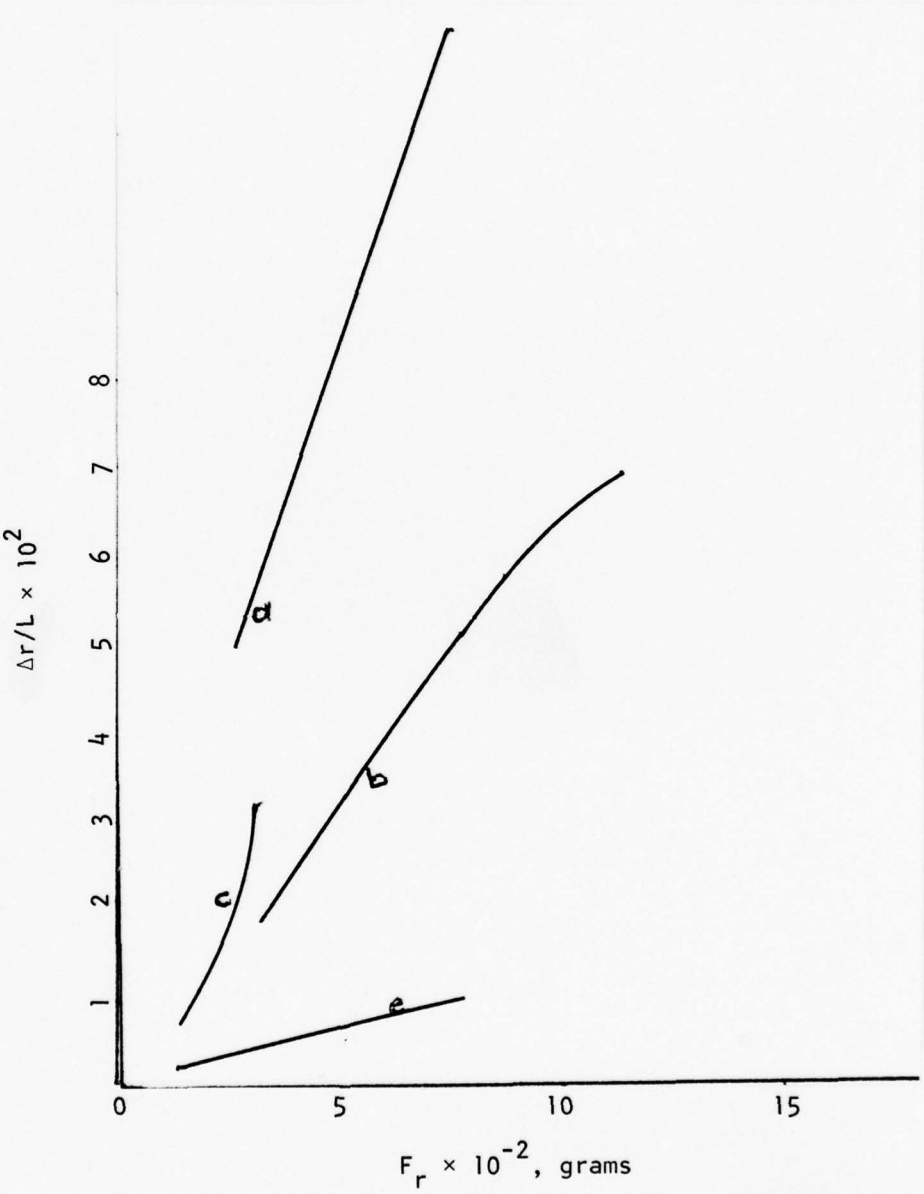

Figure 32. Radial Displacement vs. Radial Load, C-4: Extension

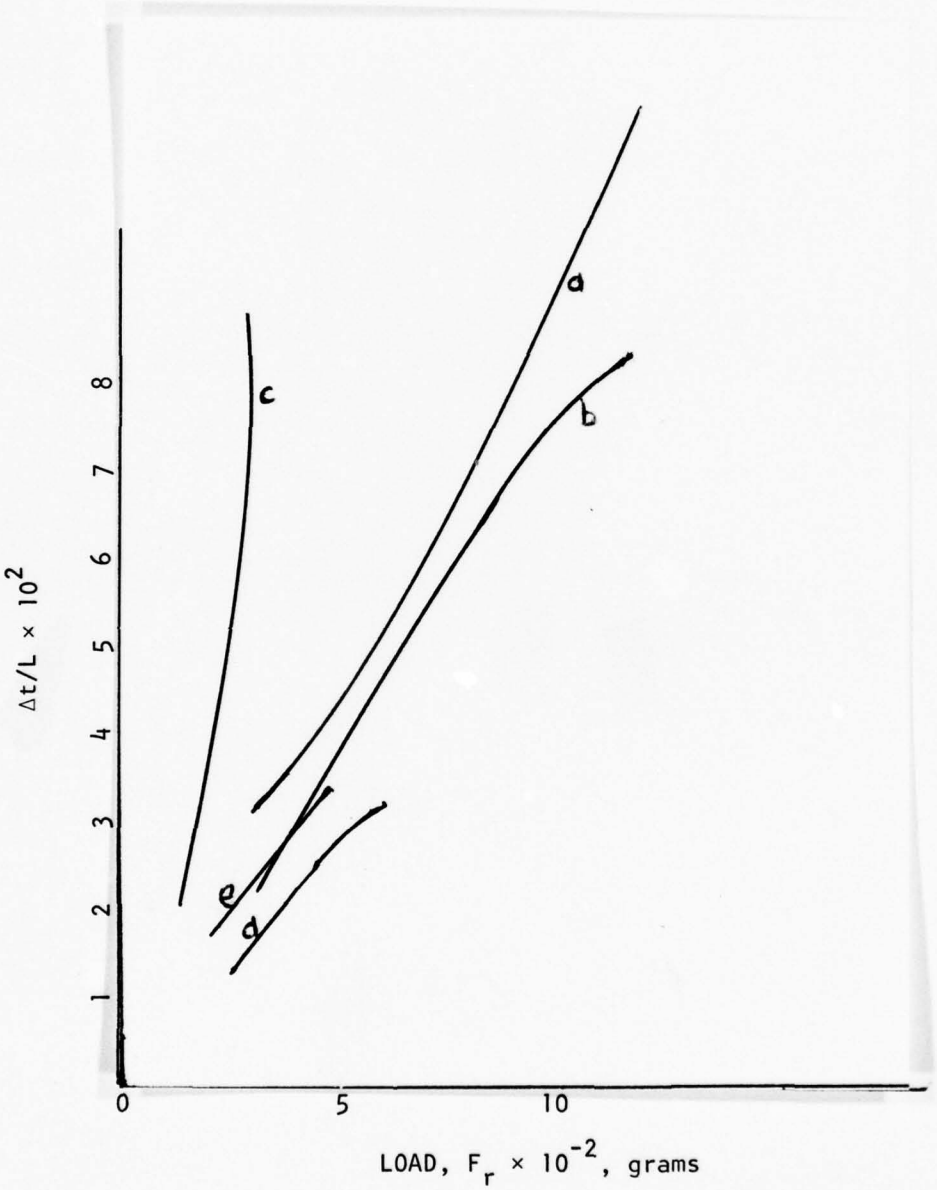

Figure 33. Tangential Displacement vs. Radial Load, C-4: Extension

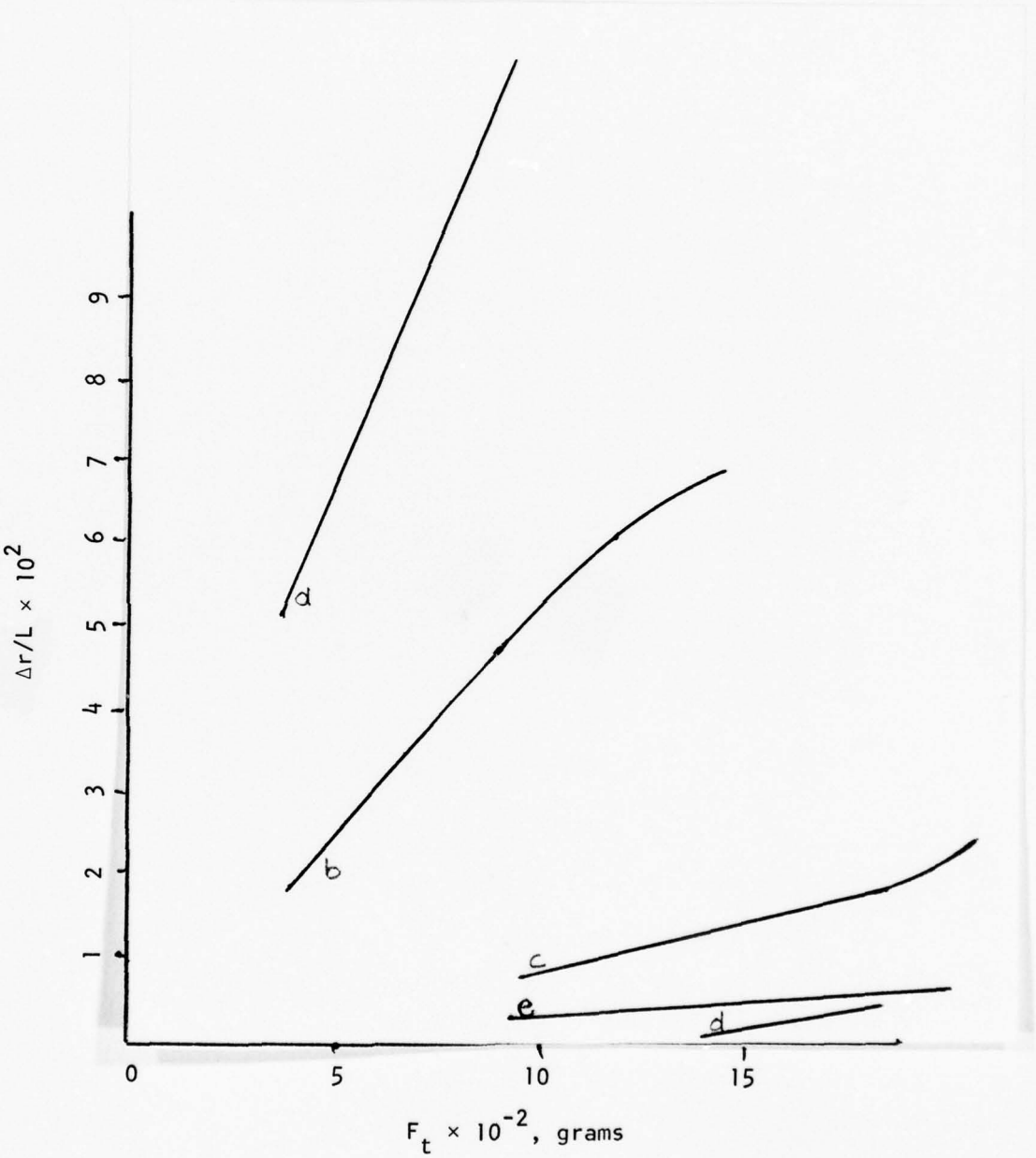

Figure 34. Radial Displacement vs. Tangential Load, C-4: Extension

Relationship	Sequence "Coefficient" × 10^4				
	a	b	c	d	e
$\Delta t/F_t$	0.872	0.658	0.350	0.125	0.143
$\Delta r/F_r$	0.556	0.678	0.925	0.112	0.112
$\Delta t/F_r$	1.030	0.850	2.560	0.645	0.625
$\Delta r/F_t$	1.200	0.560	0.122	0.097	0.037

Table 1. Displacement vs. Load

This data is for the C-4 vertebrae, chosen because it most closely approximates the "end" of the torso, viewed as a column subjected to bending. A constituative matrix hypothesis is made:

Δr - radial finite displacement calculated from ΔX and ΔY.

Δt - tangential finite displacement calculated from ΔX and ΔY.

F_r - radial load component of total applied.

F_t - tangential load component of total applied.

a_{ij} - coefficient; i = t, r; j = t, r.

Then,

$$\begin{bmatrix} \Delta r \\ \Delta t \end{bmatrix} = \begin{bmatrix} a_{rr} & a_{rt} \\ a_{tr} & a_{tt} \end{bmatrix} \begin{bmatrix} F_r \\ F_t \end{bmatrix} \tag{1}$$

multiplying the determinant (1),

$$\Delta r = a_{rr}F_r + a_{rt}F_t \tag{2}$$

$$\Delta t = a_{tr}F_r + a_{tt}F_t \tag{3}$$

dividing (2) by F_r,

$$\Delta r/F_r = a_{rr} + a_{rt}F_t/F_r = K_1 \tag{4}$$

where K_1 is the quantity expressed in Fig. 29 for the appropriate sequence of $\Delta r/F_r$. Now, dividing (3) by F_t,

$$\Delta t/F_t = a_{tr}F_r/F_t + a_{tt} = K_2 \tag{5}$$

where K_2 is the appropriate quantity for $\Delta t/F_t$ from the column of sequences in Fig. 29. Likewise,

$$\Delta t/F_r = a_{tr} + F_t a_{tt}/F_r = K_3 \tag{6}$$

$$\Delta r/F_t = F_r a_{rr}/F_t + a_{rt} = K_4 \tag{7}$$

if we define the force relationship, where g can be deduced from Fig. 30:

$$1/g = F_t/F_r = \cot \alpha \tag{8}$$

$$g = F_r/F_t = \tan \alpha \tag{9}$$

Then from substitution of Eqs. (8) and (9) into (5) and (6), and (4) and (7), respectively,

$$\Delta r = F_r a_{rt}/g + F_r a_{rr} \tag{10}$$

$$\Delta t = F_t a_{tt} + gF_t a_{tr} \tag{11}$$

Because the graphical data is not correlative, it is unlikely $a_{rt} = a_{tr}$. Therefore, this matrix does provide sufficient data to deduce the material properties constants a_{rr}, a_{tt}, a_{rt} or a_{tr}. This is essential if resulting displacement is to be predicted from an applied

load of known total value and geometric orientation to the specimen. However, there is a geometric and material dependence between F_r and F_t, and no data is available for either $F_r = 0.0$ or $F_t = 0.0$; therefore, desired a_{ij}'s will not be independent values. The trend of increasing stiffness with sequential progression is evidenced by the resolved radial and tangential data graphed in Figs. 31, 32, 33 and 34.

To solve for these a_{ij}'s, the application of strain energy theory is plausible.

Castigliano's Theorem. When an elastic body is acted upon by forces there is a resultant displacement in the direction of the applied force. The work done on the body by the acting forces is the product of force and displacement summed for each incremental force and each incremental displacement over the entire body. Strain energy is determined similarly and the principal of virtual work defines the difference equal to zero. The combination of this information derives Castigliano's Theorem which states that the derivative of the strain energy with respect to an applied force gives the displacement, of the point of application of the force, in the direction of the force.

It is intended to use the application of the "strain energy", the work of a normalized displacement, to the bent torso to predict the displacement at the end, C-4 vertebrae, for some applied external load. A basic premise of application is that the radius of curvature of the bending (or arced) torso is very much greater than the dimensions of the specimen cross-section. This appears plausible and will be assumed to be so, to allow application of the theorem. (See Fig. 12.)

The appropriate "piece" of the specimen to provide the strain energy is pictured in Fig. 35. θ for Fig. 35, and the following developments, is 180° minus θ, as defined in Fig. 11 and presented in Appendix A.

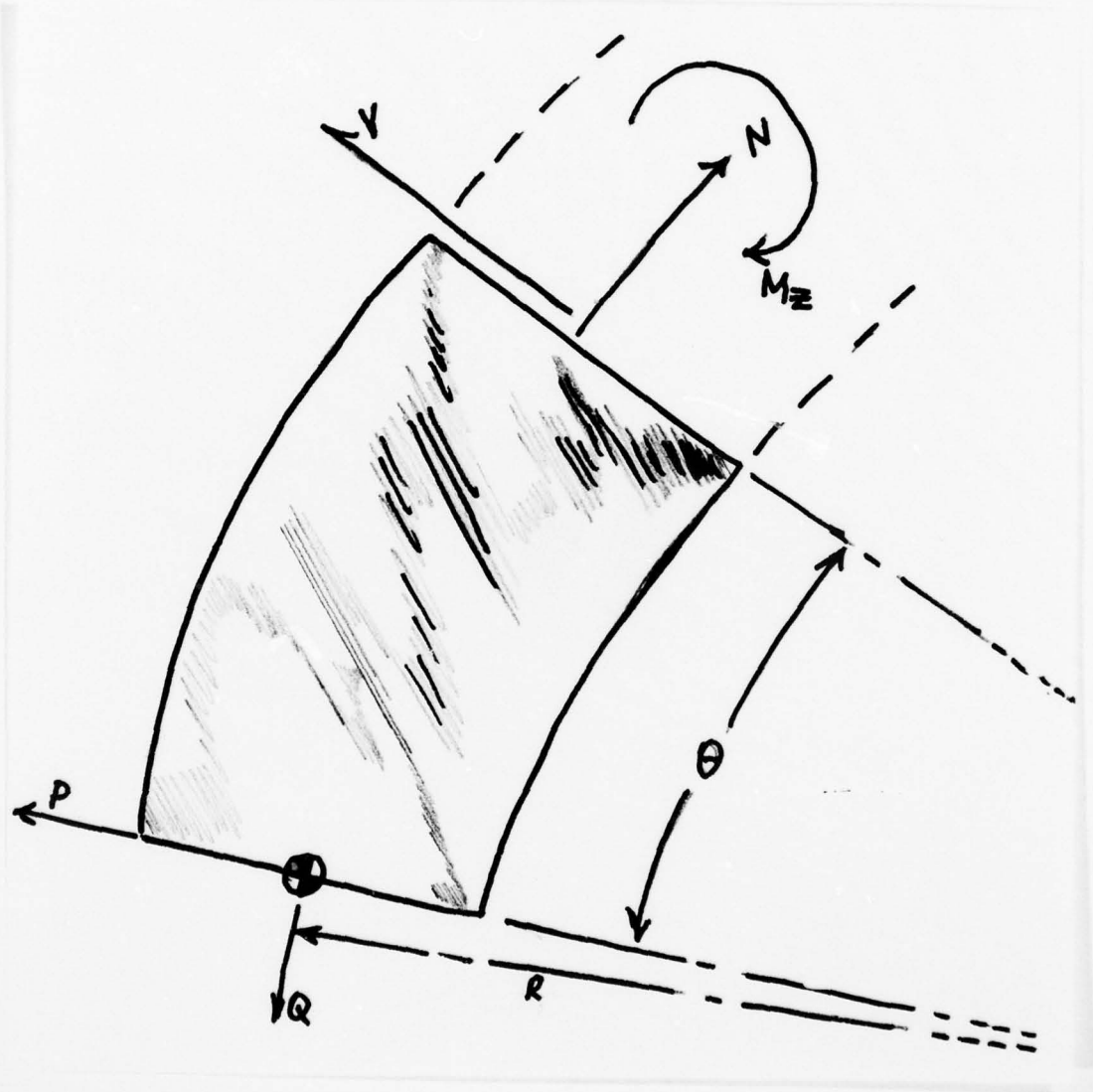

Figure 35. Castigliano's Finite Element Section

To compute the appropriate displacements, the moment about the centroid of a finite piece, the radial or shear load and the normal or tangential load must be calculated.

From Fig. 35,

$$M_z = -PR \sin\theta + QR(1 - \cos\theta) \tag{12}$$

$$N = P \sin\theta + Q \cos\theta \tag{13}$$

$$V = -P \cos\theta + Q \sin\theta \tag{14}$$

The basic form of Castigliano's theorem for displacement, Δ, in the direction of an applied external load, W, is,

$$\Delta = \partial U/\partial W$$

where U is the strain energy

$$\Delta = (1/EI) \int M_z(\partial M_z/\partial W)Rd\theta + (1/EA) \int N(\partial N/\partial W)Rd\theta + (2(1 + \nu)/EA) \int V(\partial V/\partial W)Rd\theta. \tag{15}$$

Taking P, the radial load, and substituting Eqs. (12), (13) and (14) into (15),

$$\Delta r = \frac{1}{EI} \int_0^\theta M_z \frac{\partial M_z}{\partial p} Rd\theta + \frac{1}{EA} \int_0^\theta N \frac{\partial N}{\partial P} Rd\theta + \frac{2(1+\nu)}{EA} \int_0^\theta V \frac{\partial V}{\partial P} Rd\theta$$

$$= \frac{1}{EI} \int_0^\theta (-PR \sin\theta + QR(1 - \cos\theta))(-R \sin\theta)Rd\theta \tag{16}$$

$$+ \frac{1}{EA} \int_0^\theta (P \sin\theta + Q \cos\theta)\sin\theta \, Rd\theta + \frac{2(1+\nu)}{EA} \int_0^\theta (-P \cos\theta + Q \sin\theta)(-\cos\theta)Rd\theta$$

$$\Delta r = \frac{R^3}{EI}\int_0^\theta (P\sin^2\theta - Q\sin\theta + Q\sin\theta\cos\theta)d\theta$$

$$+ \frac{R}{EA}\int_0^\theta (P\sin^2\theta + Q\sin\theta\cos\theta)d\theta + \frac{2(1+\nu)R}{EA}\int_0^\theta (P\cos^2\theta - Q\sin\theta\cos\theta)d\theta. \tag{17}$$

$$\Delta r = \frac{R^3}{EI}\left[P\left(\frac{\theta}{2} - \frac{\sin 2\theta}{4}\right) + Q\cos\theta + Q\left(\frac{1}{2}\sin^2\theta\right)\right]_0^\theta$$

$$+ \frac{R}{EA}\left[\left(P\left(\frac{\theta}{2} - \frac{\sin 2\theta}{4}\right) + Q\left(\frac{1}{2}\sin^2\theta\right)\right]_0^\theta + \frac{2(1+\nu)R}{EA}\left[\left(P\left(\frac{\theta}{2} + \frac{\sin 2\theta}{4}\right) - Q\left(\frac{1}{2}\sin^2\theta\right)\right]_0^\theta. \tag{18}$$

Simplifying and collecting terms,

$$\Delta r = \frac{R^3}{4EI}\left[P(2\theta - \sin 2\theta) + Q(4\cos\theta + 2\sin^2\theta)\right]_0^\theta$$

$$+ \frac{R}{4EA}\left[P(2\theta - \sin 2\theta) + Q(2\sin^2\theta)\right]_0^\theta + \frac{(1+\nu)2R}{4EA}\left[P(2\theta + \sin 2\theta) - Q(2\sin^2\theta)\right]_0^\theta. \tag{19}$$

So, for a semicircular arc, $\theta = \pi$,

$$\Delta r = \frac{\pi R^3 P}{2EI}\left[1 + (3 + 2\nu)\frac{I}{RA}\right] - \frac{2QR^3}{EI}. \tag{20}$$

Using the same process of the tangential load Q,

$$\Delta t = \partial U/\partial Q$$

where U is the strain energy

$$\Delta t = (1/EI)\int_0^\theta M_z(\partial M_z/\partial Q)Rd\theta + (1/EA)\int_0^\theta N(\partial N/\partial Q)Rd\theta$$

$$+ \frac{2(1+\nu)}{EA}\int_0^\theta V(\partial V/\partial Q)Rd\theta. \tag{21}$$

Taking Q as the tangential load and substituting (12), (13) and (14) into (21),

$$\Delta t = \frac{1}{EI}\int_0^\theta (-PR\sin\theta + QR(1-\cos\theta))(R(1-\cos\theta))Rd\theta$$
$$+ \frac{1}{EA}\int_0^\theta (P\sin\theta + Q\cos\theta)(\cos\theta)Rd\theta + \frac{2(1+\nu)}{EA}\int_0^\theta (-P\cos\theta + Q\sin\theta)(\sin\theta)Rd\theta. \tag{22}$$

$$\Delta t = \frac{R^3}{EI}\int_0^\theta (-P\sin\theta + P\sin\theta\cos\theta + Q - Q(2\cos\theta) + Q\cos^2\theta)Rd\theta$$
$$+ \frac{R}{EA}\int_0^\theta (P\sin\theta\cos\theta + Q\cos^2\theta)Rd\theta + \frac{2(1+\nu)R}{EA}\int_0^\theta (-P\cos\theta\sin\theta + Q\sin^2\theta)Rd\theta. \tag{23}$$

$$\Delta t = \frac{R^3}{EI}\left[P\cos\theta + P\left(\frac{1}{2}\sin^2\theta\right) + Q\theta - 2Q\sin\theta + Q\left(\frac{\theta}{2} + \frac{\sin2\theta}{4}\right)\right]_0^\theta$$
$$+ \frac{R}{EA}\left[P\left(\frac{1}{2}\sin^2\theta\right) + Q\left(\frac{\theta}{2} + \frac{\sin2\theta}{4}\right)\right]_0^\theta + \frac{2(1+\nu)R}{EA}\left[-P\left(\frac{1}{2}\sin^2\theta\right) + Q\left(\frac{\theta}{2} - \frac{\sin2\theta}{4}\right)\right]_0^\theta. \tag{24}$$

Simplifying and collecting terms,

$$\Delta t = \frac{R^3}{4EI}\left[Q(6\theta + \sin2\theta - 8\sin\theta) + P(4\cos\theta + 2\sin^2\theta)\right]_0^\theta$$
$$+ \frac{R}{4EA}\left[2P\sin^2\theta + Q(2\theta + \sin2\theta)\right]_0^\theta + \frac{2(1+\nu)R}{4EA}\left[-2P\sin^2\theta + Q(2\theta - \sin2\theta)\right]_0^\theta. \tag{25}$$

for a semicircular arc; $\theta = \pi$,

$$\Delta t = \frac{\pi R^3 Q}{2EI}\left[3 + (3+2\nu)\frac{I}{RA}\right] - \frac{2PR^3}{EI}. \tag{26}$$

To apply these results the overall configuration of the animal must be considered as the weights of the body components enter the problem (Fig. 1), as the specimen is initially deformed by the body weight, before applying any external loads. To acquire a reasonable included angle, θ, the lateral view photographs of the flexion experiment were reviewed. A translucent multiple arc protractor was placed over the photograph and manipulated until a best-fit arc was achieved along the extremities of the spinous processes with the diameter parallel to a horizontal line through the marked origin of the plane of the photograph (Fig. 11). The angle θ was measured from the horizontal to the tip (C-4) of the displaced specimen. Therefore, $\pi - \theta$ degrees is the appropriate included angle for application to the results of applying Castigliano's Theorem. The resolved component values of vertical and horizontal applied external load are geometrically solved for tangential and radial forces, P and Q, respectively. The value of "ν" was chosen as 0.3. With a given value of "ν", the axial and shear (non-bending) contributions of Eqs. (19) and (25) can be combined into an effective axial coefficient of contribution multiplied by $\frac{R}{EA}$ (constant). The bending multiplier operates on $\frac{R^3}{EI}$ (constant). The data is then aligned, accumulating the calculated "known" values, K's, and the unknown coefficients, E's, R's, etc., into the configuration,

$$K_1 = \frac{R^3}{EI} (K_2) + \frac{R}{EA} \qquad (27)$$

A least squares curve fitting program was developed (Appendix B) to calculate the coefficient and intercept of the experimental values of radial and tangential load and displacements. Measured components of load and experimental deflections were introduced into the application of

Castigliano's Theorem, for a circular arc loaded at the tip, in an effort to determine the geometric and material properties of the specimen at each necroptic stage.

Application of the least-squares curve fitting procedure to the sets (five for all sequences excepting d which has four) of Eq. (27) for each sequence, for radial and tangential load versus displacement, with the "best-fit" calculation providing a best $\frac{EI}{R^3}$ and a best $\frac{EA}{R}$, determined by the experimentally originated constants. This data is tabulated for a variety of attempts in Appendix B, for given θ, P and Q and variations of "ν" in Eqs. (19) and (25). The bending coefficient, the inverse is calculated and tabulated, became stiffer as the necropsy progressed. This indicates the osseous spine is most stable and actually becomes more vulnerable to displacement by loading when acting with the contribution of the musculature and substructures of the intact torso. This is contrary to the original hypothesis.

A review of this unsuccessful approach using Castigliano's Theorem prompted the renewed concept that the external radial and tangential loads, P and Q, respectively, were in fact artificially placed to force a deformation, so a correlative displacement versus load relationship would evolve and yield the constitutive relationships. However, this contribution to the calculated so-called bending and axial coefficients, Eq. (27), was an element to be subtracted, effective K - no applied load, when attempting to arrive at the kinesis of the trunk as a function of component weight - the P and Q merely serving to achieve the "unit-response" coefficient in the direction of external load application. Again, the data depicted an increasingly more rigid structure as necropsy progressed.

Manipulation of "ν" and adjustments in acting weight did not change the analytical forecast of a more stiffening anatomical

specimen as parts were removed. Data is tabulated in Appendix B.

Figure 36 displays the inverse bending coefficient, $\frac{R^3}{EI}$, versus percent of total body weight remaining. The sequence a activity is predominant and shows a drastic stiffening as weight is removed. The other sequences display a more erratic, but generally same, direction.

It can be drawn from the analytical attempts to calculate displacement due to external load, that linear theory is not an appropriate field for application to nonhomogeneous finite displacement investigation. Specifically, the redundancy of torso substructure contribution to load, the assumed elasticity of the torso, and the geometry of application of the applied external load were sufficiently confounding to preclude separation of the multiplicity of concurrent phenomenon into idealized, individual, constitutive measures of participation as was desired. The hypothesis that the more rigid structure is the intact torso, becoming less able to resist displacement due to external load through removal of musculoskeletal substructure, cannot be substantiated by this analytical bioengineering endeavor which, for reasons discussed, points strongly to the opposite supposition. A nonlinear simplistic model will now be approached.

Simplistic Torso Displacement. An initial hypothesis was that the torso receives a measurable amount of stability from the musculature and substructures. To gain an engineering perspective of that condition, the spine was visualized as a homogeneous elastic bar, with constant geometric properties, fortified to support an external load by an axial spring, accepting load through a frictionless pulley at the top (cranially), and restrained at the base by a coil spring (Fig. 37). This is an amplification of the fixed-base strength-of-materials beam bending problem (Fig. 37).

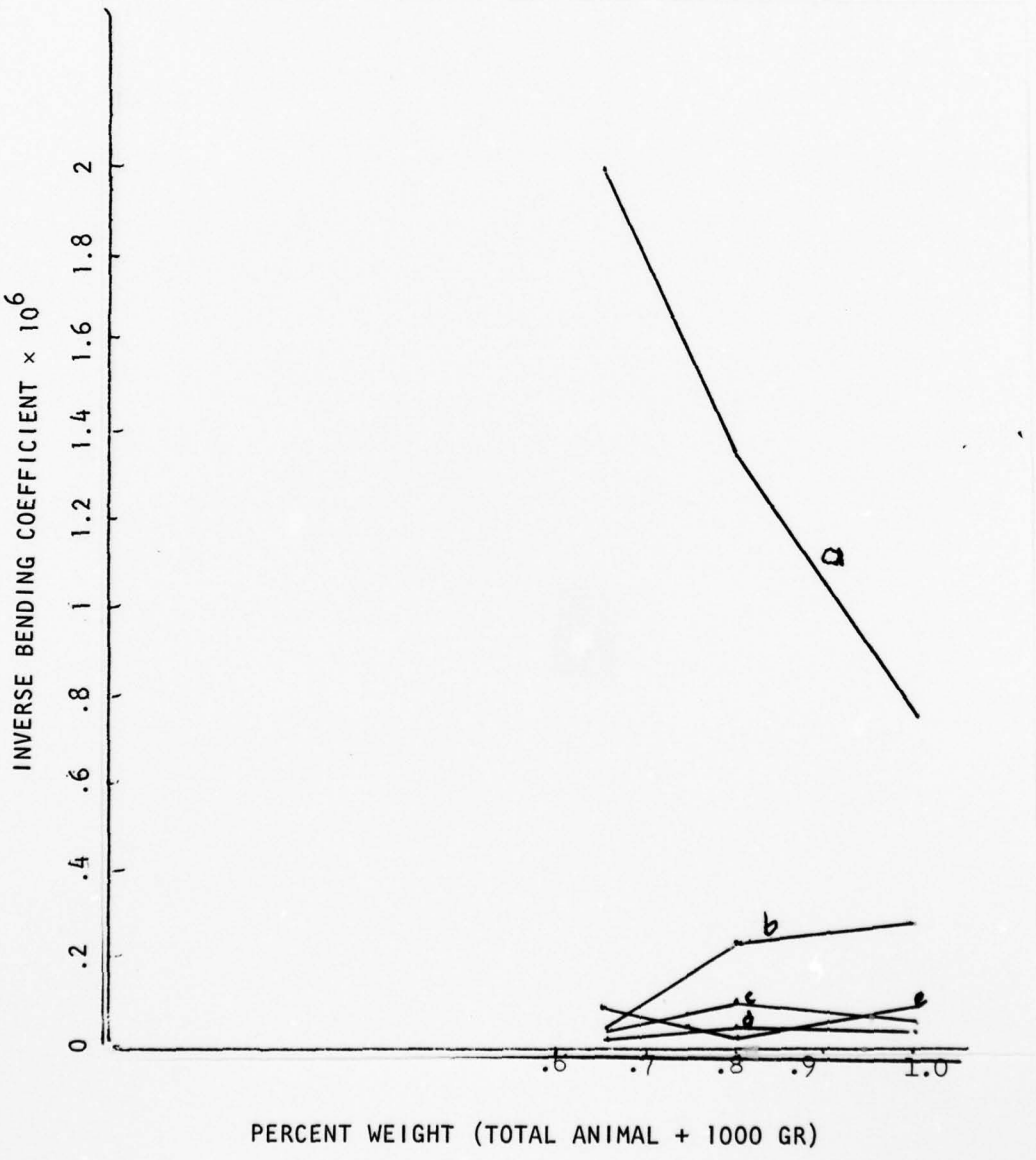

Figure 36. Inverse "Coefficient" vs. Animal Weight

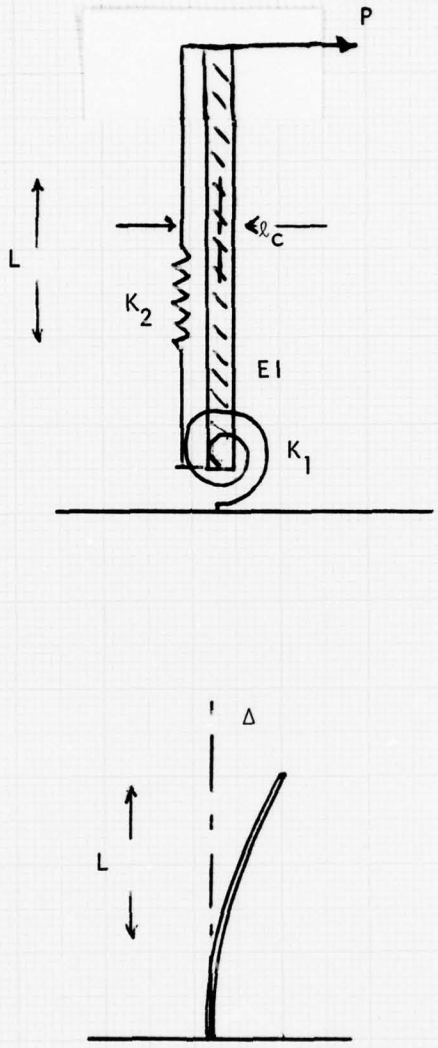

Figure 37. Spring Bar Model of Torso

Then,

$$\Delta end = \underset{\text{beam}}{PL^3/3EI} + \underset{\text{coil spring}}{PL^2/K_1} \tag{28}$$

We begin by calculating the strain, :

$$= (dS - dS_0)/dS_0 = -y(d^2w/dx^2) \tag{29}$$

where dS is,

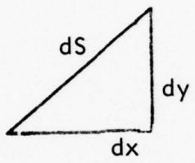

Then

$$\ell_f(y) = \int_0^{\ell} dS = \int_0^{\ell_c} (dS/dx)\,dx$$

$$= \int_0^{\ell_c} \sqrt{1 + (dy/dx)^2}\; dx = \int_0^{\ell} 1 + \tfrac{1}{2}(dy/dx)^2\; dx \tag{30}$$

Therefore

$$L_f - L_0 = \int_0^{\ell} \tfrac{1}{2}(dw/dx)^2 dx = \Delta S. \tag{31}$$

Examining the load bearing features of the contrived system:

$$P_{\text{externally applied}} = P_{\text{beam}} + F_{\text{spring}} \tag{32}$$

and mechanically,

$$F_{spring} = K(\Delta S). \tag{33}$$

Proceeding with the integration,

$$\Delta S = \int_0^{\ell} \frac{1}{2}(dw/dx)^2 dx \tag{34}$$

deriving the moment equation,

$$EI(d^2w/dx^2) = P(X - L) \tag{35}$$

$$EI(dw/dx) = P(X^2/2 - LX) \tag{36}$$

which, solving for dw/dx gives,

$$dw/dx = P/EI(X^2/2 - LX) \tag{37}$$

$$(dw/dx)^2 = (P/EI)^2(X^4/4 - X^3L + X^2L^2) \tag{38}$$

then substituting into (34),

$$\begin{aligned} \Delta S &= \frac{1}{2}\int_0^{\ell} (P/EI)^2(X^4/4 - X^3L + X^2L^2) \\ &= \frac{1}{2}(P/EI)^2(L^5/20 - L^5/4 + L^5/3) = (P/EI)^2(L^5/15) \end{aligned} \tag{39}$$

$$\Delta S/L = \quad = C(PL^2/EI)^2. \tag{40}$$

If P, E and I are assumed constant, the relationship indicates,

$$= C'L^4 \tag{41}$$

This is a fundamentally nonlinear expression. The experimental data indicates the quantity $\Delta L/L$ increases as the base of the torso is approached, Appendix . In sequence a, C-4 and T-3 do exhibit larger values of the specialized "strain", $\Delta L/L$, than locations lower on the torso. This is contrary to subsequent sequences which have smaller calculated values for $\Delta L/L$ near the unrestrained end of the specimen.

The plotted $\Delta L/L$ versus load component, of external force (Figs. 13, 14, 15, 16, 31, 32, 33 and 34), is a linear relationship which does not substantiate the nonlinear formula of Eq. (41). However, subsequent attempts to linearly unravel the constitutive relationships of load and displacement were frustrated. This lends credence to the possibility that the investigation of the kinesiology of the locked torso is an exercise demanding a nonlinear approach.

SUMMARY

In each subsequent sequence the torso offered a stiffer response to load and the data shows a convergence to the slope relationship of normal deformation and load in the bony spine. The extensive network of muscular redundant support and resolution of load prevented a static vector definition of independent load application to axial and tangential.

The preposition of this thesis that the stiffer engineering structure is the total torso which would exhibit more flexible properties through necropsy is not supported by the data which, in fact, evidences a contrary trend.

Presented evidence does allow relative understanding of the magnitude of load carried at each level of the torso and at what position the individual substructures of the body may be most active in providing support.

CONCLUSION

The predominant result of this thesis is to confirm the nonlinearity of torso kinesiology, and exhaust the linear engineering applications to bending displacement in an effort to achieve some effective modulus which would create a method of accomplishing a predictive "fit". This was not successful. The nonlinearities of Eqs. (1) and (41) appear to be substantiated by the lack of success using Castigliano's Theorem (linear, strain energy).

Qualitatively the general contributions of the musculature and substructures of the primate torso have been presented. The extensive trunk stability provided by the upper thoracic region, in the Rhesus, was observed during the experimental necropsy sequences. Torsional resistance by musculature and integument were identified with respect to degrees of pelvic rotation (Fig. 28).

To enhance the success of the continuation of this thesis, the load geometry necessarily must include some pure axial and pure shear measurements to remove the dependent relationship. Additionally, a more precise method of charting greater numbers of spinal Steinmann pins would allow concentration of efforts on other torso kinesiologies. The flextural movement predominated in the theoretical investigations of this thesis due to greater quantities of data being extractable from multiply exposed photographs of that posture.

The redundancy of torso substructures coupled with geometric considerations of external load application are basic contingencies, necessarily solved, to allow determination of component contribution through continued investigation.

AD-A060 837 AIR FORCE INST OF TECH WRIGHT-PATTERSON AFB OHIO SCH--ETC F/G 6/16
KINESIOLOGY OF THE LOCKED TORSO AS A FUNCTION OF COMPONENT WEIG--ETC(U)
MAR 78 A J NESTLE

UNCLASSIFIED AFIT/GAE/AA/78M-10 AMRL-TR-78-63 NL

2 OF 2
AD
A060837

END
DATE FILMED
1-79
DDC

BIBLIOGRAPHY

1. Andriacchi, A., et al. "A Model for Studies of Mechanical Interactions Between the Human Spine and Rib Cage," Journal of Biomechanics, 1: 497-507 (1974).

2. Barham, J. N. and Wooten, E. P. Structural Kinesiology. New York: McMillian Publishing Co., Inc., 1973.

3. Bartelink, D. L. "The Role of Abdominal Pressure in Relieving the Pressure on the Lumbar Intervertebral Disks," Journal of Bone and Joint Surgery, 39B: 718 (1957).

4. Braer, M. R. An Introduction to Kinesiology. Englewood Cliffs: Prentice-Hall, Inc., 1968.

5. Brown, R. H., et al. "Spinal Analysis Using a Three Dimensional Radiograph Technique," Journal of Biomechanics, 9: 335-65 (1976).

6. Brown, T., et al. "Some Mechanical Tests on the Lumbo-Sacral Spine with Particular Reference to the Intervertebral Disks: A Preliminary Report," Journal of Bone and Joint Surgery, 39A: 1135 (1957).

7. Combs, Steven W., Major, USAF MC, 6570 Aerospace Medical Research Laboratory, personal communications.

8. Cramer, H. J., et al. "A Distributed Parameter Model of the Inertially Loaded Human Spine," Journal of Biomechanics, 9: 115-30 (1976).

9. Croll, J. G. and Walker, A. C. Elements of Structural Stability. New York: John Wiley and Sons, Inc., 1972.

10. Danielson, D. A. "Mechanics of Muscular Organs," Journal of Biomechanics, 10: 355-6 (1977).

11. Dempster, W. T. Study of Hinge Points on the Human Body. AF Contract No. AF18(600)-43, Project No. M996, Quarterly Report. Wright-Patterson AFB, OH: Wright Air Development Center, March 1952.

12. Denslow, J. S. and Chace, J. A. "Mechanical Stresses in Human Lumbar Spine," The Journal of the American Osteophatic Association, 61: 705-12 (May 1962).

13. Edwards, W. E. The Study of Monkey, Ape and Human Morphology and Physiology, Relating to Strength and Endurance. Phase I: The Relationship of Human Size to Strength. ARL-TDR-63-19. Holloman AFB, NM: 6571 Aerospace Medical Research Laboratory, July 1963. (AD 412 448).

14. Edwards, W. E. The Study of Monkey, Ape, and Human Morphology and Physiology, Relating to Strength and Endurance. Phase IV: The Musculoskeletal Anatomy of the Thorax and Brachium of a Adult Female

Chimpanzee. ARL-TD-65-3. Holloman AFB, NM: 6571 Aerospace Medical Research Laboratory, April 1965. (AD 462 433).

15. Eie, N. and Welsh, P. "Measurements of the Intra-Abdominal Pressure in Relation to Weight Bearing of the Lumbosacral Spine," Journal of Oslo City Hospitals, 12: 206-17 (October 1962).

16. Elftman, H. "Biomechanics of Muscle," Journal of Bone and Joint Surgery, 48A: 363-77 (March 1966).

17. Evans, F. G. Biomechanical Studies of Musculoskeletal System. Springfield: Charles C. Thomas Publishers, 1961.

18. Farfan, H. F. The Orthopedic Clinics of North America. Vol. 6, No. 1, Symposium on the Lumbar Spine. Philadelphia: W. B. Saunders Company, January 1975.

19. Farfan, H. F., et al. "The Effects of Torsion on the Lumbar Intervertebral Joints: The Role of Torsion in the Production of Disk Degeneration," Journal of Bone and Joint Surgery, 52A: 468-97 (April 1970).

20. Flugge, W. Handbood of Engineering Mechanics. New York: McGraw-Hill Book Company, 1962.

21. Fung, Y. C., et al. Biomechanics: its Foundations and Objectives. New York: Prentice-Hall, Inc., 1972.

22. Gaylord, E. H. Jr. and Gaylord, C. N. Structural Engineering Handbook. New York: McGraw-Hill, Inc., 1968.

23. Godden, W. G. Numerical Analysis of Beam and Column Structures. Englewood Cliffs: Prentice-Hall, Inc., 1965.

24. Gregersen, G. G. and Lucus, D. B. "An in Vivo Study of the Axial Rotation of the Human Thoracolumbar Spine," Journal of Bone and Joint Surgery, 49A-2: 247-62 (March 1967).

25. Grey, H. Anatomy of the Human Body. Philadelphia: Lea and Febiger, Inc., 1961.

26. Hall, A. S., et al. Schaum's Outline Series of Theory and Problems of Machine Design. New York: McGraw-Hill Book Company, 1961.

27. Hetenyi, U. Beams on Elastic Foundations. Ann Arbor, Michigan: University of Michigan Press, 1946.

28. Hirsch, C. "The Reaction of Intervertebral Disks to Compression Forces," Journal of Bone and Joint Surgery, 37A: 1188 (1957).

29. Hurtly, W. C. and Rubinstein, M. R. Dynamics of Structures. Englewood Cliffs: Prentice-Hall, Inc., 1964.

30. Hyman, L. H. Comparative Vertebrate Anatomy. Chicago: University of Chicago Press, 1942.

31. Kazarian, L. E. "Creep Characteristics of the Human Spinal Column," Symposium on the Lumbar Spine-Orthopedic Clinics of North America, 6: 3-18 (January 1975).

32. Kazarian, L. E. and Graner, G. A. Compressive Strength Characteristics of Human Vertebral Column. AMRL-TR-77-14. Wright-Patterson AFB, OH: 6570 Aerospace Medical Research Laboratory, February 1977.

33. Kazarian, L. E. The Primate as a Model for Crash Injury. AMRL Rpt 751175. Wright-Patterson AFB, OH: 6570 Aerospace Medical Research Laboratory, April 1975.

34. King, A. I. Survey of State of the Art of Human Byodynamic Response. Navy - TR No. 7 - N0014-75-C-1015. Arlington, Virginia: Department of the Navy, ONR, Structural Mechanics Program (Code 474), March 1977.

35. King, A. I. Survey of State of the Art of Human Byodynamic Response. Navy - TR No. 8 - N0014-75-C-1015. Arlington, Virginia: Department of the Navy, ONR, Structural Mechanics Program (Code 474), April 1977.

36. King, A. I. "Elastic Deformation Characteristics of the Spine," Biomechanics, 4: 413-29 (April 1971).

37. Kulak, R. F., et al. "Nonlinear Behavior of Human Intervertebral Disks under Axial Load," Journal of Biomechanics, 9: 377-86 (September 1976).

38. Licht, S. ed. Orthotics Etcerta. Baltimore: Waverly Press, Inc., 1966.

39. Lovett, R. W. "The Mechanism of the Normal Spine and its Relation to Scoliosis," Boston Medical and Surgical Journal, CLIII: 349-358 (September 1905).

40. Lucas, B. D. and Bresler, B. Stability of the Ligamentous Spine. Technical Report No. 40. San Francisco and Berkeley: Biomechanics Laboratory, University of California, 1961.

41. Marton, G. M. P. Analysis of Dynamic Response of the Human Vertebral Column. Thesis, GAW/MC/74-6. Wright-Patterson AFB, OH: Air Force Institute of Technology, June 1974.

42. Morris, J. M. and Markoff, K. L. "Biomechanics of the Lumbosacral Spine," Spine, __: 312-31,

43. Morris, J. M., et al. "Role of the Trunk in Stability of the Spine," Journal of Bone and Joint Surgery, 43A: 327-51 (April 1961).

44. "Muscles, Bones and Numbers," MOSAIC, (November/December 1976).

45. Nachemson, A. and Elfstrom, G. "Introvital Dynamic Pressure Measurements in Lumbar Discs: A Study of Common Movements, Maneuvers and Exercises," Scandanavian Journal of Rehabilitory Medicine, 1 (Syp 1): 1-40 (1970).

46. Nachemson, A. "The Load on Lumbar Disks in Different Positions of the Body," Clinical Orthopaedics and Related Research, 45: 107-22 (1966).

47. Nash, W. A. Schaum's Outline Series of Theory and Problems of Strength of Materials. New York: McGraw-Hill, Inc., 1957.

48. Nicholas, W. and Lucas, W. M. Jr. Matrix Analysis for Structural Engineers. Englewood Cliffs: Prentice-Hall, Inc., 1968.

49. Palazatto, Anthony N., Professor, Air Force Institute of Technology, personal communications.

50. Panjaki, M. and White, A. A. III "A Mathematical Approach for Three Dimensional Analysis of the Mechanics of the Spine," Journal of Biomechanics, 4: 203-11 (1971).

51. Prescott, J. Applied Elasticity. New York: Dover Press, Inc., 1976.

52. "Primates," Encyclopedia Britanica, Vol. 14, 1030 (1974).

53. Pestel, E. C. and Leckie, F. A. Matrix Methods in Elastomechanics. New York: McGraw-Hill Book Company, 1963.

54. Przemieniecki, J. S. Theory of Matrix Structural Analysis. New York: McGraw-Hill, Inc., 1968.

55. Ray, C. D. Medical Engineering. Chicago: Yearbook Medical Pubs, Inc., 1974.

56. Ricci, B. Experiments in Physiology of Human Performance. Philadelphia: Lea and Febiger, Inc., 1970.

57. Rivello, R. M. Theory and Analysis of Flight Structures. New York: McGraw-Hill Book Company, 1969.

58. Saczalski, K. et al. Aircraft Crashworthiness. Charlottesville: Union Press of Virginia, 1975.

59. Schultz, A. B. "A Biomechanical View of Scoliosis," Spine, 1: 162-71 (September 1976).

60. Seto, W. W. Schaum's Outline Series of Theory and Problems of Mechanical Vibrations. New York: McGraw-Hill Book Company, 1972.

61. Smith, J. W. and Walemsley "Factors Affecting the Elasticity of Bone," Journal of Anatomy, 93: 503-23 (1959).

62. Steindler, A. Kinesiology of the Human Body under Normal and Pathological Conditions. Springfield: Charles C. Thomas Publishers, 1955.

63. Swindler, D. R. and Wood, C. D. An Atlas of Primate Gross Anatomy. Seattle: University of Washington Press, 1973.

64. Tanz, S. S. "Motion of the Lumbar Spine: A Roentgenalogic Study," American Journal of Roentgenology, 69: 399-412 (1953).

65. Tong, P. and Fung Y. C. "The Stress Strain Relationship for the Skin," Journal of Biomechanics, 9: (1976).

66. Tong, P. and Rossettos, J. N. Finite Element Method. Boston: MIT Press, 1977.

67. Torvik, Peter J., Professor, Air Force Institute of Technology, Wright-Patterson AFB, OH, personal communications.

68. Tuma, J. J. Schaum's Outline of Theory and Problems of Structural Analysis. New York: McGraw-Hill, Inc., 1969.

69. Wang, C. T. Applied Elasticity. New York: McGraw-Hill, Inc., 1953.

70. Wang, P. C. Numerical and Matrix Methods in Structural Applications to Computers. New York: Wiley, John and Sons, Inc., 1966.

71. Wells, D. A. Schaum's Outline Series of Theory and Problems of Lagrangian Dynamics. New York: McGraw-Hill Book Company, Inc., 1967.

72. Wells, K. F. Kinesiology. Philadelphia: W. B. Saunders Company, 1966.

73. White, A. A. III "Kinematics of Normal Spine as Related to Scoliosis," Biomechanics, 4: 405-11 (1971).

74. White, A. A. III, et al. "A System for Defining Position and Motion of the Human Body Parts," Medical and Biological Engineering, 13: 261-65 (March 1975).

75. Wiles, P. "Movements of Lumbar Vertebrae During Flexion and Extension," Procedures of the Royal Society of Medicine, 28: 647-52 (1935).

76. Williams, M. and Lissuer, H. R. Biomechanics of Human Motion. Philadelphia: W. B. Saunders Company, 1962.

APPENDIX A

Flexion. Raw Data. Sequence letters refer to the stage of the necropsy, as described in the procedure section. The step is the increment of applied load. The abdominal pressure differential is measured by the transducer (Fig. 9) from the Blakemore Esophageal tube (Fig. 10) as described in Section III, Preparation.

Sequence	Step	Total Load (grams)	Abdominal Pressure Differential	
			Millivolts	psi (@ 0°C)
a	1	0.	.255	.246
	2	481.9	.271	.262
	3	940.5	.323	.312
	4	1397.6	.366	.354
	5	1855.8	.655	.629
b	1	0.		
	2	481.9	.120	.116
	3	939.2	.210	.203
	4	1397.2	.280	.270
	5	1855.8	.750	.725
c	1	481.9		
	2	939.9	.266	.257
	3	1397.2	.330	.319
	4	1855.8	.395	.381
	5	2229.2	.446	.431
d	1	481.9	.158	.152
	2	939.2	.163	.158
	3	1397.8	.162	.156
	4	1855.8	.167	.166
e	1	481.9	(visceration step and following)	
	2	940.5		
	3	1397.8		
	4	1855.8		
	5	2309.4		
f	1	481.9		
	2	940.5		
	3	1397.8		
	4	1855.8		
	5	2309.4		

Table 2. Flexion: Applied Load and Abdominal Press Differential

Flexion (contd). Coordinates of end and insert of spinal Steinmann pins from marked origin (millimeters). Sequence and step are as described for Table 2. The X_i and Y_i, and X_e and Y_e, are coordinates, measured in millimeters, of the inserted (surgically drilled into the spine) and exposed ends, respectively, of the small spinal Steinmann pins (Fig. 11).

		C-4				T-3			
Sequence	Step	X_i	Y_i	X_e	Y_e	X_i	Y_i	X_e	Y_e
a	1	199.50	189.0	167.90	215.82	143.86	211.46	156.96	188.50
	2	7.63	-6.54	15.26	-2.18	11.99	-5.45	7.63	-6.54
	3	22.90	-25.00	27.25	-17.44	27.25	-8.72	19.62	-13.08
	4	27.25	-29.43	37.06	nc	37.06	-2.18	26.16	-10.90
	5	44.00	-49.05	56.60	-50.14	56.68	-31.61	41.42	-31.60
b	1	222.22	147.20	202.74	196.20	not measurable			
	2	4.36	-7.63	10.50	-11.99				
	3	8.72	-16.35	16.40	-19.62				
	4	11.99	-25.07	21.08	-25.07				
	5	13.06	-30.50	26.16	-30.50				
c	1	225.54	114.17	113.72	107.91	not measurable			
	2	9.81	-2.18	2.18	-6.54				
	3	4.36	-10.90	6.54	-10.90				
	4	6.54	-16.35	9.81	-17.40				
	5	8.72	-22.89	11.99	-23.98				
d	1	252.62	32.4	171.02	72.00	191.20	70.20	203.80	106.20
	2	nc	nc	nc	nc	nc	nc	nc	nc
	3	4.50	-4.50	5.40	-2.70	4.50	-2.70	6.30	-3.60
	4	7.20	-4.50	9.90	-2.70	8.10	-3.60	9.90	-3.60
e	1	267.12	19.42	176.60	64.75	200.85	99.9	53.65	86.02
	2	1.85	-3.70	3.70	-2.70	3.70	-3.70	3.70	-2.77
	3	4.60	-4.60	5.55	-3.10	6.48	-5.92	6.48	-4.63
	4	6.47	-5.50	6.47	-4.60	8.32	-8.32	8.33	-6.47
	5	7.40	-6.50	nc	nc	11.10	-10.54	9.25	-9.25
f	1	not measurable				180.00	52.20	192.60	88.20
	2					2.70	-5.40	4.50	-3.60
	3					4.50	-9.00	9.90	-8.10
	4					7.20	-10.80	11.70	-9.90
	5					9.00	-11.70	12.60	-12.60

Table 3. Flexion: C-4, T-3; Spinal Steinmann Pin Positions

Flexion (contd). Sequence and step are as described for Table 2. The X_i and Y_i, and X_e and Y_e, are coordinates, measured in millimeters, of the inserted (surgically drilled into the spine) and exposed ends, respectively, of the small spinal Steinmann pins (Fig. 11).

		T-8				L-2			
Sequence	Step	X_i	Y_i	X_e	Y_e	X_i	Y_i	X_e	Y_e
a	1	106.82	161.32	69.72	200.56	9.80	85.02	-45.78	52.00
	2	4.36	-4.36	9.80	-1.09	2.18	nc	3.27	1.52
	3	9.80	-7.63	17.44	-4.36	5.45	1.10	6.54	2.61
	4	18.53	-14.70	22.85	-8.72	nc	nc	7.63	3.27
	5	26.18	-21.80	40.33	-15.26	9.80	2.18	13.08	5.45
b	1	113.36	148.24	189.66	198.36	14.17	82.84	-51.23	115.54
	2	6.54	-6.54	8.72	-3.27	2.18	nc	1.09	1.09
	3	9.81	-9.81	11.99	-5.45	3.27	nc	2.18	2.18
	4	10.90	nc	19.62	-7.63	nc	nc	5.45	5.45
	5	13.08	-11.99	22.89	-8.72	4.36	nc	6.54	6.54
c	1	113.36	130.80	87.20	182.03	17.44	76.30	-49.05	109.00
	2	4.36	-1.09	3.27	-1.09	nc	nc	2.18	nc
	3	7.63	-3.27	7.63	-2.18	nc	nc	3.27	nc
	4	10.50	-4.36	10.90	-3.27	nc	nc	4.36	nc
	5	16.35	-6.54	15.26	-7.63	nc	nc	5.45	nc
d	1	170.10	92.70	162.00	144.00	66.60	77.40	21.60	126.00
	2	nc	nc	nc	nc	nc	nc	nc	nc
	3	5.40	-1.80	4.50	nc	4.50	-1.80	4.50	nc
	4	8.10	-1.80	8.10	nc	8.10	nc	8.10	nc
e	1	164.65	86.02	155.40	140.60	52.73	65.68	3.70	116.55
	2	3.70	-2.77	3.70	-2.77	1.85	nc	3.33	.93
	3	6.48	-4.63	8.33	-4.62	2.78	nc	5.18	1.85
	4	8.33	-6.47	11.10	-7.40	3.70	nc	8.33	1.48
	5	10.54	-9.25	13.87	-10.17	4.63	nc	10.18	1.48
f	1	129.60	75.60	118.80	126.00	28.80	58.50	-15.30	104.40
	2	1.80	-2.16	5.40	-2.70	1.80	nc	3.60	.90
	3	4.50	-5.40	10.80	-7.20	3.60	-.90	7.20	nc
	4	5.40	-8.10	14.40	-9.90	4.50	-1.80	9.90	nc
	5	6.84	-9.90	17.10	-13.50	6.30	-2.70	11.70	nc

Table 4. Flexion: T-8, L-2; Spinal Steinmann Pin Positions

Flexion (contd). Sequence and step are as described for Table 2. The X_i and Y_i, and X_e and Y_e, are coordinates, measured in millimeters, of the inserted (surgically drilled into the spine) and exposed ends, respectively, of the small spinal Steinmann pins (Fig. 11).

		L-6			
Sequence	Step	X_i	Y_i	X_e	Y_e
a	1	-16.00	14.00	-34.00	14.00
	2	nc	nc	nc	nc
	3	nc	nc	nc	nc
	4	nc	nc	nc	nc
	5	nc	nc	nc	nc
b	1	-27.25	35.97	-82.84	34.88
	2	nc	nc	nc	nc
	3	nc	nc	nc	nc
	4	nc	nc	nc	nc
	5	nc	nc	nc	nc
c	1	-30.52	33.79	-85.02	34.88
	2	nc	nc	nc	nc
	3	nc	nc	nc	nc
	4	nc	nc	nc	nc
	5	nc	nc	nc	nc
d	1	-20.70	45.9	-31.50	56.70
	2	nc	nc	nc	nc
	3	3.60	2.70	-5.40	1.80
	4	3.60	2.70	-5.40	1.80
e	1	0.	32.37	-51.80	42.55
	2	nc	nc	nc	nc
	3	nc	nc	nc	nc
	4	nc	nc	nc	nc
	5	nc	nc	nc	nc
f	1	17.10	30.60	-64.80	39.60
	2	nc	nc	nc	nc
	3	nc	nc	nc	nc
	4	nc	nc	nc	nc
	5	nc	nc	3.60	1.8

Table 5. Flexion: L-6; Spinal Steinmann Pin Positions

Flexion (contd). Sequence and step designations are as defined in Table 2. Theta, "θ" is the arc of a best fit circle, superimposed on the displaced torso (Fig. 11). All loads are in grams. The radial and tangential components is the resolution of load "F" in Fig. 11 into components consistent with P and Q in Fig. 35, viewing the torso as a semicircular arc. Horizontal and vertical components are the resolution of force "F" (Fig. 11) into loads parallel to the x, horizontal, and y, vertical axis.

Sequence	Step	θ(°)	Radial Load (grams)	Tangential Load (grams)	Horizontal Load (grams)	Vertical Load (grams)	α(°)
a	1	64.95					
	2	62.20	-242.34	416.45	255.36	408.60	-41.0
	3	55.90	-408.39	827.14	455.96	801.90	-42.0
	4	54.00	-534.79	1291.18	730.24	1191.60	-42.0
	5	46.60	-438.41	1791.70	969.65	1582.30	-37.0
b	1	52.90					
	2	50.37	-127.72	464.59	276.35	394.70	-31.0
	3	47.49	-203.13	916.88	538.63	769.30	-30.0
	4	44.79	-237.56	1376.69	801.29	1144.40	-28.5
	5	43.19	-264.34	1836.64	1064.30	1520.00	-27.0
c	1	43.00					
	2	40.70	-60.66	937.88	565.60	750.60	-4.0
	3	38.97	-48.03	1396.29	840.80	1115.80	-3.0
	4	36.86	4.56	1855.68	1116.80	1482.00	-5.0
	5	34.38	101.86	2226.82	1341.50	1730.30	-6.0
d	1	12.06					
	2	12.06	673.98	652.82	795.50	497.60	11.0
	3	10.10	1036.58	937.61	1185.33	740.68	10.0
	4	9.96	1379.89	1240.76	1573.70	983.40	10.0
e	1	7.09					
	2	5.68	763.86	548.54	814.40	470.25	11.0
	3	5.26	1141.33	806.93	1210.50	698.90	nc
	4	4.89	1522.05	1061.51	1607.00	927.90	nc
	5	4.50	1903.13	1308.05	1999.90	1154.70	nc
f	1	6.50	not calculated; Δx, Δy not measurable				
	2	5.00					
	3	4.50					
	4	3.00					
	5	2.50					

Table 6. Flexion: Displacement (θ), Load Direction (α) and Component Resolution

Flexion (contd). Sequence and step are unchanged from Table 2. Bending measured, in degrees, is the change from original location of the small spinal Steinmann pins as the torso is displaced by loading. As in Fig. 11, increased "F" will effectively decrease θ and evidence some bending of the spine visualized by an in plane rotation of the C-4, T-3, etc., pins as the vertebrae bend in conforming to the new equilibrium. ΔX and ΔY are the changes, measured in millimeters of X_i and Y_i (Fig. 11) and Table 2, 3, 4. ΔL is the hypotenuse of the ΔX, ΔY sided triangle and is the combined displacement. $\Delta L/L$ is the normalized displacement, dividing by L, the millimeter length from the rim of the pelvis to the inserted spinal pin along the arc of the spine. Δr and Δt are radial and tangential resolutions of ΔX and ΔY.

C-4 (306.9 mm = L)

Sequence	Step	Bending (°)	ΔL	$\Delta L/L$	Δx	Δy	Δr	Δt
a	1	41.0 initial						
	2	6.0	10.60	.061	7.63	6.54	-2.22	9.79
	3	18.0	33.9	.110	22.90	-25.00	-7.86	32.97
	4	25.0	40.1	.130	27.25	-29.43	-7.79	39.34
	5	32.0	65.9	.210	44.0	-49.05	-5.41	65.67
b	1							
	2	4.0	8.87	.029	4.36	7.63	-3.09	8.22
	3	7.0	18.53	.060	8.72	16.35	-6.16	17.47
	4	10.0	27.78	.090	11.99	25.07	-9.15	26.23
	5	12.0	33.17	.108	13.06	30.50	-11.35	31.17
c	1							
	2	constant	6.89	.022	2.18	6.54	-2.61	6.38
	3		11.73	.038	4.36	10.90	-3.47	11.21
	4		17.60	.057	6.54	16.35	-4.57	17.00
	5		28.87	.094	8.72	22.89	-5.73	23.81
d	1							
	2	constant	.0	.0	.0	.0	.0	.0
	3		6.36	.021	4.5	4.5	3.63	5.22
	4		8.49	.027	7.2	4.5	6.31	5.68
e	1							
	2	constant	4.14	.013	1.85	3.70	1.47	3.86
	3		6.50	.021	4.60	4.60	4.15	5.01
	4		8.49	.027	6.47	5.50	5.97	6.03
	5		9.84	.032	7.40	6.50	6.86	7.06

Table 7 (Contd).

Sequence	Step	Bending (°)	ΔL	ΔL/L	Δx	Δy	Δr	Δt
f	1							
	2	constant			not measurable			
	3							
	4							
	5							

Table 7. Flexion: C-4, Vertebral Bending and Normalized Displacements

Flexion (contd). Sequence and step are unchanged from Table 2. Bending measured, in degrees, is the change from original location of the small spinal Steinmann pins as the torso is displaced by loading. As in Fig. 11, increased "F" will effectively decrease θ and evidence some bending of the spine visualized by an in plane rotation of the C-4, T-3, etc., pins as the vertebrae bend in conforming to the new equilibrium. ΔX and ΔY are the changes, measured in millimeters of X_i and Y_i (Fig. 11) and Table 2, 3, 4. ΔL is the hypotenuse of the ΔX, ΔY sided triangle and is the combined displacement. ΔL/L is the normalized displacement, dividing by L, the millimeter length from the rim of the pelvis to the inserted spinal pin along the arc of the spine.

		T-3 (L = 249.3 mm)			T-8 (L = 191.7 mm)		
Sequence	Step	Bending (°)	ΔL	ΔL/L	Bending (°)	ΔL	ΔL/L
a	1	63.0 initial			47.0 initial		
	2	5.0	13.10	.052	1.5	6.16	.032
	3	13.0	28.60	.114	3.0	12.42	.064
	4	25.0	37.10	.148	4.0	23.65	.123
	5	33.0	64.90	.260	9.0	34.06	.177
b	1				57.5 initial		
	2	constant	not		2.0	9.24	.048
	3		measurable		4.0	13.87	.070
	4				6.0	14.66	.076
	5				7.0	17.74	.092
c	1				27.0 initial		
	2	constant	not		1.0	4.49	.023
	3		measurable		1.5	8.30	.040
	4				2.0	11.36	.059
	5				3.0	17.60	.092

Table 8 (Contd).

		T-3 (L = 249.3 mm)			T-8 (L = 191.7 mm)		
Sequence	Step	Bending (°)	ΔL	ΔL/L	Bending (°)	ΔL	ΔL/L
d	1						
	2	constant	0.	0.	constant	0.	
	3		5.29	.021		5.69	.029
	4		8.86	.035		8.29	.043
e	1						
	2	constant	4.13	.016	not measurable		
	3		8.53	.034			
	4		11.13	.044			
	5		15.05	.060			
f	1				80.0 initial		
	2	constant	6.03	.024	3.0	2.81	.014
	3		10.06	.040	6.0	7.02	.036
	4		12.97	.052	8.0	9.73	.051
	5		14.76	.059	9.0	12.23	.063

Table 8. Flexion: T-3, T-8; Vertebral Bending and Normalized Displacements

Flexion (contd). Sequence and step are unchanged from Table 2. Bending measured, in degrees, is the change from original location of the small spinal Steinmann pins as the torso is displaced by loading. As in Fig. 11, increased "F" will effectively decrease θ and evidence some bending of the spine visualized by an in plane rotation of the C-4, T-3, etc., pins as the vertebrae bend in conforming to the new equilibrium. ΔX and ΔY are the changes, measured in millimeters of X_i and Y_i (Fig. 11) and Table 2, 3, 4. ΔL is the hypotenuse of the ΔX, ΔY sided triangle and is the combined displacement. $\Delta L/L$ is the normalized displacement, dividing by L, the millimeter length from the rim of the pelvis to the inserted spinal pin along the arc of the spine.

		L-2 (L = 87.3 mm)			L-6 (L = 30.6 mm)		
Sequence	Step	Bending (°)	ΔL	ΔL/L	Bending (°)	ΔL	ΔL/L
a	1	27.0 initial					
	2	constant	0.		stationary		
	3		6.63	.075			
	4		7.70	.088			
	5		10.03	.115			
b	1	26.0 initial					
	2	1.5	not measurable		stationary		
	3	2.0					
	4	3.0					
	5	4.0					
c	1	not measurable					
	2				stationary		
	3						
	4						
	5						
d	1						
	2		.0	.0	constant	.0	.0
	3		4.84	.055		4.50	.147
	4		.0	.0		4.50	.147
e	1	50.0 initial					
	2	1.0	4.62	.053	constant	1.85	.060
	3	2.0	7.46	.085		2.78	.092
	4	3.0	10.54	.120		3.70	.120
	5	4.0	13.08	.150		4.30	.140
f	1						
	2	constant	1.80	.021	stationary		
	3		3.70	.040			
	4		4.85	.055			
	5		6.88	.078			

Table 9. Flexion: L-2, L-6; Vertebral Bending and Normalized Displacements

Flexion (contd). Sequence and step are unchanged. Axial rotation is out-of-plane movement of the inserted spinal pins measured about the normal axis of the spine (Fig. 11 - out of page movement of C-4, T-3, etc.).

		Axial Rotation (degrees)				
Sequence	Step	C-4	T-3	T-8	L-2	L-6
a	1					
	2					
	3	12.0	8.0	1.5	no movement	
	4	13.0	12.0	1.0		
	5	7.0	12.0	5.0		
b	1					
	2					
	3	3.0		2.0	0.5	
	4	3.0		2.0	1.0	
	5	2.0		1.0	1.0	
c	1	*	*	*	*	*
	2					
	3					
	4					
	5					
d	1	no movement	*	*	*	*
	2					
	3					
	4					
e	1	*	*	*	*	*
	2					
	3					
	4					
	5					
f	1	*	*	*	*	*
	2					
	3					
	4					
	5					

*not measurable

Table 10. Flexion: Axial Rotation of Vertebrae Pins

Extension. Raw Data. Sequence letters refer to the stage of the necropsy, described in the procedure section. The step is the increment of applied load. The abdominal pressure differential is measured by the transducer (Fig. 9) from the Blakemore Esophageal tube (Fig. 10) as described in Section III, Preparation.

Sequence	Step	Total Load (grams)	Abdominal Pressure Millivolts	Differential psi (@ 0°C)
a	1	1390.5	.194	.188
	2	1848.8	.268	.259
	3	2305.8	.353	.341
	4	2764.4	.436	.422
b	1	1390.5	.101	.0976
	2	1847.8	.184	.1779
	3	2305.8	.269	.260
	4	2764.4	.363	.351
c	1	935.5	.129	.124
	2	1317.5	.198	.191
	3	1776.1	.288	.278
	4	2149.3	.380	.367
d	1	939.9	.119	.115
	2	1397.2	.118	.114
	3	1855.8	.190	.183
e	1	481.9	(visceration)	
	2	939.2		
	3	1397.2		
	4	1855.8		
	5	2309.4		
f	1	939.9		
	2	1397.2		
	3	1855.8		
	4	2309.4		

Table 11. Extension: Applied Load and Abdominal Press Differential

Extension (contd). Coordinates of end and insert of spinal Steinmann pins from marked origin (millimeters). Sequence and step are as described for Table 2. The X_i and Y_i, and X_e and Y_e, are coordinates, measured in millimeters, of the inserted (surgically drilled into the spine) and exposed ends, respectively, of the small spinal Steinmann pins (Fig. 11).

		C-4				T-3			
Sequence	Step	X_i	Y_i	X_e	Y_e	X_i	Y_i	X_e	Y_e
a	1	not measurable				not measurable			
	2								
	3								
	4								
b	1	not measurable				not measurable			
	2								
	3								
	4								
c	1	not measurable				76.30	180.94	73.03	159.14
	2					10.90	-6.54	8.72	-5.45
	3					21.80	-11.99	17.44	-11.99
	4					35.97	-20.70	28.34	-17.44
d	1	191.90	70.30	171.00	66.50	not measurable			
	2	4.75	-6.65	-4.75	-11.40				
	3	8.55	-17.10	-15.20	-24.70				
e	1	not measurable				not measurable			
	2								
	3								
	4								
	5								
f	1	not measurable				154.80	84.60	136.80	59.40
	2					3.60	-.90	.90	-7.20
	3					9.00	-15.30	.90	-13.50
	4					12.60	-20.70	1.80	-19.80
	5					14.40	-26.10	2.70	-24.30

Table 12. Extension: C-4, T-3; Spinal Steinmann Pin Locations

Extension (contd). Sequence and step are as described for Table 2. The X_i and Y_i, and X_e and Y_e, are coordinates, measured in millimeters, of the inserted (surgically drilled into the spine) and exposed ends, respectively, of the small spinal Steinmann pins (Fig. 11).

		T-8				L-2			
Sequence	Step	X_i	Y_i	X_e	Y_e	X_i	Y_i	X_e	Y_e
a	1	104.60	147.15	124.26	134.07	87.20	69.70	104.64	61.47
	2	4.36	-4.36	1.09	-4.36	-4.36	.44	nc	-2.18
	3	7.63	-8.72	5.45	-7.63	1.05	-1.09	-1.09	-4.36
	4	10.50	-14.17	6.54	-13.06	2.18	-4.36	-4.36	-5.45
b	1	197.29	159.14	125.35	134.07	69.76	73.03	165.20	81.20
	2	nc	nc	5.45	-6.54	2.18	-1.09	1.40	-5.60
	3	nc	nc	9.80	-10.90	1.09	-2.18	1.40	-9.80
	4	nc	nc	14.17	-20.71	2.18	-3.27	4.20	-14.00
c	1	67.58	154.78	100.28	146.06	47.96	82.84	100.28	58.86
	2	10.90	-5.45	6.54	-7.13	3.27	-2.18	1.09	-4.36
	3	20.70	-10.90	11.99	-16.35	6.54	-4.36	3.27	-8.72
	4	31.61	-17.44	18.53	-26.16	10.90	-7.63	5.45	-15.26
d	1	not measurable				118.75	36.10	137.75	18.05
	2					.95	-1.90	nc	-1.90
	3					2.26	-5.32	nc	-1.90
e	1	not measurable				103.60	55.50	146.15	15.72
	2					nc	nc	nc	-2.77
	3					nc	nc	nc	-4.62
	4					nc	nc	nc	-7.40
	5					nc	nc	nc	-9.25
f	1	131.40	84.60	124.20	47.40	84.60	52.20	124.00	12.60
	2	1.8	-5.40	-1.80	-3.60	nc	nc	nc	-2.70
	3	5.4	-9.00	-2.70	-7.20	nc	nc	nc	-4.50
	4	6.3	-13.50	-3.60	-10.8	nc	nc	nc	-7.20
	5	8.1	-16.20	-4.50	-12.6	nc	nc	nc	-9.00

Table 13. Extension: T-8, L-2; Spinal Steinmann Pin Locations

Extension (contd). Sequence and step are as described for Table 2. The X_i and Y_i, and X_e and Y_e, are coordinates, measured in millimeters, of the inserted (surgically drilled into the spine) and exposed ends, respectively, of the small spinal Steinmann pins (Fig. 11).

		L-6			
Sequence	Step	X_i	Y_i	X_e	Y_e
a	1	94.80	32.70	104.64	32.70
	2	nc	nc	nc	nc
	3	nc	nc	nc	nc
	4	nc	nc	nc	nc
b	1	246.2	42.0	305.2	42.0
	2	nc	nc	nc	nc
	3	nc	nc	nc	nc
	4	nc	nc	nc	nc
c	1	56.68	32.70	98.10	32.70
	2	1.70	-1.74	1.09	-2.18
	3	3.27	-2.62	1.74	-4.36
	4	3.92	-4.36	3.27	-7.63
d	1	91.20	21.80	130.15	6.65
	2	nc	nc	nc	-.95
	3	nc	nc	nc	-1.90
e	1	not measurable			
	2				
	3				
	4				
	5				
f	1	85.50	18.90	117.00	4.50
	2	nc	nc	nc	nc
	3	nc	nc	nc	nc
	4	nc	nc	nc	nc
	5	nc	nc	nc	nc

Table 14. Extension: L-6; Spinal Steinmann Pin Locations

Extension (contd). Sequence and step are unchanged. Bending is the in plane rotation of the spinal Steinmann pins (Fig. 11) from an initial angle to some new position as a result of conforming to the bending of the complete torso. ΔL is the Pythagorean resolution of Δx_i and Δy_i taken from Tables 12-14. L is the millimeter length from the rim of the pelvis to the insert of the Steinmann pin (Fig. 11) along the arc of the spine (L values in Tables 3, 4, 5 for C-4, T-3, T-8, respectively).

SEQ	STEP	C-4 Bending (°)	C-4 ΔL	C-4 ΔL/L	T-3 Bending (°)	T-3 ΔL	T-3 ΔL/L	T-8 Bending (°)	T-8 ΔL	T-8 ΔL/L
a	1	45.0 initial			not measurable			38.0 initial		
	2	-6.0	7.87					-4.0	6.16	.032
	3	-10.0	19.52					-5.0	11.59	.060
	4	-12.5	31.47					-12.5	16.73	.090
b	1	not measurable			not measurable			34.0 initial	0.	
	2							-4.0	nc	
	3							-8.0	nc	
	4							-13.0	nc	
c	1	not measurable			not			52.0 initial	not meas	
	2				measurable	12.71	.05	-4.0	3.93	.060
	3					24.87	.099	-6.0	7.86	.148
	4					41.50	.166	-16.0	13.36	.188
d	1				not measurable			not measurable		
	2		8.17							
	3		9.11							
e	1	not measurable			not measurable			60.0 initial		
	2							-4.0		
	3							-8.0		
	4							-10.0		
	5							-14.0		
f	1	not measurable			not measurable			11.0 initial		
	2							-6.0	3.71	.019
	3							-11.0	7.75	.04
	4							-16.0	24.23	.126
	5							-18.0	29.80	.153

Table 15. Extension: C-4, T-3, T-8; Bending and Normalized Displacement

Extension (contd). Sequence and step are unchanged. Bending is the in plane rotation of the spinal Steinmann pins (Fig. 11) from an initial angle to some new position as a result of conforming to the bending of the complete torso. ΔL is the Pythagorean resolution of Δx_i and Δy_i taken from Tables 12-14. L is the millimeter length from the rim of the pelvis to the insert of the Steinmann pin (Fig. 11) along the arc of the spine (L values in Tables 3, 4, 5 for C-4, T-3, T-8, respectively).

		L-2			L-6		
Sequence	Step	Bending (°)	ΔL	ΔL/L	Bending (°)	ΔL	ΔL/L
a	1				not measurable		
	2		2.22	.025			
	3		2.51	.028			
	4		4.87	.055			
b	1	13.0 initial			not measurable		
	2	-.8	2.43	.027			
	3	-2.6	2.43	.027			
	4	-4.5	3.93	.045			
c	1	-11.0 initial					
	2	-4.0	3.93	.045	constant	2.43	.079
	3	-7.0	7.86	.090		4.19	.136
	4	-11.0	13.36	.153		5.86	.191
d	1	-22.0 initial			not measurable		
	2	-1.0	2.12				
	3	-2.0	5.78				
e	1	-42.0 initial			not measurable		
	2	-2.0					
	3	-4.0					
	4	-5.0					
	5	-7.0					
f	1	-35.0 initial			not measurable		
	2	-2.0	5.69	.065			
	3	-4.0	10.49	.120			
	4	-5.0	14.89	.170			
	5	-6.0	18.10	.207			

Table 16. Extension: L-2, L-6; Bending and Normalized Displacement

Extension (contd). Sequence and step are unchanged. Axial rotation is out-of-plane movement of the inserted spinal pins measured about the normal axis of the spine (Fig. 11 - out of page movement of C-4, T-3, etc.).

Sequence	Step	C-4	T-3	T-8	L-2	L-6
a	1	*	*			*
	2					
	3					
	4			1.0	1.0	
b	1	*	*	*	*	*
	2					
	3					
	4					
c	1	*	*			
	2					
	3				3.0	constant
	4			2.0	5.0	
d	1	*	*	*	*	*
	2					
	3					
e	1	*	*	*	*	*
	2					
	3					
	4					
	5					
f	1	*	*	*	constant	*
	2					
	3					
	4					
	5					

*not measurable

Table 17. Extension: Axial Rotation of Vertebral Pins

Side-Bending. Raw Data. Sequence letters refer to the stage of the necropsy, described in the procedure section. The step is the increment of applied load. The abdominal pressure differential is measured by the transducer (Fig. 9) from the Blakemore Esophageal tube (Fig. 10) as described in Section III, Preparation.

Sequence	Step	Total Load (grams)	Abdominal Pressure Millivolts	Differential psi (@ 0°C)
a	1	1317.5	.193	.186
	2	1774.8	.194	.188
	3	2223.6	.300	.290
	4	2691.4	.520	.503
b	1		not measurable	
	2			
	3			
	4			
c	1		not measurable	
	2			
	3			
	4			
d	1		not measurable	
	2			
	3			
e	1	481.9		
	2	939.9		
	3	1398.5		
	4	1855.8		
	5	2309.4		
f	1		not measurable	
	2			
	3			
	4			
	5			

Table 18. Side-Bending: Applied Load and Abdominal Press Differential

Side-Bending (contd). Coordinates of end and insert of spinal Steinmann pins from marked origin (millimeters). Sequence and step are as described for Table 2. The X_i and Y_i, and X_e and Y_e, are coordinates, measured in millimeters, of the inserted (surgically drilled into the spine) and exposed ends, respectively, of the small spinal Steinmann pins (Fig. 11).

		C-4				T-3			
Sequence	Step	X_i	Y_i	X_e	Y_e	X_i	Y_i	X_e	Y_e
a	1	not measurable				127.53	176.56	137.30	187.46
	2					9.80	-9.80	8.72	-6.54
	3					15.26	-18.53	15.26	-13.08
	4					17.44	-27.25	19.62	-20.70
b	1				not measurable				
	2								
	3								
	4								
c	1				not measurable				
	2								
	3								
	4								
d	1				not measurable				
	2								
	3								
e	1	186.30	36.90	195.30	58.50	not measurable			
	2	5.40	-1.80	4.50	-1.80				
	3	9.00	-1.80	9.00	-1.80				
	4	14.40	-4.50	13.50	-1.80				
	5	15.30	-7.20	18.00	-2.70				
f	1				not measurable				
	2								
	3								
	4								
	5								

Table 19. Side-Bending: C-4, T-3; Spinal Steinmann Pin Locations

Side-Bending (contd). Sequence and step are as described for Table 2. The X_i and Y_i, and X_e and Y_e, are coordinates, measured in millimeters, of the inserted (surgically drilled into the spine) and exposed ends, respectively, of the small spinal Steinmann pins (Fig. 11).

		T-8				L-2			
Sequence	Step	X_i	Y_i	X_e	Y_e	X_i	Y_i	X_e	Y_e
a	1	88.25	159.14	89.36	179.89	not measurable			
	2	7.60	-1.09	5.45	nc				
	3	11.95	-4.36	9.80	-1.09				
	4	16.35	-10.60	14.20	-3.20				
b	1				not measurable				
	2								
	3								
	4								
c	1				not measurable				
	2								
	3								
	4								
d	1				not measurable				
	2								
	3								
e	1	120.60	95.40	117.00	126.90	not measurable			
	2	1.80	-1.80	1.80	-.90				
	3	3.60	-3.60	1.80	-1.80				
	4	5.40	-5.40	1.80	-4.50				
	5	7.20	-7.20	1.80	-6.30				
f	1				not measurable				
	2								
	3								
	4								
	5								

Table 20. Side-Bending: T-8, L-2; Spinal Steinmann Pin Locations

Side-Bending (contd). Sequence and step are as described for Table 2. The X_i and Y_i, and X_e and Y_e, are coordinates, measured in millimeters, of the inserted (surgically drilled into the spine) and exposed ends, respectively, of the small spinal Steinmann pins (Fig. 11).

		L-6			
Sequence	Step	X_i	Y_i	X_e	Y_e
a	1	147.20	25.00	163.50	15.28
	2	nc	nc	nc	nc
	3	nc	nc	nc	nc
	4	nc	nc	nc	nc
b	1		not measurable		
	2				
	3				
	4				
c	1		not measurable		
	2				
	3				
	4				
d	1		not measurable		
	2				
	3				
e	1	85.50	18.90	117.00	4.50
	2	nc	nc	nc	nc
	3	nc	nc	nc	nc
	4	nc	nc	nc	nc
	5	nc	nc	nc	nc
f	1		not measurable		
	2				
	3				
	4				
	5				

Table 21. Side-Bending: L-6; Spinal Steinmann Pin Locations

Side-Bending (contd).

		C-4			T-3		
Sequence	Step	Bending (°)	ΔL	ΔL/L	Bending (°)	ΔL	ΔL/L
a	1	not measurable			6.5 initial	13.85	.055
	2				nc	24.00	.096
	3				nc	32.35	.129
	4				nc		
b	1						
	2						
	3						
	4						
c	1						
	2						
	3						
	4						
d	1						
	2						
	3	no others measurable					
e	1						
	2						
	3						
	4						
	5						
f	1						
	2						
	3						
	4						
	5						

Table 22. Side-Bending: C-4, T-3; Bending and Normalized Displacement

Side-Bending (contd).

		T-8			L-2		
Sequence	Step	Bending (°)	ΔL	ΔL/L	Bending (°)	ΔL	ΔL/L
a	1	38.0 initial			12.2 initial		
	2	-4.0	6.16	.032	-1.2	2.22	.025
	3	-5.0	11.59	.060	-2.0	2.51	.028
	4	-12.50	17.63	.090	-2.5	4.87	.055
b	1						
	2						
	3						
	4						
c	1						
	2			no others measurable			
	3						
	4						
d	1						
	2						
	3						
e	1	11.0 initial			-35.0 initial		
	2	6.0	3.71	.019	-2.0	5.69	.065
	3	11.0	7.75	.040	-4.0	10.49	.120
	4	16.0	24.23	.126	-5.0	14.89	.170
	5	18.0	29.80	.153	-6.0	18.10	.207
f	1						
	2						
	3						
	4						
	5						

No bending or ΔL data was measurable for L-6.

Table 23. Side-Bending: T-8, L-2; Bending and Normalized Displacement

Rotation.

Sequence	Degrees	Abdominal Pressure Differential (millivolts/psi @ 0°C)
a	0	.059/.057
	20	.061/.058
	40	.060/.058
	60	.069/.066
	90	.072/.069
	110	.091/.087
	130	-
	150	.050/.048
	0	
b	0	
	20	.028/.027
	40	.024/.023
	60	.018/.017
	90	.019/.018
	110	.042/.040
	130	.046/.044
	150	.041/.039
	0	.034/.032
c	0	.144/.139
	20	.148/.143
	40	.149/.144
	60	.151/.146
	90	.153/.147
	110	.159/.153
	130	.161/.155
	150	.162/.156
	0	
d	0	.031/.029
	20	.034/.032
	40	.040/.038
	60	.047/.045
	90	.060/.058
	110	.082/.079
	130	.117/.113
	150	.156/.150
	0	.027/.026

Table 24. Rotation: Degrees and Abdominal Press Differential

APPENDIX B

Applying a least squares program to Eqs. (19) and (25), varying ν, with P and Q, the radial and tangential load components (Appendix A, Table 5), equal to stated values; i.e., no weight adjustment for body components.

Sequence	ν	Bending "Coefficient"	Axial "Coefficient"
a	0.3		
b	0.3	$.47 \times 10^{-3}$	$.74 \times 10^{-3}$
c	0.3	$.38 \times 10^{-3}$	$.17 \times 10^{-3}$
d	0.3		
e	0.3	$.51 \times 10^{-3}$	$.13 \times 10^{-3}$
a	0.5	$-.17 \times 10^{-2}$	$.21 \times 10^{-2}$
b	0.5	$.45 \times 10^{-3}$	$.66 \times 10^{-3}$
c	0.5	$.38 \times 10^{-3}$	$.15 \times 10^{-3}$
d	0.5		
e	0.5	$.51 \times 10^{-3}$	$.11 \times 10^{-3}$
a	0.0	$-.16 \times 10^{-2}$	$.29 \times 10^{-2}$
b	0.0	$.49 \times 10^{-3}$	$.89 \times 10^{-3}$
c	0.0	$.33 \times 10^{-3}$	$.33 \times 10^{-3}$
d	0.0		
e	0.0	$.52 \times 10^{-3}$	$.15 \times 10^{-3}$

Table 25. Theoretical Coefficients: Varying ν

Castigliano's theorem for = 0.3 and adjustments in (1) weight added for the head, 1055.5 gr, (2) shoulders, 1270.5 gr, and an estimated (3) remainder, 1000 gr (see Appendix C).

Sequence	Weight Added	Bending "Coefficient"	Axial "Coefficient"
a	(1)	.0020	.025
b		.000047	.0012
c		-.001	.0015
d		.000099	.00023
e		.000029	.00023
a	(1),(2)	.0013	.0167
b		.00024	.0035
c		.0001	-.00013
d		.000023	.00060
e		.000047	.000025
a	(1),(2),(3)	.00075	.0093
b		.00028	.0040
c		.000058	.0011
d		.000093	-.00057
e		.000041	-.00019

Table 26. Theoretical Coefficients: Varying Effective Applied Load

Castigliano's theorem, solving for radial displacement.

```
      PROGRAM LESS(INPUT=/SC,OUTPUT)
   13 READ*,TH,P,Q,DELX,DELY,W
      IF(EOF(5LINPUT))15,22
   22 CONTINUE
      PS=P
      QS=Q+1055.49
      THJ=TH*.0174532
      Z1=COS(THJ)
      Z2=SIN(THJ)
      Z5=PS*Z1
      Z6=QS*Z2
      Z3=Z5-Z6
      Z7=QS*Z1
      Z8=PS*Z2
      Z4=Z7+Z8
      P=Z3
      Q=Z4
      THS=180.-TH
      A1=THS*.0174532
      A2=2.0*A1
      A3=SIN(A1)
      A4=A3**2.0
      A5=SIN(A2)
      A6=COS(A1)
      A7=4.0*A6
      A8=A2-A5
      A10=2.0*A4
      C11=A8*P
      C12=A7+2.0*A4
      C13=C12*Q
      C14=-1.0*4.0*Q
      C1=C11+C13+C14
      C15=2.0*Q*A4
      C2=C11+C15
      A40=A2+A5
      C17=P*A40
      C18=Q*2.0*A4
      C3=C17-C18
      PT=0.0
      QT=QS-Q
      T5=PT*Z1
      T6=QT*Z2
      T3=T5-T6
      T7=QT*Z1
      T8=PT*Z2
      T4=T7+T8
      P0=T3
      Q0=T4
```

```
      T11=A8*P0
      T13=C12*Q0
      T14=-1.0*4.0*Q0
      T1=T11+T13+T14
      T15=2.*Q0*A4
      T2=T11+T15
      T17=P0*A6*0
      T18=Q0*2.*A4
      T3=T17-T18


      C1=C1-T1
      C2=C2-T2
      C3=C3-T3
      THS=180.-THS
      V=0.3
      EX2=1.0+V
      EX1=C2+2.0*C3*EX2
      EX=C1/EX1
      DELS = DELX
      DELX=DELX*Z1-DELY*Z2
      DELY = DELY*Z1+DELS*Z2
      WHYX=DELX/EX1
      WHYY=DELY/EX1
      B4=C1/W
      B5=C2/W
      B6=C3/W
      B7=DELX/W
      B8=DELY/W
      PRINT*,THS," PLOAD=",PS," QLOAD=",QS," RADL=",R," TANGL=",Q
      PRINT*,".........."," C1=",C1," C2=",C2," C3=",C3
      PRINT*,".........."," X=",EX," Y=",WHYX
      PRINT*,"..........",W,B4,B5,B6,B7
      PRINT*,".........."," DELR=",DELX," DELT=",DELY
      GO TO 13
  15  STOP
      END
```

Castigliano's theorem, solving for tangential displacement.

```
      PROGRAM LESS(INPUT=/80,OUTPUT)
   13 READ*,TH,P,Q,DELX,DELY,W
      IF(EOF(5LINPUT))15,22
   22 CONTINUE
      PS=P
      QS=Q
      THJ=TH*.0174532
      Z1=COS(THJ)
      Z2=SIN(THJ)
      Z5=PS*Z1
      Z6=QS*Z2
      Z3=Z5-Z6
      Z7=QS*Z1
      Z8=PS*Z2
      Z4=Z7+Z8
      P=Z3
      Q=Z4
      THS=180.-TH
      A1=THS*.0174532
      A2=2.0*A1
      A3=SIN(A1)
      A4=A3**2.0
      A5=SIN(A2)
      A6=COS(A1)
      A7=4.0*A6
      A8=A2-A5
      A10=2.0*A4
      D1=3.0*A2
      D2=-1.0*8.0*A3
      D3=D1+A5+D2
      D4=D3*Q
      D5=4.0*A6+2.0*A4
      D6=D5*P
      C1=D4+D6-4.0*P
      D7=2.0*P*A4
      D8=Q*(A2+A5)
      C2=D7+D8
      D9=Q*(A2-A5)
      C3=D9-D7
      PT=0.0
      QT=QS-Q
      T5=PT*Z1
      T6=QT*Z2
      T3=T5-T6
      T7=QT*Z1
      T8=PT*Z2
      T4=T7+T8
      P0=T3
      Q0=T4
```

```
      T4=B3*C0
      T6=B5*B0
      T1=T4+T6-4.*B0
      T7=2.*B0*A4
      T8=C0*(A2+A5)
      T2=T7+T8
      T9=C0*(A2-A5)
      T3=T9-T7

      C1=C1-T1
      C2=C2-T2
      C3=C3-T3
      THS=180.-THS
      V=0.3
      EX2=1.0+V
      EX1=C2+2.0*C3*EX2
      EX=C1/EX1
      DELS = DELX
      DELX=DELX*Z1-DELY*Z2
      DELY = DELY*Z1+DELS*Z2
      WHYX=DELX/EX1
      WHYY=DELY/EX1
      B4=C1/W
      B5=C2/W
      B6=C3/W
      B7=DELX/W
      B8=DELY/W
      PRINT*,THS," PLOAD=",PS," QLOAD=",QS," RADL=",R," TANGL=",Q
      PRINT*,".....","  C1=",C1,"  C2=",C2,"  C3=",C3
      PRINT*,".....","      X=",EX,"      Y=",WHYY
      PRINT*,".....",W,B4,B5,B6,B8
      PRINT*,".....","      DELR=",DELX,"      DELT=",DELY
      GO TO 13
15    STOP
      END
```

Least squares program. Read X and Y from previous Castigliano's solution to get a best fit bending and axial relationship for given values of data from Appendix A; θ, P and Q (Table 6), and ΔX, ΔY (Table 7).

```
      PROGRAM JON(INPUT=/80,OUTPUT)
      B1=0.
      B2=0.
      B3=0.
      B4=0.
      B5=0.
      B6=0.
11    READ*, X,Y
      PRINT*,X,Y
      IF(EOF(5LINPUT))15,22
 22   CONTINUE
      A1=Y*Y
      A2=-2.0*X*Y
      A3=-2.0*Y
      A4=X*X
      A5=2.*X
      A6=1.
      B1=B1+A1
      B2=B2+A2
      B3=B3+A3
      B4=B4+A4
      B5=B5+A5
      B6=B6+A6
      GO TO 11
 15   C1=B4*2.
      C2=-1.*B3/C1
      C3=-1.*B5/C1
      D1=B5*C2
      D2=B5*C3
      E1=B2+D1
      E2=2.*B4+D2
      AM=E1/E2
      AB=C2+(B5*AM)
      PRINT*,"BENDING COEFFICIENT=",A1,"AXIAL COEFFICIENT=",AB
      STOP
      END
```

APPENDIX C

	Animal #1	Animal #2
Species	Rhesus	Cynomologus
Tattoo ho	Q78	38
Weight (lbs)	19.0	11.5
Circ, chest (inches)	15.5	13.5
Circ, shoulders (inches)	21.25	14.75
Length (inches)	35.0	24.5
Steinmann pins	C-4,T-3,T-8,L-2,L-6	T-8,L-2,L-6
Sequence	Experiment 1: Bending	Experiment 2: Torsion

Animals were administratively controlled on AMRL Form 70, September 1971, "Laboratory Animal Disposition Request".

	Percent of Total Body Weight: Animal #1
Pelt	7.7
Arms, en bloc	16.2
Abdominal Muscles	4.4
Viscera	17.0
Spinal Muscles	3.9
Osseous Spine/Pelvis	41.0

Table 27. Primate Description

VITA

Arthur Jonathan Nestle was born on 9 September 1947, in Amsterdam, New York. He graduated from high school in Canajoharie, New York, in 1965, and attended Syracuse University from which he received the degree of Bachelor of Science (Aeronautical Engineering) in June 1969. Upon graduation, he received a commission in the United States Air Force through the ROTC Program. He was employed as an associated engineer (pyrotechnics) for McDonnell Douglas Corporation, St. Louis, Missouri, until called to active duty in August 1969. He completed avionics maintenance officer training at Lowry AFB, Denver, Colorado, in July 1970. He then served as Squadron Maintenance Supervisor and Branch Chief in the 5th Avionics Maintenance Squadron (SAC), Minot AFB, North Dakota, until July 1973, and the 36th Avionics Maintenance Squadron (USAFE), Bitburg AB, West Germany, until June 1976. During this time he attended the University of Utah from which he received the degree of Masters of Human Resources Management in April 1975. He entered the School of Engineering, Air Force Institute of Technology, in June 1976.

Permanent address: Box 182
Palatine Bridge, New York 13428

SECURITY CLASSIFICATION OF THIS PAGE (When Data Entered)

REPORT DOCUMENTATION PAGE		READ INSTRUCTIONS BEFORE COMPLETING FORM
1. REPORT NUMBER AMRL-TR-78-63	2. GOVT ACCESSION NO.	3. RECIPIENT'S CATALOG NUMBER
4. TITLE (and Subtitle) KINESIOLOGY OF LOCKED TORSO AS A FUNCTION OF COMPONENT WEIGHT		5. TYPE OF REPORT & PERIOD COVERED MS Thesis
		6. PERFORMING ORG. REPORT NUMBER GAE-AA/78M-10
7. AUTHOR(s) Arthur J. Nestle, Capt, USAF		8. CONTRACT OR GRANT NUMBER(s)
9. PERFORMING ORGANIZATION NAME AND ADDRESS Air Force Institute of Technology (AFIT/EN) Wright-Patterson AFB, OH 45433		10. PROGRAM ELEMENT, PROJECT, TASK AREA & WORK UNIT NUMBERS 61102F 2312-V3-12
11. CONTROLLING OFFICE NAME AND ADDRESS Aerospace Medical Research Laboratory, Aerospace Medical Division, Air Force Systems Command, Wright-Patterson AFB, OH 45433		12. REPORT DATE MARCH 1978 13. NUMBER OF PAGES 135
14. MONITORING AGENCY NAME & ADDRESS(if different from Controlling Office)		15. SECURITY CLASS. (of this report) Unclassified 15a. DECLASSIFICATION/DOWNGRADING SCHEDULE

16. DISTRIBUTION STATEMENT (of this Report)

Approved for public release; distribution unlimited.

17. DISTRIBUTION STATEMENT (of the abstract entered in Block 20, if different from Report)

18. SUPPLEMENTARY NOTES

APPROVED FOR PUBLIC RELEASE,
IAW AFR 190-17.

JOSEPH P. HIPPS, Major, USAF
Director of Information
OCT 5 1978

19. KEY WORDS (Continue on reverse side if necessary and identify by block number)

Kinesiology
Biomechanics
Abdominal Cavity
Spine
Castigliano's Theorem
Primate

20. ABSTRACT (Continue on reverse side if necessary and identify by block number)

Two subhuman primates were utilized to experimentally record the contribution of the musculoskeletal substructures to overall torso stability. Each specimen was euthenized and four small diameter surgical pins drilled into the spinous processes. A Stengstaken-Blakemore esophageal tube was threaded into the proximal esophagus and balloons inflated to define the diaphragm. One experiment consisted of static load application to the torso so that flextural, extensive and lateral bending were introduced. Abdominal pressure was taken from a transducer and multiple exposure photography used to measure the vertebral deformations

DD FORM 1 JAN 73 1473 EDITION OF 1 NOV 65 IS OBSOLETE

SECURITY CLASSIFICATION OF THIS PAGE (When Data Entered)

corresponding to load increment from 0-2309 grams. A second experiment involved rotation of the pelvis, with the C-4, C-5 vertebrae fixed, from 0-110° and associated pressure recorded. For each experiment a progressive necropsy was accomplished and experimental steps repeated.

Deformation measured, from scaled photographs, versus applied load was graphically compared. Both quantities were geometrically reduced along the axis of the spine and slope data tabulated.

Relative reaction to loading for vertebrae C-4, T-3, T-8, L-2 and L-6 is tabulated for abdominal pressure and deformation in flexion, extension and side bending and abdominal pressure from torsion.

Castigliano's theorem was applied to a circular arc representation of the bent torso.